# Characterization of the 10-stages R5900 Hamamatsu photomultipliers for the hadronic ATLAS calorimeter

Gerard Montarou, N. Bouhemaid, P. Grenier, M. Crouau, G.-S. Muanza, S. Poirot, F. Vazeille, I. Gil-Botella, S. Gonzalez de La Hoz

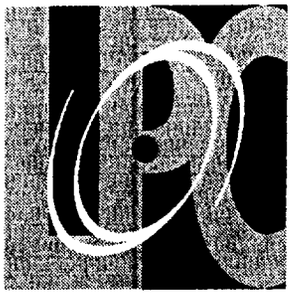

Laboratoire de Physique Corpusculaire
de Clermont-Ferrand



# Characterization of the 10-stages R5900 Hamamatsu photomultipliers for the hadronic ATLAS calorimeter

**G. Montarou, N. Bouhemaid, Ph. Grenier, M. Crouau, G.S. Muanza, S. Poirot, F. Vazeille**

***LPC Clermont-Ferrand***
*IN2P3/CNRS*
*Université Blaise Pascal*
*63177 AUBIERE CEDEX France*

**I. Gil Botella, S. González de la Hoz**

***IFIC-Instituto de Fisica Corpuscular***
*Centro Mixto Universidad de Valencia*
*Avda. Dr. Moliner, 50*
*46100 BURJASSOT Espagne*

**PCCF RI 9705**

# Characterization of the 10-stages R5900 Hamamatsu photomultipliers for the hadronic ATLAS calorimeter

**G. Montarou, N. Bouhemaid, Ph. Grenier, M. Crouau, G.S. Muanza, S. Poirot, F. Vazeille**

**LPC CLERMONT**
**Université BLAISE PASCAL**
**F-63177 Aubiere Cedex**

**I. Gil Botella, S. Gonzàlez de la Hoz**

**IFIC-Instituto de Fisica Corpuscular**
**Centro Mixto Universidad de Valencia**
**Avda. Dr. Moliner, 50**
**E-46100 Burjassot**

**Abstract**

This report summarizes the measurements done at Clermont on the R5900 Hamamatsu photomultipliers for the ATLAS hadronic calorimeter. These measurements had been performed on different developements of the R5900, and finally on a set of PMTs (15) used in a scale-1 prototype ("Module 0") of a sector of the calorimeter barrel. Section 1 reminds what are the TILECAL specifications. Then, we justify the choice of testing the R5900 PMT for the TILECAL readout. Section 3 decribes the uniformity results. Section 4 is devoted on the amplifications measurements. Section 5 reports the dark current measurements on the set of PMTs used in "Module 0". Section 6 describes the R5900 linearity and its improvement. Section 7 reports the data on the magnetic sensitivity without and with an optimised shielding. Finally one describes in section 8 the voltage divider optimisation.

# 1. Specifications for the TILECAL readout system

## 1.1 Readout system.

A suitable device for the read-out of the fibers of the ATLAS hadronic calorimeter (TILECAL) should fullfill some specific constraints:

1) linearity of the device response over the whole dynamic range,

2) good detection efficiency, especially quantum efficiency at the specific light wavelength emitted by the used fibers,

3) magnetic field insensitivity,

4) compacity,

5) low cost.

First preliminary studies on the possible use of a large sensitive area avalanche photodiode (APD) as a suitable device for the read-out of the fibers had forced us to go back to a more classic readout system since neutron radiations induce irreversible damages on such a device.

So far, the most frequent system used for the light read-out remains the PMT, and the constraints listed above have different implications on the different parts of a PMT structure:

1) and 3) are directly related to the dynode structure.

2) is affected by the photocathode and the first dynode.

4) and 5) depend on the technology used for the PMT manufacturing.

## 1.2 Dynamic range and linearity

Simulations of the TILECAL calorimeter response and test beam studies provide indications on the specifications that should fullfill the PMT in the final ATLAS configuration. These specifications are the following:

The energy deposited in one cell of the calorimeter goes from 1.5 TeV (high energy jet) down to 350 MeV for the muon responses.

The amplification of the PMT should be large enough to obtain a correct linearity over the entire dynamic range, but not too large to not saturate the input of the digitizing circuit. Using a calorimeter detection efficiency of the order of 50 photoelectrons/GeV, the dynamical range of photoelectron (p.e.) before amplification goes from 50K p.e for 1 TeV/PMT down to some p.e.

Such a dynamics does not allow to operate the PMT with a too large amplification, since a PMT gain of $10^6$ would induce the anode charge values up to 8 $10^3$ pC, i.e. an anode current [1] up to 530 mA.

An amplification of $10^5$ induces the anode charges up to 800 pC; i.e. an anode current up to 53 mA. An amplification of $10^5$ is found to be a correct nominal value for the PMT gain.

[1] Calorimeter pulse recording indicates that the pulse width is of the order of 15 ns

### 1.3 Detection efficiency

The light coming from the scintillating tiles is collected and transfered to the PMT by wavelength shifting fibers. The main characteristic of these fibers is that the light is absorbed at some wavelength and remitted at an another wavelenght. Figure (1) presents the absorption and emission spectra for Kuraray Y11 fibers. The light is absorbed with a maximum peak around 420 nm and emitted at 480 nm. So, a good detection efficiency is directly correlated to a high quantum efficiency of the photocathode at that specific wavelength. Typical quantum efficiencies at 480 nm for different PMTs are indicated in Table (1).

Nevertheless we have to keep in mind that the quantum efficiency is not the only parameter involved in the detection efficiency, since the first dynode collection efficiency is also determinant to improve the overall PMT detection efficiency.

| Firm | Type | size ($\phi \times L$) | Photocathode | Q.E. (480 nm) | Multiplier type |
|---|---|---|---|---|---|
| Hamamatsu | R1924 | 25×43 | Sb-K-Cs | 16 ~ 18% | CF-10 |
| = | R3991 | 19×28 | Sb-K-Cs | 16 ~ 18% | CF-10 |
| = | R4162 | 19×35 | Sb-K-Cs | 16 ~ 18% | CF-10 |
| Philips | XP2072B | 34×109 | Sb-K-Cs | 20 ~ 22% | LF-10 |
| = | XP2052B | 34×99 | Sb-K-Cs | 16 ~ 18% | LF-10 |
| = | XP2961 | 23×98 | X-tended | 22 ~ 20% | LF-8 |
| EMI | 9111B | 25×43 | Sb-K-Cs | 20 ~ 21% | CF-10 |
| = | 9112B | 25×43 | Sb-Rb-Cs | 21 ~ 22% | CF-10 |

*Table 1 : Compilation of the main characteristics of some conventional but compact PMTs. The quantum efficiency is indicated at 480 nm. LF (CF) corresponds to a linear (circular) focusing configuration for the multiplier.*

### 1.4 Response uniformity

The PMT response should be independent of the impinging point of the light on the PMT photocathode. The bundle diameter (D) directly depends on the number of fibers (M). For 1 mm diameter fibers, an empirical formula of the dependence between D and M is:

$$M = 0.778D^2$$

The number of fibres per cell, as calculated in a preliminary study is given in Table (2). Using the previous formula, the fibre bundle section is less than 14 mm but this effect

could imply a dependence of the calorimeter efficiency as a function of the illuminated tiles. An usual corrective method to overcome such a dependence is to use a light mixer, as an intermediate light collector between the fiber bundle and PMT photocathode.

| | Sampling 1 | Sampling 2 | Sampling 3 |
|---|---|---|---|
| Barrel | $28 \rightarrow 40$ | $40 \rightarrow 86$ | $60 \rightarrow 92$ |
| External Barrel | $22 \rightarrow 68$ | $32 \rightarrow 140$ | $142 \rightarrow 152$ |

*Table 2 : Number of fibres per cell in the 3 samplings of Barrel and External Barrels.*

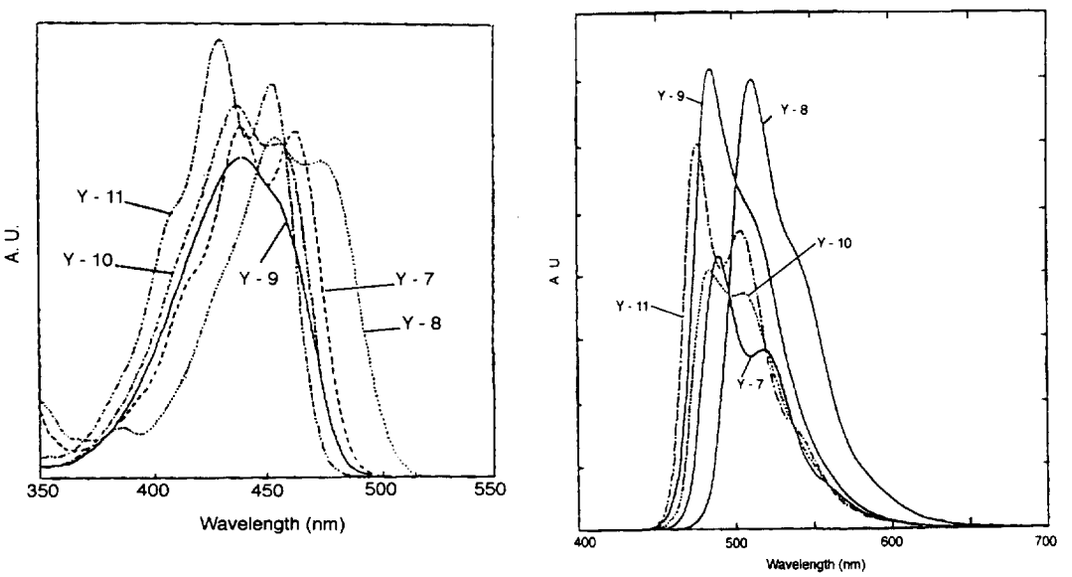


*Figure 1 : Absorption (right) and emission (left) spectrum for the Kuraray fibers. The used fibers are refered as Y11.*

### 1.5 Compacity

Each PMT should be associated with its voltage divider and an optical connector to the fibers bundle (plastic light guide). Moreover, on the same board than the divider are also implanted an integrator circuit for current measurement, a shaper and possibly a compressor. The whole system forms a compact block: the PMT block as represented on Figure (2).

The PMT blocks are implanted in a mechanical structure (the "drawer") that can move inside a girder located at the upper part of each calorimeter sector. Figure (3) presents the foreseen design of the "drawer" and the space available for the block implantation (24 PMT blocks in a drawer). These two pictures show clearly that the PMT compacity is one of the main constraint for the final choice.

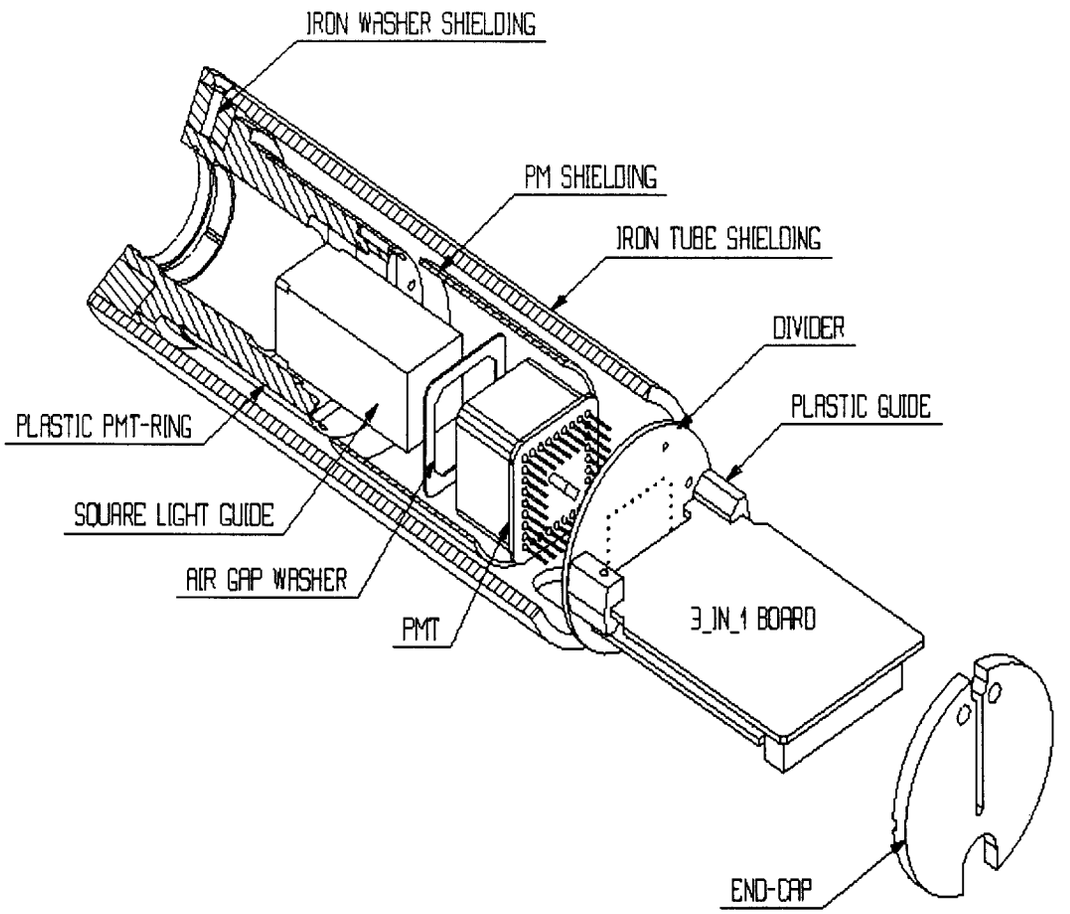


*Figure 2 : Top: PMT block assembly drawing. Bottom: PMT block Photo. The overall dimensions are 15 cm long and 5 cm diameter.*

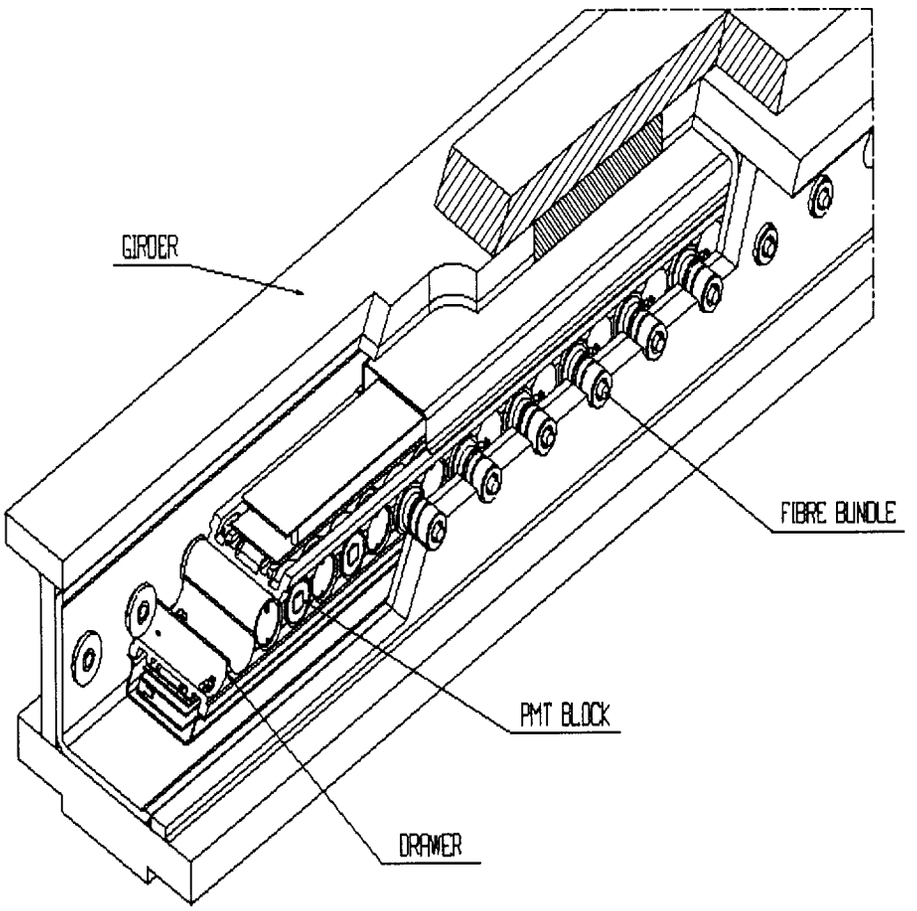


*Figure 3 : The "Drawer" concept and the arrangement of PMT blocks inside the "Drawer".*

### 1.6 Magnetic field sensitivity

Simulations done in the ATLAS framework show that two residual magnetic fields could induce perturbations on the PMT operation in the drawer. Figure (4) indicates the two orientations of the main components of these residual fields which are both perpendicular to the main axis of the PMT.

The simulations indicate that the longitudinal field would not exceed 5 Gauss, and the transversal field would be less than 20 Gauss.

Most of the conventional PMTs are very sensitive to the magnetic field. The insensitivity could be obtained using a magnetic shielding but the more the PMT is intrinsically affected by the magnetic field, the more the shielding would be important and therefore heavy (using soft iron as primary shielding).

Including a safety factor, we fixed first to 800 (250) Gauss the maximum value of the residual transverse (longitudinal) component of the magnetic field at the PMT location which induces a 1% variation of the PMT response with a magnetic shielding.

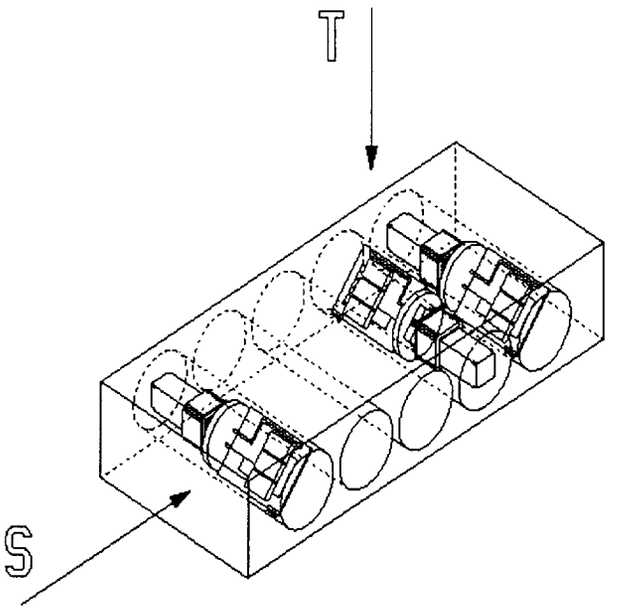


*Figure 4 : Residual magnetic fields at the PMT location.*

### 1.7 Power supply

One solution to overcome the magnetic field sensitivity could be to use a very high electric field in the amplification structure (anode to cathode voltage of 2.5 kVolts for Hamamatsu R2490-05 mesh PMT) or a focusing optics (cathode voltage of the order of 10 kVolts for DEP HPD).

Nevertheless, one should keep in mind that the difficulties of the design of the power source increase with the range needed to supply the device.

Moreover, the cost of the resistors increases significantly for values above 1 kVolt. Therefore, we fixed the device high voltage to be less that 1000 Volts at the nominal amplification.

### 1.8 Rise time

Test beam measurements using a very fast rise time PMT (0.6 ns for the R5600 Hamamatsu) have shown that the TILECAL calorimeter pulse width for pions is of the order of 17 ns, with a rise time close to 5.5 ns. In order to be compatible with the calorimeter pulse rise time, the PMT one should be less than 2.5 ns.

### 1.9 Dark current

It had been required that the PMTs should operate in a current mode for calorimeter cells calibration using integrated charges from minimum bias events or from a Cesium source system. The dynamical range of such calibration currents is between some tens and hundreds of nA. This constrained the maximum dark current to be less than some few nA at the nominal amplification.

# 2. Choice of the PMT

## 2.1 Existing PMTs

The actual manufactured PMTs are of different types, with different photocathode and dynode configurations. Some of them have characteristics well suited to the Tilecal constraints. Other characteristics induce clear disadvantages. Let us review the most typical manufactured PMTs together with their main characteristics.

- Conventional Linear Focusing PMT.
  - good linearity over a large dynamic range,
  - not compact,
  - intrinsically very sensitive to magnetic field.
- Mesh PMT.
  - compact,
  - very insensitive to magnetic field,
  - good linearity,
  - high cost,
  - high value of power supply.
- Circular Focusing PMT, i.e. circular implementation of the dynodes
  - compact,
  - poor linearity,
  - rather insensitive to magnetic field.

Any PMT of the three types listed above needs at least 1000 Volts to achieve a gain of at least $10^5$. A present R and D on ceramic PMTs is promising and could lead to the development of very attractive new types of read-out systems for high energy physics. These products are not yet avalaible, so we consider a new kind of PMTs recently manufactured by the Hamamatsu company: the R5900 square PMT.

In fact this PMT was developed from an outset of an earlier existing PMT, the R5600. Since the first generation, a constant improvement of the characteristics of this PMT has been performed by the Hamamatsu company. Now, this PMT is also available with a multianode configuration. Let us summarize that evolution as follows:

1) generation #1 of R5900 was built up by juxtaposing four R5600 dynodes structures in the same metal package.

2) generation #2 was an evolution of only the dynode structure in the same metal package. It clearly improves the uniformity of the PMT.

3) generation #3 is mainly an optimisation of the input optical structure between the photocathode and the first dynode in order to improve the collection efficiency.

We will now give a presentation of this PMT, indicating for each component what were the main evolutions since the generation #1.

## 2.2 Description of the 5900 PMT

### a) General description

The first advantage of such a PMT becomes clear when looking at the Figure (5). This figure shows the size of the R5900, i.e. overall dimensions equal to $28 \times 28 \times 20$ mm if we take into account only the housing (one should add 8 mm for the pins). The PMT weight is of the order of 25 g. The area of the photocathode (shaded area) corresponds to a square of $19 \times 19$ mm$^2$ (now $18 \times 18$ mm$^2$). The second interesting general characteristic of the R5900 is that the housing package is made of metal. The connections through this package are achieved by a set of 32 pins. One important point of the R5900 series is that the PMT metal housing is connected to the cathode potential. So, operating the tube under negative high voltage implies that the housing is brought to a negative high voltage.

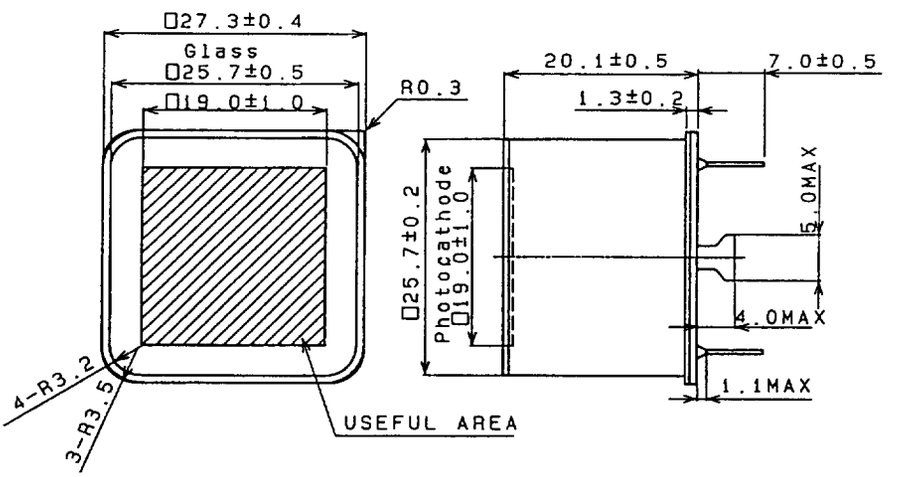


*Figure 5: Overall dimensions of the R5900 as indicated by Hamamatsu. The shaded area corresponds to the photocathode area (Hamamatsu documentation).*

The Figure (6) presents the general dynamic characteristics of the R5900 series:

- a spectral response between 300 and 650 nm,
- a 10-stages amplification, i.e. a gain of the order of $10^6$ at the nominal HV value ($< 900$ Volts),
- a typical anode dark current of the order of the nA at the nominal HV value.

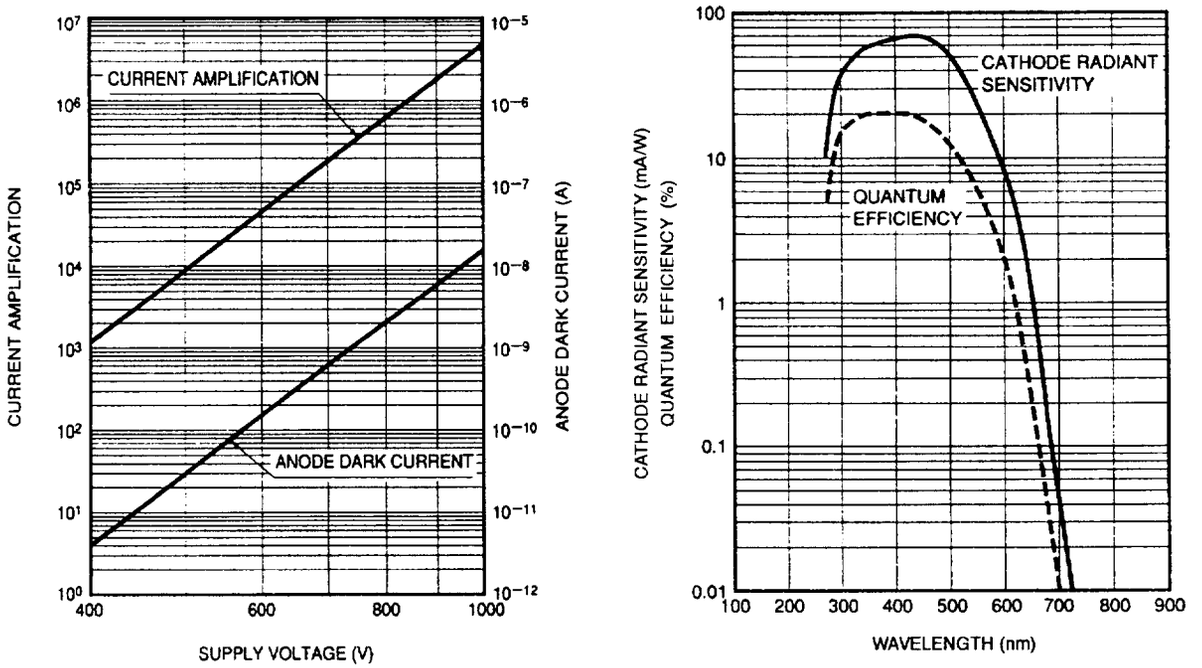


*Figure 6: Typical spectral response of the R5900 series on the right. Typical current amplification and anode dark current on the left. The typical amplification is of the order of* $10^6$ *for a voltage of 800 Volts with a 1.5:1.5:1.5:1:1:1-1:0.5 repartition (Hamamatsu documentation).*

The amplification curve shows also one of the main advantages of the R5900 series: the low supply voltage. The maximum supply voltage, as recommanded by Hamamatsu, should not exceed 1000 Volts. It clearly implies a lot of advantages for the design of the power supply system in comparison with a PMT that needs a higher HV (cost and quality of the electronic components, power dissipation for a large number of PMTs).

Figure (7) indicates the main temporal characteristics of the R5900:

- a fast time response; i.e. a typical rise time of 1.4 ns,
- a typical Transit Time Spread (FWHM) of 0.33 ns.

Nevertheless, one of the most promising characteristic remains the relative large magnetic field insensitivity of the R5900, compared to a classical PMT. Figure (8) presents the relative output variation as a function of the magnetic field flux density for different orientations of the magnetic field.

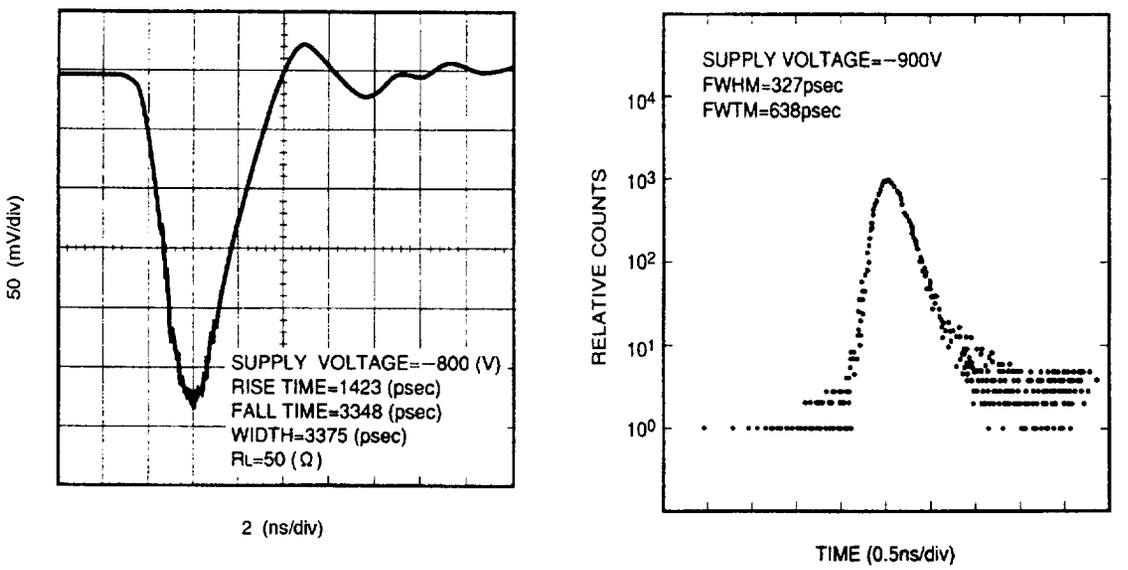


*Figure 7: Typical temporal response of the R5900 series: typical time response on the left. Typical Transit Time Spread on the right (Hamamatsu documentation).*

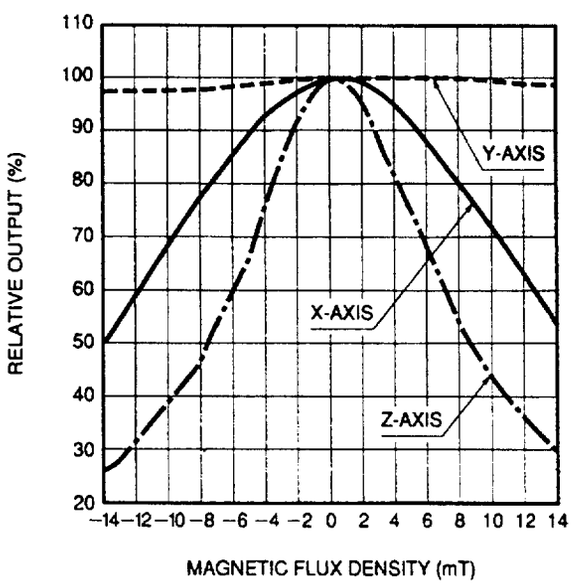


*Figure 8: Relative output variation of a R5900 as a function of the magnetic flux density for different orientations of the magnetic field (Hamamatsu documentation).*

We will have now a deeper insight look at the different components of the PMT.

**b) The photocathode**

The main characteristics of the photocathode are indicated in Table (3):

| Photocathode characteristics | |
|---|---|
| Cathode Material | Sb-$K^2$-Cs |
| Window Material | Borosilicate |
| Spectral response | $300 - 650nm$ |
| Maximum response | $420nm$ |
| Typ. Cath. Sens. $(\mu A/Lm)$ | 70.0 |
| Min. Cath. Sens. $(\mu A/Lm)$ | 60.0 |
| Minimum effective area (mm *times* mm) | $18 \times 18$ |

*Table 3 : R5900 Photocathode characteristics. Hamamatsu documentation.*

These characteristics are measured using a DC luminous flux from a Tungsten Lamp operated at 2856 $K$. The incident luminous flux used for that measurement is in the range of $10^{-4}$ $lm$, i.e. a photocathode current of the order of 10 $nA$. The photocathode is of bialkaki type (Sb-$K^2$-Cs), with a maximum spectral response at 420 nm. The material used for the windows is borosilicate glass. The photocathode sensitivity is: 70$\mu$A/lm for the typical value, and 60$\mu$A/lm for the minimum value.

A bialkali photocathode is generally very resistive, causing a poor collection efficiency over a wide range of voltages even for photoemission currents as low as 10 $nA$. So the photocurrent is linear with the light flux, but if the photocathode current is too large ($\sim$ 100 $nA$), effects of the surface resistance of the photocathode could be very large, and the linearity of the photocathode response is significantly deteriorated.

When the light is directed to the center of the sensitive area, one could have a huge drop of potential between the illuminated area and the edge of the photocathode. Moreover, the larger the photocathode diameter is (and/or smaller the light-spot diameter), the more severe is that effect.

In the pulsed mode case, the local surface potential of the photocathode current is sustained for a while by the electrical charge associated with the photocathode capacitance so that the maximum current (higher than the DC limit) could be maintained during the pulse duration.

Moreover, the global resistivity of the photocathode depends also on the electrical connection between the photocathode and the metal housing. In the two first generations that connection was achieved using two contact points as shown on Figure (9). In the last generation, the overall resistivity of the photocathode is reduced using anAluminium coating between the photocathode and the metal package, thus the electrical connection gets better.

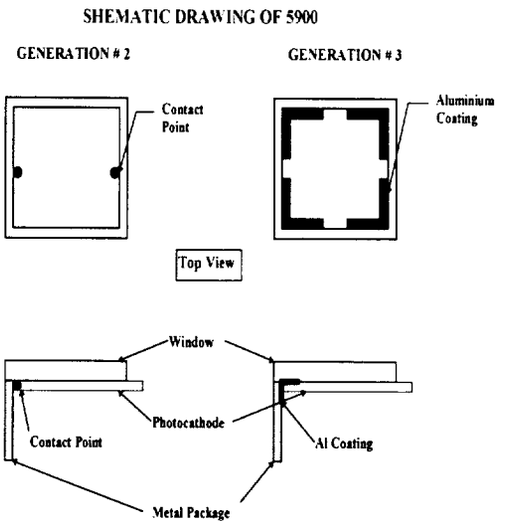


*Figure 9: Connection between the photocathode and the metal housing for generations #2 and #3 of the R5900.*

A test of the photocathode resistivity consists in measuring the variation of the photocathode current as a function of the voltage between the photocathode and the first dynode. The experimental set-up used for that measurement is shown on Figure (10): the light intensity is monitored by the way of a photodiode. The PMT adjusted photocurrent is of the order of a few tens of nA. It should rise-up to a plateau that corresponds to the full collection efficiency (including the PMT quantum efficiency): the faster the photocurrent goes to the plateau, the less resistive is the photocathode, and the best is the photocathode quality.

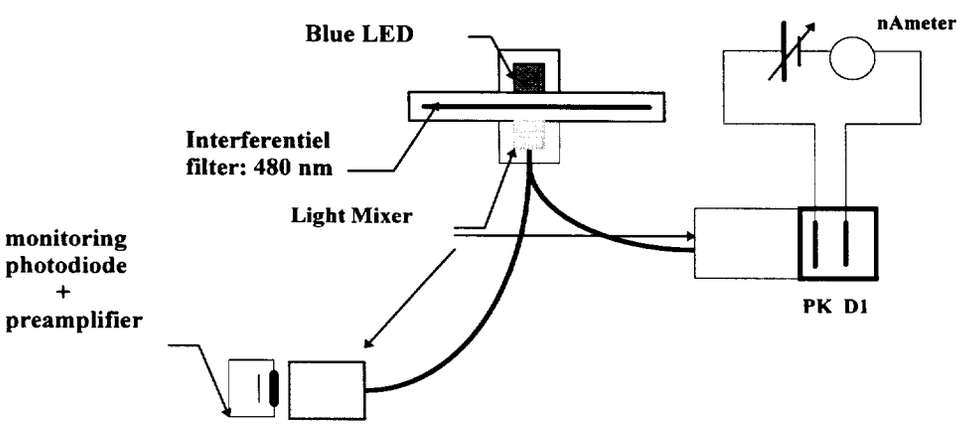


*Figure 10: Experimental setup used for the photocathode current measurements.*

The photocathode current is measured operating the PMT with a specific configuration of the voltage divider as shown on Figure (11). In this measurement, one uses only the photocathode and all the others dynodes tied together as an anode. The photocurrent is measured between the photocathode and the ground.

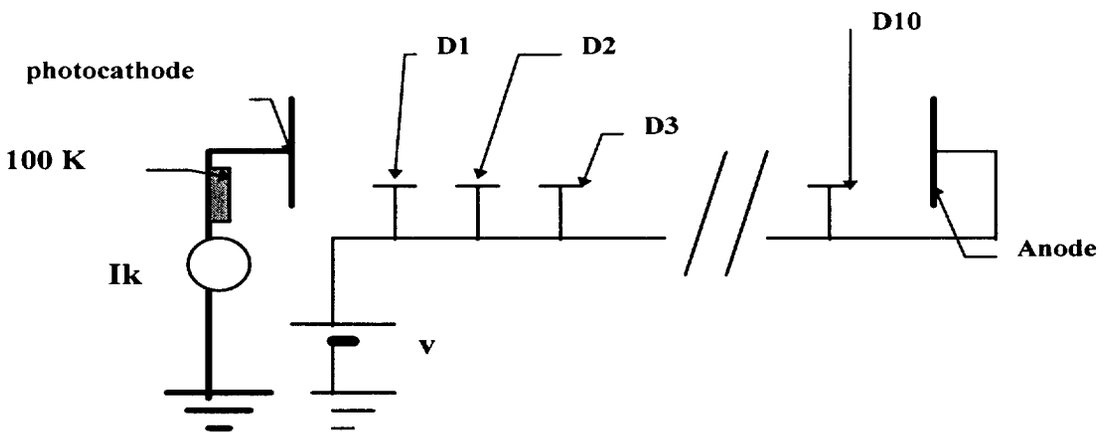


*Figure 11: Specific voltage divider configuration used for the photocathode current measurements.*

The results are shown on Figure (12) for a sample (7) of PMTs of generation #2 (with contact point connection), and for a sample (8) of PMTs of generation #3. The improvements between generation #2 and generation #3 appear clearly.

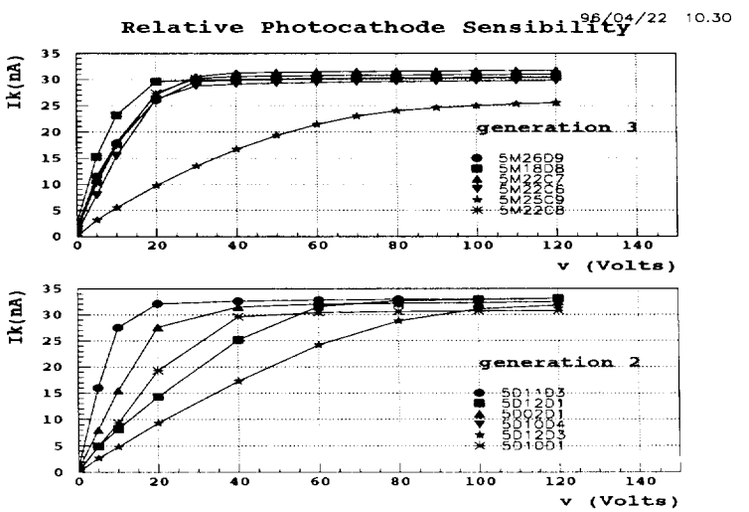


*Figure 12: Results of photocathode current measurements for a set of R5900 of generation #2, and generation #3.*

As this set of sample concerns only 8 PMTs, we perform the test on a set of 15 PMTs of generation #3 used to equip the "Module 0". [2] Figure (13) shows the results of these tests when the light flux was adjusted and monitored by the photodiode to have roughly a photocurrent of the order of 10 $nA$. Most of the R5900 present the same behaviour, i.e. the photocurrent rises-up to a plateau above 20 Volts. However, the 5M25C9 needs at least 40 Volts to get its saturation value, which is significantly lower by about 20 % in comparison to the 14 other PMTs. It indicates that this specific PMT has a high photocathode resistivity. This behaviour appears more clearly on Figures (14) for a light flux corresponding to a photocurrent of the order of 30 $nA$.

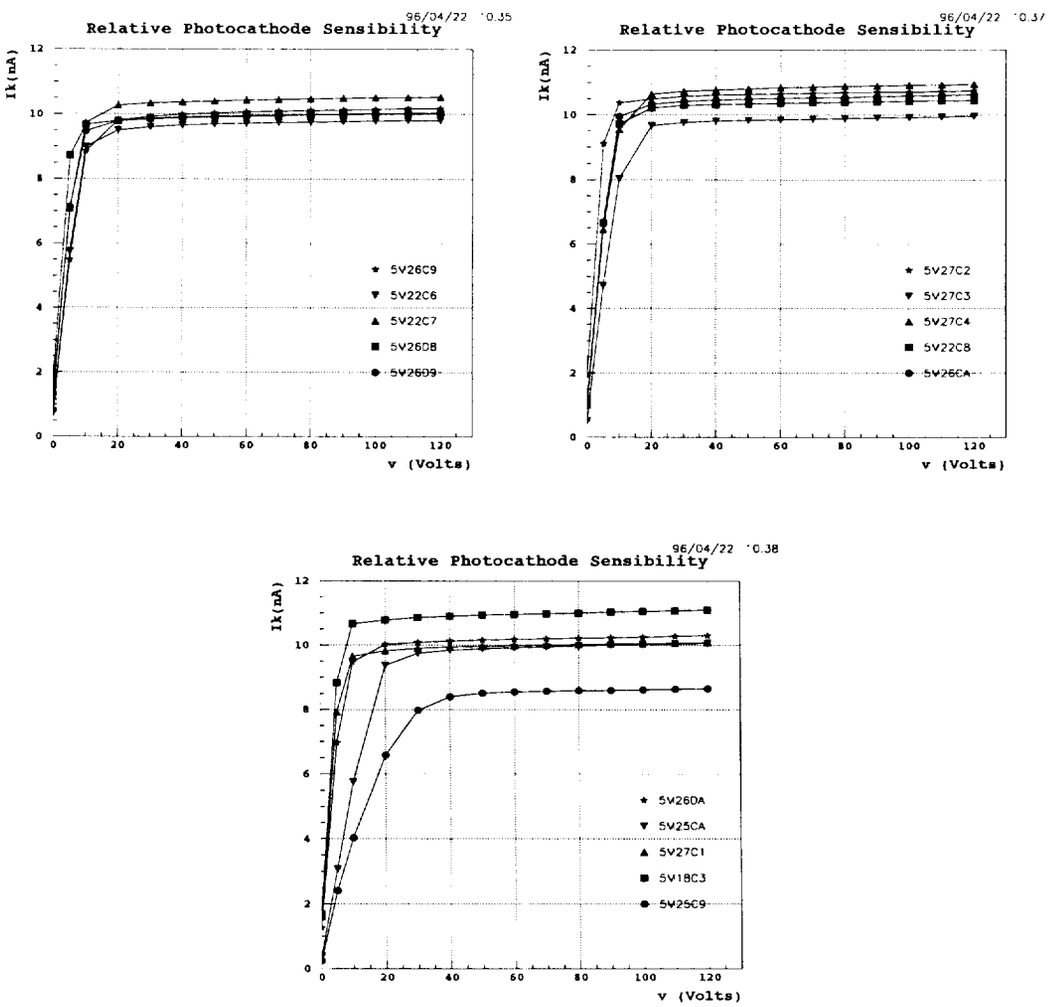


*Figure 13: Photocathode current (nA) as a function of voltage (Volts) between photocathode and all the other dynodes tied together as an anode. The saturation photocurrent is adjusted roughly to 10 nA, and monitored by the photodiode.*

[2] "Module 0" is a full scale barrel sector of the calorimeter tested at CERN

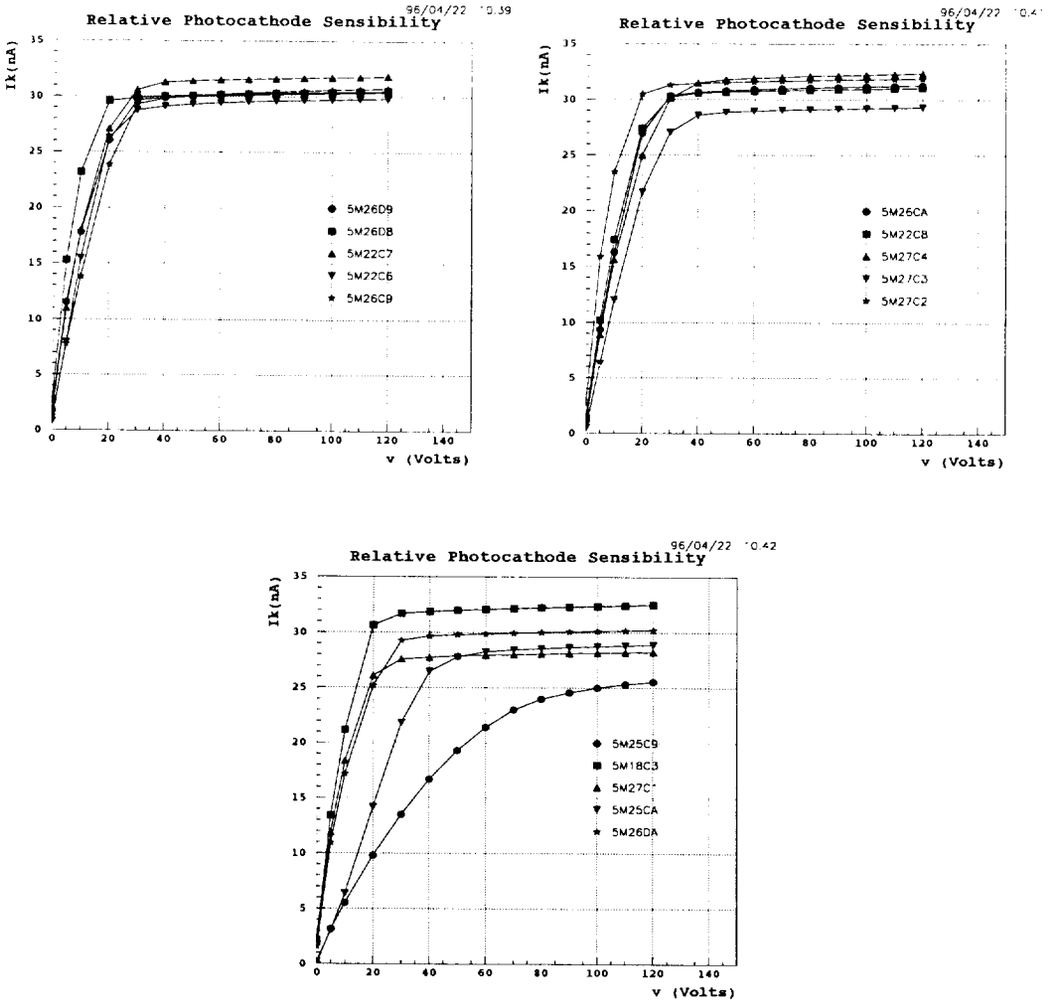


*Figure 14: Photocathode current (nA) as a function of voltage (Volts) between photocathode and all the other dynodes tied together as an anode. The saturation photocurrent is adjusted roughly to 30 nA, and monitored by the photodiode.*

Part a) of Figure (15) represents the correlation between the values corresponding to a photocurrent of the order of 10 $nA$ and the values corresponding to a photocurrent of the order of 30 $nA$. In both cases, the efficiency is estimated relatively to a reference PMT (#5M26DA) and assuming that we have an accurate monitored light source by the way of the photodiode read-out current (we estimate the measurement error due to the monitoring to be of the order 1.5 % on the photocurrent value). This figure shows that the data at 10 $nA$ and 30 $nA$ are correlated at least for the extreme values. Part b) of Figure (15) presents the efficiency estimated relatively to the #5M26DA PMT from the average of the 30 $nA$ and the 10 $nA$ data.

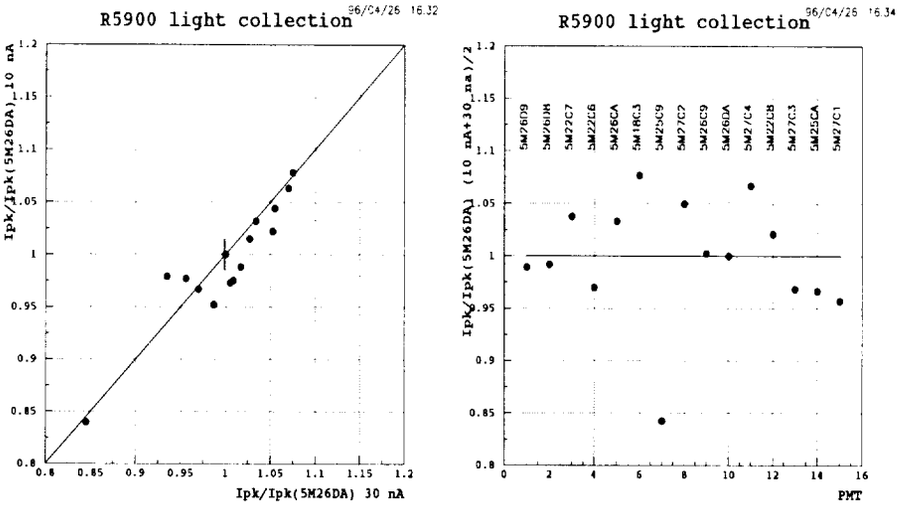


*Figures 15: a) on the left is shown the correlation between the values corresponding to a photocurrent of 10 nA and the values corresponding to a photocurrent of 30 nA. In both cases, the efficiency is estimated relatively to the #5M26DA PMT. We estimate the measurement error due to the monitoring to be of the order* 1.5 % *on the photocurrent value. b) on right is presented the efficiency estimated relatively to #5M26DA PMT from the average of the 30 nA and the 10 nA data.*

### b) The metal dynode structure

This is the most original part of that PMT, first used in the R5600 circular PMT. This concept had been then applied in order to obtain a large square effective area PMT by the juxtaposition of 4 R5600 metal dynode structures. An insight view of the R5900 is shown on Figure (16).

Each stage is made of a thin metallic plate with the dynode profile obtained by micro-graving.

The multiplier configuration is build-up by stacking such metallic plates; the distance between two plates is of the order of 1 mm. Secondary emission is achieved by means of a deposition of Sb-$K^2$-Cs. A plane of thin metallic stripes is put between the photocathode and the first dynode plane, as shown on Figure (17), in order to focus the photoelectrons and so ensures the detection efficiency. The whole dynode block is then very compact and allows a good magnetic insensitivity of the PMT.

Since the generation #1, a constant evolution has been performed by Hamamatsu, up to the generation #3 for which the focusing electrodes dimensions and position have been optimised in order to improve the collection efficiency. In addition, the photocathode resistivity has been decreased by improving the contact between the photocathode and the metal package.

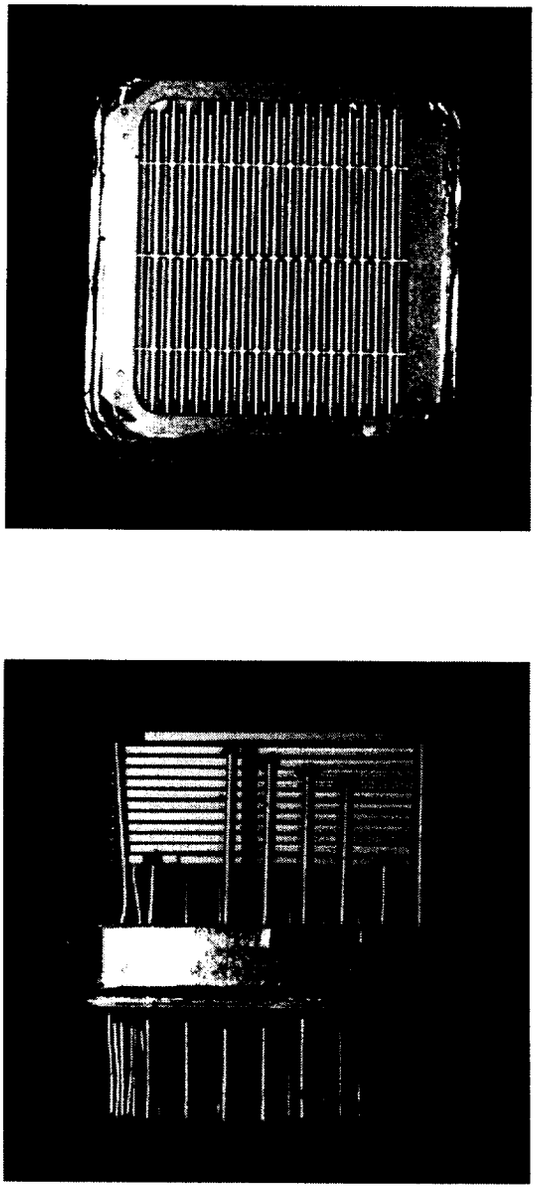

*Figure 16 : Views of the structure of a R5900 of generation #2. Top part shows the input optical structure, i.e the plane of thin metallic stripes between the photocathode and the first dynode to focus the photoelectrons and so to ensure the detection efficiency. Bottom part shows the multiplier configuration built-up of thin metallic plates with the dynode profile.*

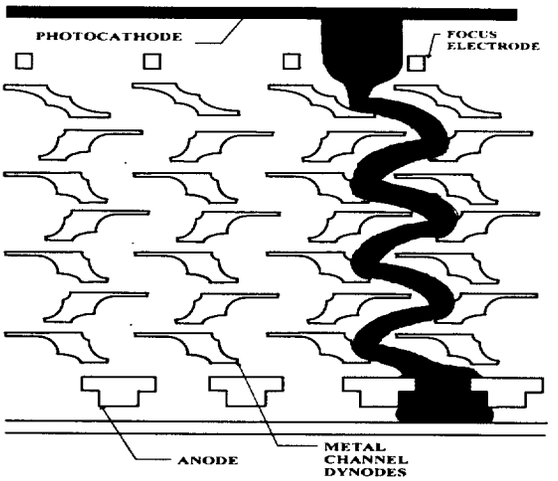


*Figure 17 : Transversal view of the R5900 for generation #2. For simplicity all the stages are not shown. On this picture is also represented a simplified electronic amplification.*

### c) R5900 photometric and radiometric characteristics

While delivering PMTs, Hamamatsu provides the measurements of some photometric and radiometric characteristics. These characteristics are:

- The "white" photocathode luminous sensitivity ($\mu$A/lm).
- The "blue" (Corning CS-58 filtered) photocathode luminous sensitivity ($\mu$A/lmb)
- The anode luminous sensitivity in (A/lm).

Figure (18) shows these characteristics for the whole set of R5900 ordered for the Module 0. These characteristics had been measured by Hamamatsu at 800 Volts and using a specific voltage repartition: 1.5:1.5:1.5:1:1-1:0.5. The average "white" photocathode luminous sensitivity is of the order of 75 $\mu$A/lm, and the "blue" cathode luminous sensitivity is on the average a factor 8.3 smaller. The PMT current amplification is equal to the ratio of the anode luminous sensitivity on the photocathode luminous sensitivity and could be estimated on average to 2.4 $10^6$ with a maximum amplification equal to 5.5 $10^6$.

### • Definitions of photometric and radiometric characteristics

The luminous sensitivity is a photometric measurement [3] used when comparing the sensitivity of photomultiplier tubes categorized in the same types. It is defined in units of Ampere per lumen (A/lm):

$$S_k(A/lm) \;=\; \frac{I_k(A)}{\Phi_\nu(lm)} \qquad (1)$$

[3] the subscripts $e$, $\nu$ designate usualy radiometric and photometric quantities respectively

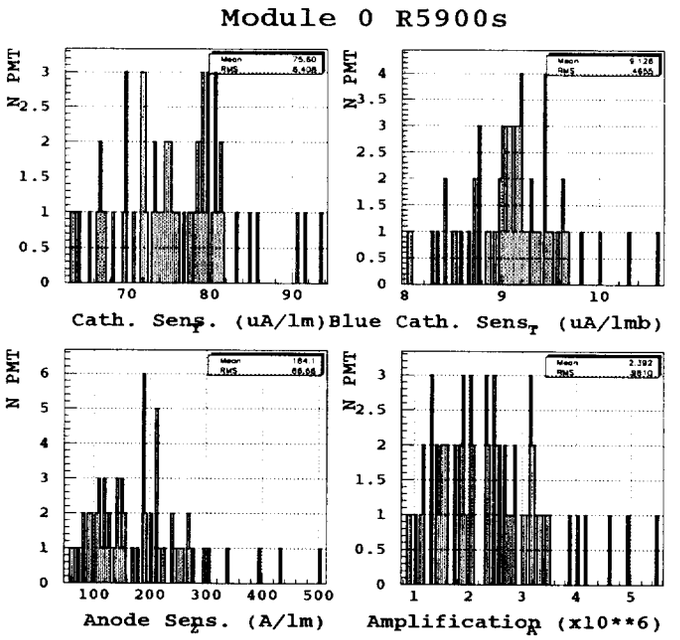


*Figure 18 : Main characteristics of the whole set (65 samples) of R5900 dedicated for Module 0.*

The luminous sensitivity is generally defined for a specific spectral distribution of the radiation, e.g., a tungsten lamp at a colour temperature of 2856K. The relative spectral irradiance of such a lamp is shown in the left part of Figure (19). By definition, the photometric measurement depends on how the radiation source appears to the human eye. The response of the "standard" light adapted human eye (photocopic vision) is denoted by the normalized function $V(\lambda)$. This function is called the photocopic luminous efficiency, and its variation as a function of $\lambda$ is also shown in the right part of the Figure (19).

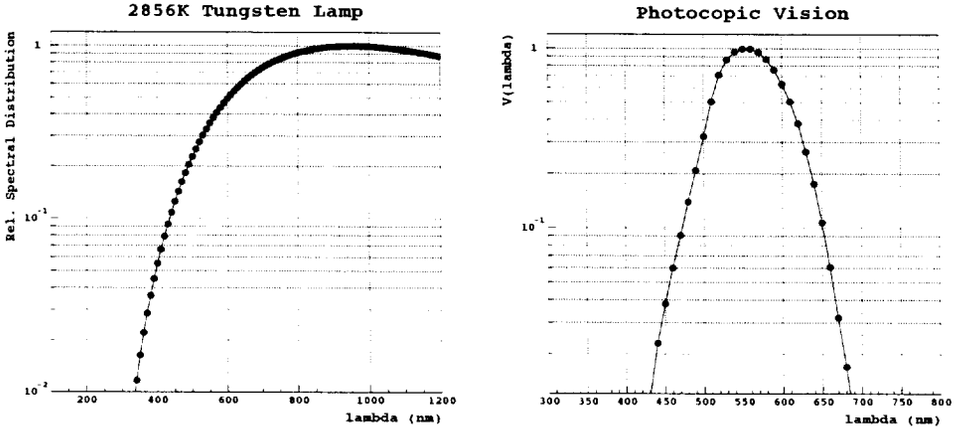


*Figure 19 : Left: relative spectral irradiance from a tungsten lamp operated at a color temperature of 2856 K. Right: photocopic luminous efficiency, $V(\lambda)$.*

Hamamatsu measures the photocathode (anode) luminous sensitivity using a luminous flux of about $10^{-4}lm$ ($10^{-8}lm$) on the PMT photocathode. Lumen is the unit of luminous flux with respect to the standard human's visual sensitivity and is defined as following: the illumination intensity on a surface one meter away from a point light source of one Candela, is one Lux, and one lumen equals the luminous flux of one lux passing through an area of one square meter.

Lumen has no physical significance for most of the PMT applications. That is why it would be better to use a radiometric measurement of the device sensitivity like the radiant sensitivity, defined as the photoelectric current from the photocathode divided by the incident radiant flux (expressed in ampere per watt).

$$S_k(A/W) \;=\; \frac{I_k(A)}{\Phi_e(W)} \tag{2}$$

The conversion from a radiometric quantity ($RQ$ in watts) to the corresponding photometric quantity ($PQ$ in lumens) requires simply to multiply the spectral radiant distribution curve by the photocopic response curve, integrating the product curve and multiplying the results by a conversion factor of 683.

$$PQ \;=\; 683 \int RQ(\lambda)\; V(\lambda)\; d\lambda \tag{3}$$

In most of the applications with photomultipliers, one used a specific radiation. This radiation could be defined as the response of the photomultiplier as a function of the wavelength of the exciting radiation. So, if $d\Phi_e$ is the incident radiant flux in a range $d\lambda$ around a specific wavelength $\lambda$, and $dI_k$ is the corresponding photocathode current, the following expression:

$$S_{k,\lambda}(A/W) \;=\; lim_{d\lambda \to 0}\left[\frac{dI_k(A)}{d\Phi_e(W)}\right]_\lambda \tag{4}$$

defines the monochromatic radiant sensitivity or spectral radiant sensitivity. Such characteristics may be on an absolute or a relative basis. The relative spectral response characteristic is the ratio of $S_{k,\lambda}$ over the radiant sensistivity at some specific wavelength $S_m$. Usually $S_m$ is choosen equal to the maximum of $S_{k,\lambda}$, so that the curves are usually normalized to the unity at the peak of the spectral response curve.

**• Estimation of PMT quantum efficiency from photometric characteristics**

Let us consider the relative radiant sensitivity of a typical R5900 photocathode as being represented by $R(\lambda)$, and assign the absolute radiant response at the peak of the response curve as $\sigma$. The complete radiant response characteristics is given by the function:

$$lim_{d\lambda \to 0}\left[\frac{dI_k(A)}{d\Phi_e(W)}\right]_\lambda \;=\; S_{k,\lambda}(A/W) \;=\; \sigma R(\lambda) \tag{5}$$

Figure (20) shows the typical relative spectral radiant sensitivity of the R5900 PMT.

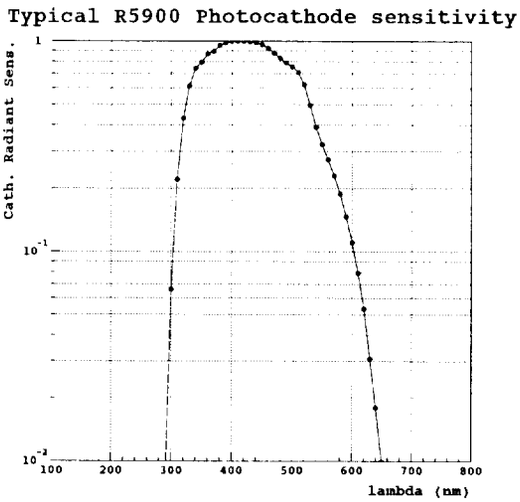


*Figure 20 : Typical Relative radiant spectral sensitivity ($R(\lambda)$ of a R5900 PMT. $S_{k,\lambda}$ is equal to $\sigma R(\lambda)$ where $\sigma$ is the absolute radiant response at the peak of the response curve.*

The average power radiated from a light source, with a spectral distribution $W(\lambda)$, seen by the photocathode, may be expressed as follows:

$$\Phi_e(W) = \int W(\lambda)d\lambda \;=\; P_0 \int W'(\lambda)d\lambda \tag{6}$$

where $W'(\lambda)$ is normalized to unity at the peak of the spectral radiation characteristics, and $P_0$ is some constant (in watts).

The response of the photocathode (in amperes) to the radiation is then given by:

$$I_k(A) \;=\; \sigma \int R(\lambda)W(\lambda)d\lambda \;=\; \sigma P_0 \int R(\lambda)W'(\lambda)d\lambda \tag{7}$$

The radiant photocathode sensitivity is:

$$S_k(A/W) \;=\; \frac{I_k(A)}{\Phi_e(W)} \tag{8}$$

substituting equations (6) and (7) in (8) gives:

$$S_k(A/W) \;=\; \frac{\sigma P_0 \int R(\lambda)W'(\lambda)d\lambda}{P_0 \int W'(\lambda)d\lambda} \;=\; \frac{\sigma \int R(\lambda)W'(\lambda)d\lambda}{\int W'(\lambda)d\lambda} \tag{9}$$

Note that $P_0$ needs not to be known. The light flux in lumen $\Phi_\nu$, represented by the total radiant flux $\Phi_e(W)$, is given by:

$$\Phi_\nu \;=\; 683 \int V(\lambda)W(\lambda)d\lambda \tag{10}$$

where $V(\lambda)$ is the spectral luminous efficiency as modelised in the right part of the Figure (19).

The luminous photocathode sensitivity in amperes per lumen is given by the ratio of expressions (7) and (10):

$$S_k(A/lm) = \frac{\sigma \int R(\lambda)W(\lambda)d\lambda}{683 \int V(\lambda)W(\lambda)d\lambda} \tag{11}$$

From equation (11) the absolute radiant response at the peak, $\sigma$, may be obtained:

$$\sigma = \frac{683S_k \int V(\lambda)W(\lambda)d\lambda}{\int R(\lambda)W(\lambda)d\lambda} = \frac{683S_k \int V(\lambda)W'(\lambda)d\lambda}{\int R(\lambda)W'(\lambda)d\lambda} \tag{12}$$

Note again that the absolute magnitude of the function $W(\lambda)$ needs not to be known. If one assumes that the shape of the spectral radiant sensitivity is the same for each PMT, one could easily deduce $\sigma$ as a characteristic of each PMT, using equation (12).

As claimed above, lumen is the unit of luminous flux with respect to the standard visual sensitivity. It has no physical significance for photomultiplier tubes which have a spectral response range beyond the visible region. That is why manufacturers often use the "blue sensitivity". This sensitivity is measured with the same standard light source as luminous sensitivity but with a colour filter placed between the source and the photocathode in order to simulate the emission spectrum of another source, mostly scintillators.

The used filter is a Corning Cs No. 5-58 polished to half stock thickness, which closely simulates the emission spectrum of a NaI(Tl) scintillator (peak wavelength 420 nanometers).

The photocathode current corresponding to 1 lumen incident on this filter is then called the photocathode blue sensitivity and is expressed in $\mu$A/lmb (b for "blue") or sometimes in $\mu$A/lmF (F for "filtered").

From manufacturer's experience, the "blue" and radiant sensitivities are empirically related:

$$\text{radiant sensitivity at 400 nm(mA/W)} \sim 8.3 \times \text{blue sensitivity } (\mu\text{A/lmb}) \tag{13}$$

As the input light distribution incident on the detector is modified with the "blue" filter, the spectral distribution of the radiation striking the photocathode becomes now $W''(\lambda)$. So the average power, seen by the photocathode, may be expressed as follows:

$$\Phi_e(W) = \int W(\lambda)''d\lambda = P_1 \int W'''(\lambda)d\lambda \tag{14}$$

where $W'''(\lambda)$ is normalized to unity at the peak of the spectral radiation characteristics, and $P_1$ is some constant (in watts). The relative spectral irradiance from a tungsten lamp operated at a color temperature of 2856 K, and transmitted by a "blue" filter is shown on Figure (21).

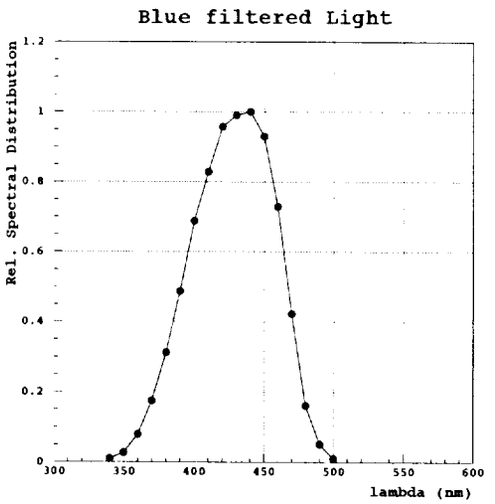


*Figure 21 : Relative spectral irradiance from a tungsten lamp operated at a color temperature of 2856 K, and transmitted by a "blue" filter Filter corrected spectral (Corning Cs No. 5-58 polished to half stock thickness).*

The response of the photocathode (in amperes) to the radiation is then given by:

$$I_k(A) = \sigma \int R(\lambda)W(\lambda)''d\lambda = \sigma P_1 \int R(\lambda)W'''(\lambda)d\lambda \tag{15}$$

The Hamamatsu "blue" photocathode luminous sensitivity corresponds to:

$$S_{kb}(A/lmb) = \frac{I_k(A)}{\Phi_\nu(lm)} = \frac{\sigma P_1 \int R(\lambda)W'''(\lambda)d\lambda}{683 P_0 \int V(\lambda)W'(\lambda)d\lambda} \tag{16}$$

$W'$ and $W'''$ are normalized functions but now $P_0$ and $P_1$ do not cancel like in the expression (11). This ratio takes into account the "blue" filter light attenuation. It should be determined first by the way of the ratio of $S_k/S_{kb}$, i.e., the ratio of expressions (11) and (16):

$$\frac{S_k}{S_{kb}} = \frac{P_0\sigma \int R(\lambda)W'(\lambda)d\lambda}{683 P_0\sigma \int V(\lambda)W'(\lambda)d\lambda} \times \frac{683 P_0\sigma \int V(\lambda)W'(\lambda)d\lambda}{P_1\sigma \int R(\lambda)W'''(\lambda)d\lambda} \tag{17}$$

$$\frac{P_0}{P_1} = \frac{S_k \int R(\lambda)W'''(\lambda)d\lambda}{S_{kb} \int R(\lambda)W'(\lambda)d\lambda} \tag{18}$$

Under the assumption that $R(\lambda)$ is typical of a set of PMT and that the experimental conditions for sensitivity measurements do not change, the ratio $S_k/S_{kb}$ should remain constant and allows to estimate the ratio $P_0/P_1$.

Even though these standard characteristics are useful to select PMTs, they don't give any information about the efficiency of the PMT to convert the light from the fibres,

i.e. the quantum efficiency of the PMT at the specific wavelength they should be used in the TILECAL.

The quantum efficiency is related to the spectral radiant sensitivity by the following expression:

$$S_{k,\lambda} = \frac{\eta e}{hc/\lambda} = \frac{\eta e \lambda}{hc} \tag{19}$$

in units of Amperes per Watt, where $e$ is the charge of the electron. The quantum efficiency is:

$$\eta = \frac{hc}{e} \times \frac{S_{k,\lambda}}{\lambda} = 124 \times \frac{S_{k,\lambda}}{\lambda} \tag{20}$$

where $\lambda$ is given in nanometers, $S_{k,\lambda}$ is given in milliampere per watt, and $\eta$ is given in per cent.

**• Test of the method on two different R5900**

As a concrete application, the Hamamatsu data indicate that for PMT $\#5D17F4$, $S_k$ is equal to 80 $\mu A/lm$. Using equation (12), one obtains an estimated value of $\sigma$ equal to 83.54 mA/W, when the same value directly obtained from the measured spectra is 80.98 mA/W. There is a systematic difference between the estimated value and the measured one which is due to the sampling used for the integrations in the expressions. From some PMT measured spectra, we calculate that this systematic error is of the order of 3%.

Using the estimated value for $\sigma$ and the typical relative radiant spectral sensitivity as shown on the Figure (20), one could easily deduce the spectral radiant sensitivity, and finally the quantum efficiency for any wavelength using relation (20). For the PMT #5D17F4, we estimate the quantum efficiency to be 17.38% at 480 nm, to be compared with the value directly measured by Hamamatsu of 17.35%.

The limitation of such a method could come from the variation of the shape of the relative spectral radiant sensitivity as a function of $\lambda$ for each PMT. This fluctuation generally results in a shift of the spectral PMT sensitivity for higher values of the wavelength. Differences below 400 nm do not have any influence on the photocathode luminous sensitivity since photocopic response is equal to 0 in that range. It is not the case for wavelength in the 600 nm range. We simulate the fluctuation, as a global shift of the "typical" relative spectral radiant distribution, i.e.:

$$R(\lambda) \longrightarrow R(\lambda - \lambda_0) \tag{21}$$

where $\lambda_0$ is the value of the shift. For a PMT, we must check first the assumption that the distribution can be represented by the typical one. This is achieved by the way of the 400 nm quantum efficiency that could be estimated by two independent methods:

• using the measured "blue" photocathode sensitivity and expression (13) to estimate first 400 nm radiant sensitivity. The 400 nm quantum efficiency is then calculated from the expression (20).

• using the value of $\sigma$ and the relative spectral radiant sensitivity to first estimate the 400 nm radiant sensitivity. Finally, the 400 nm quantun efficiency is calculated from the expression (20).

For each PMT, both methods should give roughly the same value for the 400 nm quantum efficiency, and so a ratio of both estimations should be equal to 1.

The PMT #6E06D2 for which the relative spectral radiant distribution (and quantum efficiency) had been fully measured by Hamamatsu, has a luminous photocathode sensitivity ("blue" luminous sensitivity) equal to 101 $\mu$A/lm (9 $\mu$A/lmb). Using the previous method for the $\sigma$ determination, together with the measured $S_k$, and the relative spectral radiant sensitivity, we estimate $\sigma$ to 102.35 mA/W instead of 77.35 mA/W for the measured value.

Using once more the relative radiant spectral distribution, the 400 (480) nm quantum efficiency is 31.7 (21.9)%, to be compared with the Hamamatsu measured values: 21.8 % for 400 nm and 19.1 % for 480 nm.

Moreover, if one uses $S_{kb}$ together with expressions (3) and (20), one estimates that the quantum efficiency at 400 nm is 23.3 %; that is a very different estimation from the previous one (31.7%). So PMT #6E06D2 cannot be tagged as a "typical" one.

Introducing the shift in $R(\lambda)$, $P_0/P_1$ becomes:

$$\frac{P_0}{P_1} = \frac{S_k \int R(\lambda - \lambda_0) W'''(\lambda) d\lambda}{S_{kb} \int R(\lambda - \lambda_0) W'(\lambda) d\lambda} \tag{22}$$

Now we let $\lambda_0$ taking values, with 10 nm steps in the $[-50, 50]$ nanometer range. For each step, the new value of the ratio $P_0/P_1$ is calculated, and the final value of $\lambda_0$ is the one for which the difference between that new ratio $P_0/P_1$ and $\langle P_0/P_1 \rangle$ measured for typical PMTs is the minimum.

For PMT $\#6E06D2$, the shift is of the order of 30 nm and Figure (22) represents the comparison between the measured distribution and the approximated one from the 30 nm shifted typical distribution. It appears clearly that in the $[400, 500]$ nm range, both curves are almost the same. Below 350 nm there is a huge difference but that does not matter so much since in this wavelength range, the photocopic sensitivity and the Kuraray spectral distributions are equal to zero.

With the 30 nm shifted spectral radiant sensitivity, the estimated value of the 400 (480) nm quantum efficiency is 20.6 (18.50)%, to be compared with the measured values: 21.8 (19.1) %.

**• Application to the R5900s used in Module 0**

The method has been applied to the 65 R5900s used in Module 0. We define as "typical", PMTs for which the ratio is in the range $[0.95 - 1.05]$. That condition defines a subset of 37 of the initial set of 65 samples. Using only "typical" PMTs, $P_0/P_1$ spreads over a range of 2 $10^{-3}$, with an averaged value of 0.043. We should keep in mind that this ratio is completely independent from the PMTs and only reflects the operating conditions (light source and Corning filter).

For the complementary subset of non "typical" PMTs, we correct the relative radiant spectral sensitivity by a global shift of the wavelength.

As a final result, we estimate that the 480 nm quantum efficiency is on an average:

$$\langle \eta_{480} \rangle \ = \ 16.4\%$$

with a dispersion of 6.2%. In order to test the sensitivity of the corrective method on the estimated ratio $P_0/P_1$, one redoes the 480 nm quantum efficiency determination of the non "typical" PMTs with the two extreme values for $P_0/P_1$: 0.041 and 0.045. On an average, the 480 nm quantum efficiency decreases of $6.4 \pm 1\%$ when $P_0/P_1$ goes from 0.041 to 0.045.

The right part of Figure (23) represents the distribution of the ratio of the two independent estimations of the 400 nm quantum efficiency for the whole set of R5900. The final 480 nm quantum efficiency for the whole set of PMTs is also presented in the right part of Figure (23).

Table (4) summarizes the $\sigma$ values, as well as the 480 nm quantum estimation for the subset of R5900 tested at Clermont, previously to their use in Module 0. For the non "typical" PMTs, the shift ($\lambda_0$) is indicated in the last column in unit of 10 nm.

| Serial Number | $\sigma$ $(mA/W)$ | $\eta$ (%) 480 nm | $S_{kura}$ $(mA/W)$ | Shift (10 nm) |
|---|---|---|---|---|
| 5M18C3 | 81.78 | 17.53 | 79.05 | |
| 5M22C6 | 76.88 | 15.66 | 73.30 | -1 |
| 5M22C7 | 84.31 | 18.07 | 80.40 | |
| 5M22C8 | 82.00 | 16.70 | 78.19 | -1 |
| 5M25C9 | 71.98 | 14.66 | 68.63 | -1 |
| 5M25CA | 75.62 | 15.40 | 72.10 | -1 |
| 5M26C9 | 79.55 | 17.05 | 76.90 | |
| 5M26CA | 77.83 | 16.68 | 75.23 | |
| 5M26D8 | 73.27 | 15.70 | 70.82 | |
| 5M26D9 | 75.19 | 16.11 | 72.69 | |
| 5M26DA | 79.25 | 16.98 | 76.60 | |
| 5M27C1 | 81.97 | 16.01 | 76.48 | -2 |
| 5M27C2 | 79.96 | 17.14 | 76.24 | |
| 5M27C3 | 79.72 | 16.24 | 76.02 | -1 |
| 5M27C4 | 85.94 | 18.41 | 81.94 | |

*Table 4 : Compilation of the estimated characteristics of the R5900 tested at Clermont for the Module 0. For the non "typical" PMT, the shift ($\lambda_0$) is indicated in the last column in units of 10 nm.*

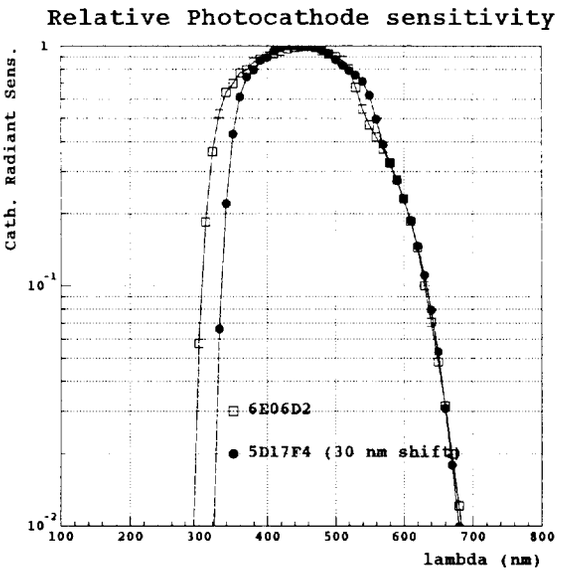


*Figure 22 : Relative radiant spectral sensitivity of a R5900 (PMT #6E06D2) that differs from the typical one. The shifted typical relative radiant spectral sensitivity is shown.*

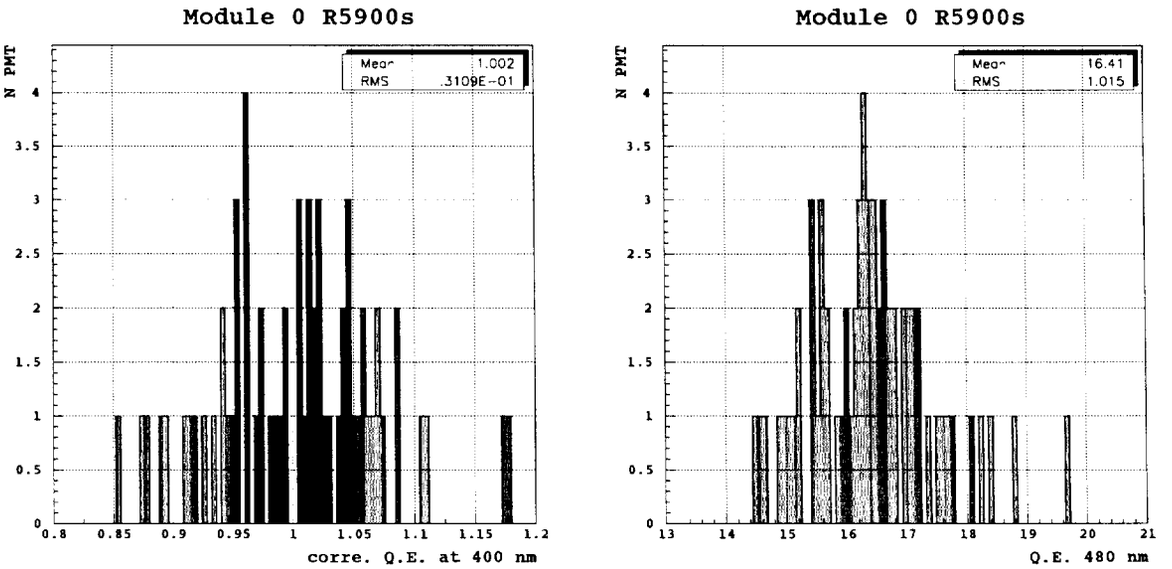


*Figure 23 : Right: Distribution of the ratio of the two independant estimations of the 400 nm quantum efficiency for the whole set of R5900. Left: 400 nm quantum efficiency of the subset of "typical" PMT.*

To cross-check the 480 nm quantum efficiency estimations, we correlate that quantum efficiencies with the 480 nm photocathode current measured at the "plateau" shown in Figure (14). This comparison shown in Figure (24) indicates clearly that these two sets of data are correlated, indicating in that way that we could have some confidence in our estimation of the 480 nm quantum efficiency.

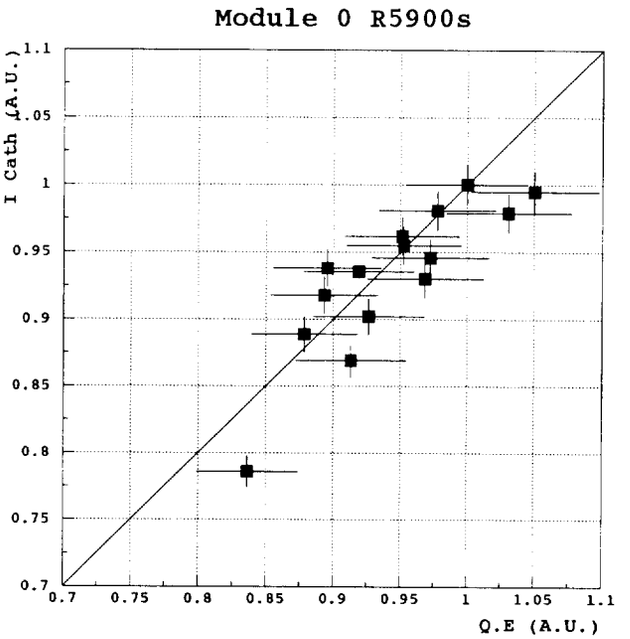


*Figure 24 : Correlation between the estimated 480 nm quantum efficiency (x-axis), and the photocathode current measured at the "plateau" with the 480 nm interferential filter (y-axis). For the subset of tested PMTs, one of the PMT has been used as a reference (#5M18C3). We fix to* 5% *the systematic error on the relative estimated 480 nm quantum efficiency, and to* 1.5% *the systematic error on the relative photocarthode current.*

# 3. Uniformity

The photocathode uniformity is defined as the variation of the photocathode current as a function of the light spot position on the photocathode.

The spatial uniformity of the PMT is the variation of the anode output response with respect to the light spot position on the photocathode.

As a matter of fact, the spatial uniformity is the product of the photocathode uniformity with the electron multiplier uniformity.

### 3.1 Photocathode uniformity

The set-up used for the photocathode uniformity measurement is presented on Figure (25). The light is provided by a blue LED operating in a continuous mode. As the photocathode uniformity is depending upon the light wavelength, the high intensity blue LED is followed by the interferential filter. Downstream, the light is focused into a fiber, providing by this way a spot light source of 1 mm diameter on the active area of the photocathode. The photomultiplier is operated as a photodiode using the first dynode and the others tied together as an anode. For convenience, the photocathode is scanned along the X-axis and the Y-axis, and for each scanned point, the current is measured using a nanoameter. In order to achieve a full photoelectron efficiency, the voltage between the photocathode and the first dynode is set up at least to 100 Volts.

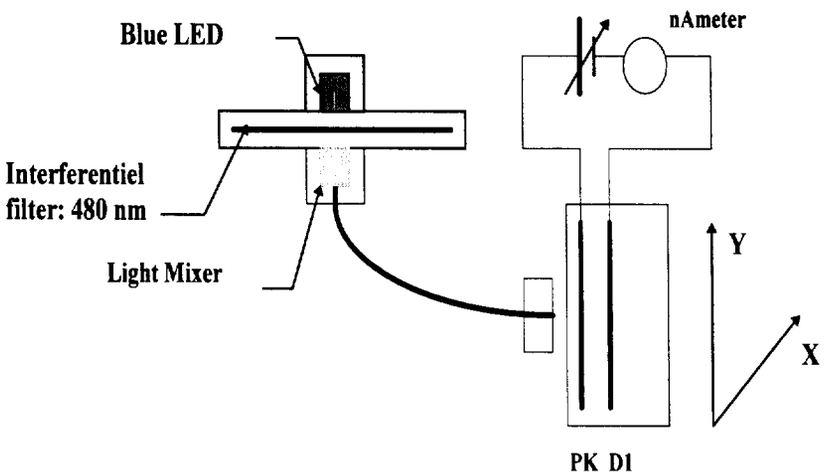


*Figure 25 : Experimental set-up used for the photocathode uniformity measurement. The light is provided by a blue LED operating in a continuous mode, followed by an interferential filter in order to select a specific light wavelength range. The photocathode current is measured with a nanoameter.*

Figure (26) shows the photocathode uniformity measured along perpendicular and transversal axis for 2 typical PMTs of the third generation (#5M22C4 and #5M22C6). These results are fully compatible with the Hamamatsu measurements and indicate that the variation does not exceed ±10% on the effective photocathode area.

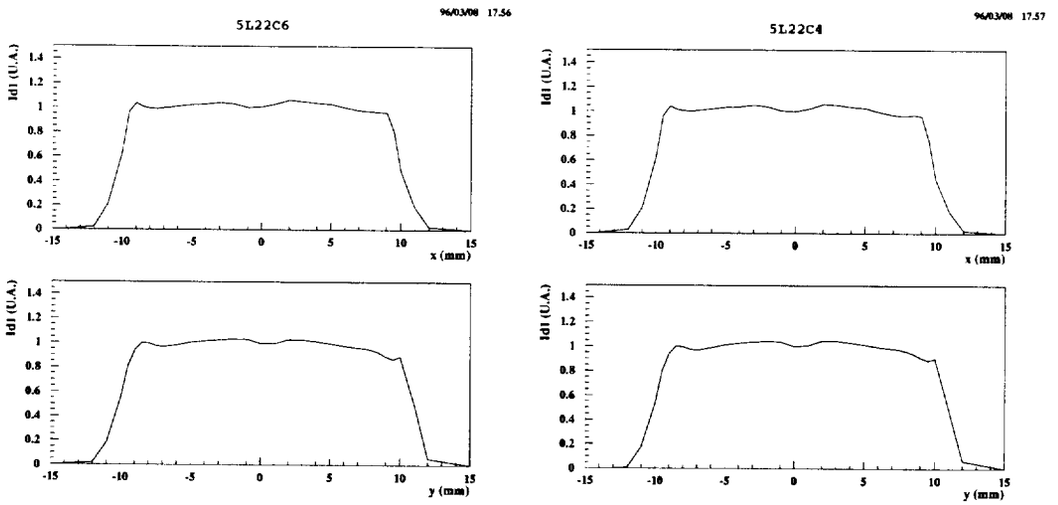


*Figure 26 : Photocathode uniformity as measured along perpendicular and transversal axis for 2 typical PMTs of the third generation: #5M22C4 and #5M22C6. The experimental set-up for this measurement is shown on Figure (25).*

### 3.2 Spatial uniformity

The experimental set-up used for the spatial uniformity measurement is almost indentical to the one shown on Figure (25). However the light is provided by a LED operating now in a pulsed mode (30 ns width), followed by an optical fiber in order to have a light spot impinging on the photocathode. The light spot was 1 mm wide and the gap was less than 1 mm. The LED pulse was generated by a classical LED driver and used also for generating the ADC gate. An automatic procedure allows to control the two motors and so to scan the whole effective area. At each point, 1000 measurements were performed in order to calculate the mean and sigma of the PMT response at that point. The mean response after pedestal substraction and temperature correction is renormalised to the central value. The HV was set to 800 Volt with a standard voltage repartition (1:1:—-1:0.5).

Figures (27) and (28) represent the spatial uniformity for two first PMTs: #4F21G1 and #4L24D6. #4F21G1 is one of the two R5900 prototypes supplied by Hamamatsu, and is representative of the first generation #1 when the dynodes structure was actually made of four R5600 dynodes structure. As shown on the x and y-profiles, these first prototypes were affected by a huge inefficiency area. Along the y direction, the ratio between the minimum and the maximum efficiency grows up to three with y in the range of the effective area (±9). Along the x direction, this ratio is limited to 1.3.

The second PMT (#4L24D6) is one prototype of the generation #2, with a single dynode structure. As shown on the x and y-profiles, there is still a variation of the response, but this variation is now limited to 50% around the central value. One should mention that for this measurement the experimental set-up was modified by using a fiber with a smaller light aperture emission cone than before. This allows to decrease the step of the scaning procedure (and so the resolution to 1 mm instead of 2 mm).

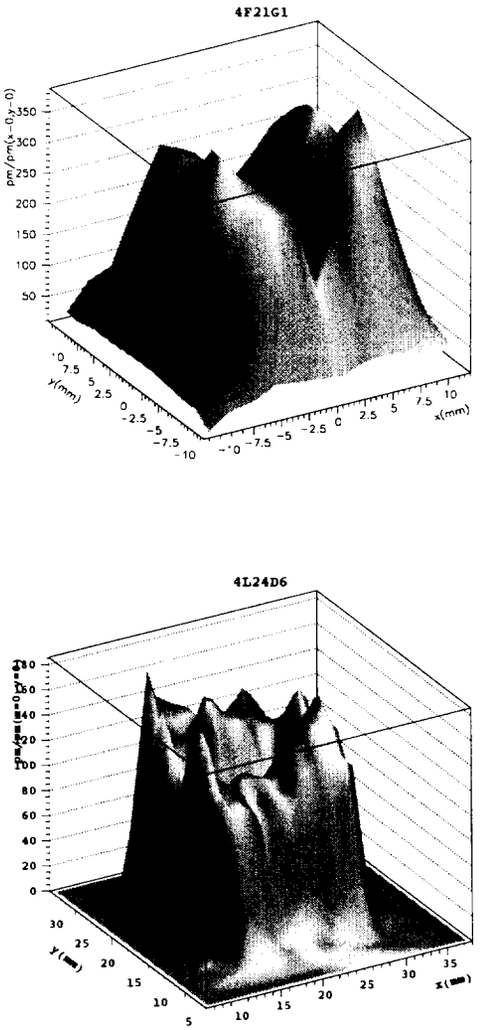


*Figure 27 : Surface representation of the variation of the response of two R5900: #4F21G1 of the first generation and #4L24D6 of the second generation. For the 4F21G1, the light spot was achieved using a large aperture emission cone so that the scanning resolution was 2 mm. For the 4L24D6, the scanning resolution was decreased to 1 mm using a fiber with a smaller light aperture emission cone.*

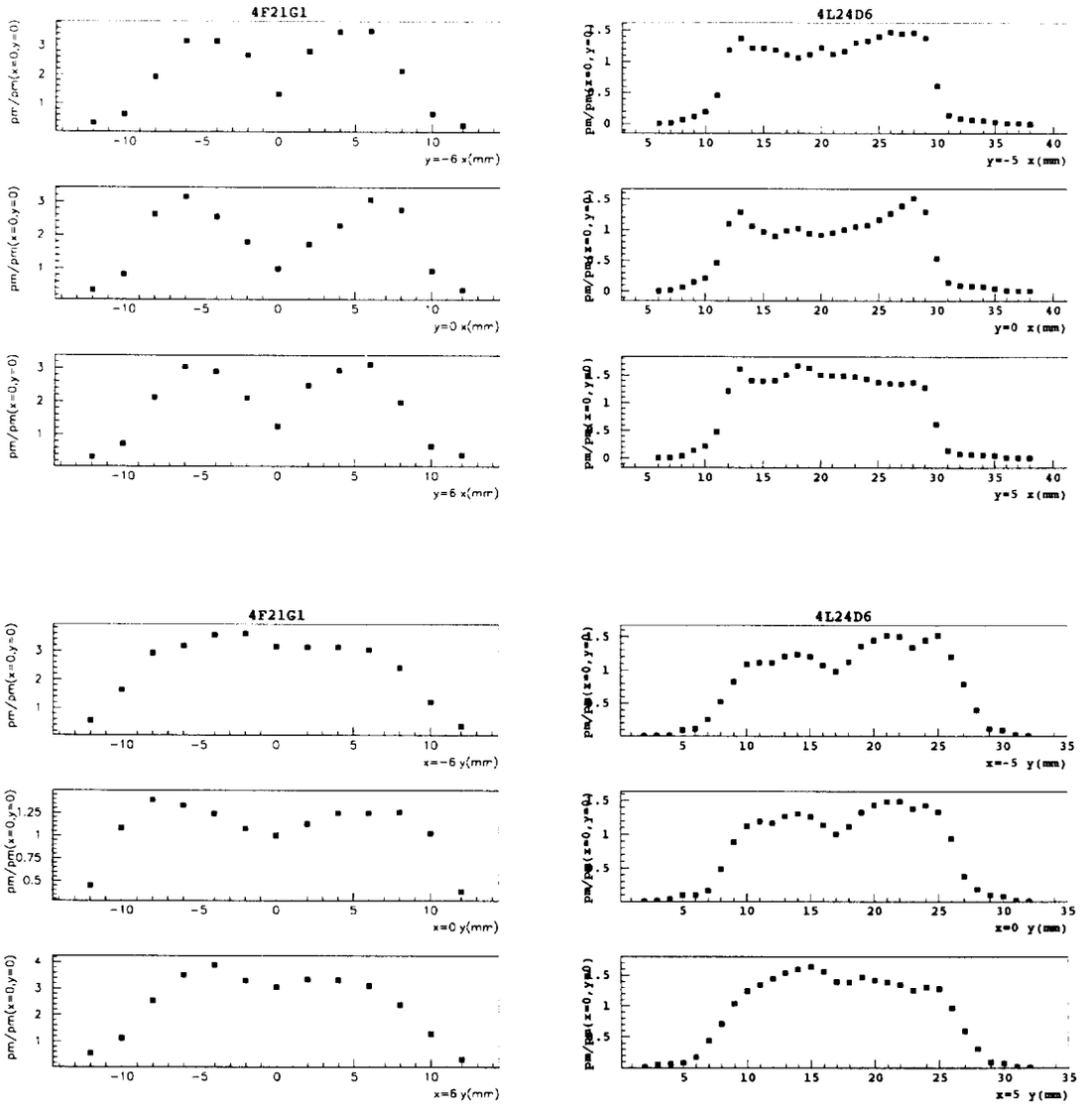


*Figure 28 : Variation of the response of two R5900: #4F21G1 of the first generation and #4L24D6 of the second generation along the x- and y-axis for 3 different values of the other coordinate: -6 mm, 0 mm and 6 mm for the 4F21G1, -5 mm, 0 mm and 5 mm for the 4L24D6. The response after pedestal substraction and temperature correction is renormalised to the central value. This central value is clearly defined as the minimum for the 4F21G1. For the 4L24D6, the central value is defined to be x=17 mm and y=21 mm in our local frame.*

The Figures (29) and (30) indicate that the spatial uniformity does not depend on the applied high voltage over a large range from 600 to 900 Volts. After that, the HV range was extended down to 500 Volts and up to 1000 Volts, that confirms that the spatial uniformity is independent under these extreme values.

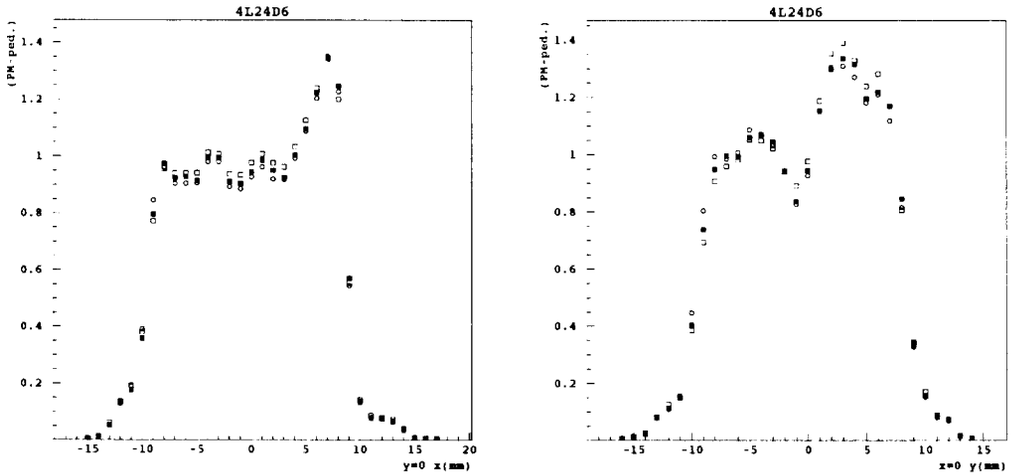


*Figure 29 : Variation of the PMT response (# 4L24D6): as a function of y coordinate and for x =0 on the left; as a function of the x coordinate and for y =0 on the right. The signal after pedestal substraction is renormalised to the mean value calculated on a central square of* $10 \times 10$ mm$^2$ *of the photocathode. Full squares correspond to a PMT voltage equal to 800 Volts, open squares correspond to a PMT voltage equal to 700 Volts, and open triangles to a PMT voltage equal to 900 Volts.*

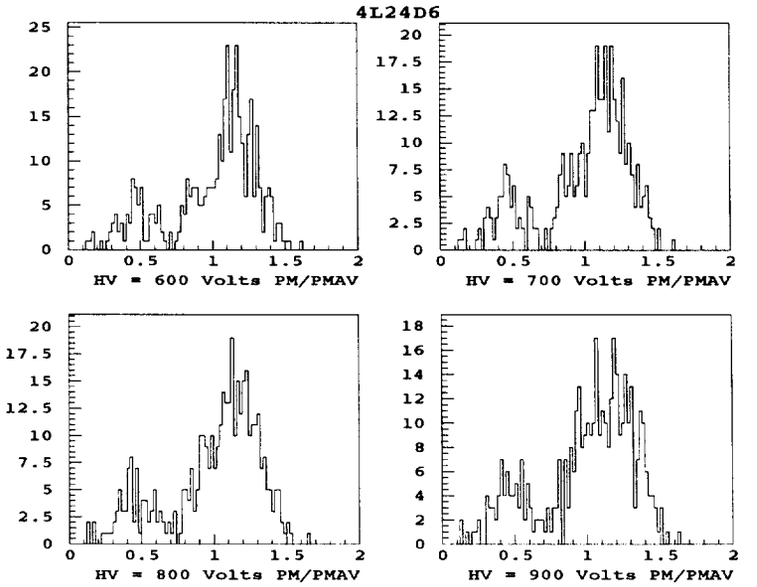


*Figure 30 : Variation of the PMT response (# 4L24D6) over a central square of* $10 \times 10$ mm$^2$ *of the photocathode. This response is renormalised to the mean value calculated on that central square and represented for different values of the PMT voltage: 600, 700, 800 and 900 Volts.*

### 3.3 Light mixer optimisation

As shown above, most of the R5900 exhibit variations in response over their photocathode surfaces, but the light extracted from the fibres inside a given bundle must be independent of the fibre location on the photocathode. An usual corrective method to overcome such a dependance is to use a "light mixer", i.e. an intermediate light guide between the fibre bundle and the PMT photocathode to mix the light coming from the fibres.

Such a light guide needs to be carefully designed; especially its shape and its length. Previous studies indicate that a parallelepiped shape light guide with a length of 1.9 times its side leads to the best performance. Moreover, parallelepiped shape is also more suitable when designing the PMT block mechanics.

The cross section of that light guide is mainly constrained by the maximum size of the fibres bundle (see Table (1)) and the accuracy in positioning the drawers (which support the light guides) in front of the bundles. The optimum cross section is $18 \times 18$ mm$^2$ and fits well with the R5900 effective photocathode area. The light mixer length remains to be optimised taking into account different constraints:

- The light attenuation in the light mixer.
- The Cerenkov light emission from particles in the "light mixer" material.
- On the other hand, the longer is the "light mixer", the better the light coming from the fibres is mixed.

An air gap between the PMT block and the fibre bundle is needed to allow the movement of the drawer. Moreover, simulations of the mixing uniformity and acceptance show that:

- The air gap between the fibre bundle and the light mixer should be no more than 1 mm.
- An air gap of a few tenths of a mm is aquedate between the light mixer and the photocathode.
- The length of the light guide should be greater than 30 mm.

Figure (31) illustrates the evolution of the uniformity and of the acceptance as a function of the light guide length, in apex units [4], for two fibre positions: fibre #1 is near the external part of the largest bundle, and fibre #1 is at the center. These results show that for a light guide of at least 1.5 times the apex ($\sim$ 38mm) the acceptance and the uniformity of the PMT response are independent from the fibre position.

In order to test the light guide, we measured the variation of a PMT (#5D10D1) response, as a function of the x and y coordinates of a $1 \times 1$ mm$^2$ illuminated window of the photocathode, moving in front of the output face of the light guide. The PMT is used now as a ponctual photodetector.

Clearly, we use a R5900 for technical convenience, but any other type of photodetector with a sufficient amplification is suitable for such a test. The signal after pedestal

[4] diameter of the circumscribed circle

substraction is renormalised to the averaged response on a $16 \times 16$ mm$^2$ central square window on the output face of the "light mixer". Figure (32) represents, in a lego representation, the renormalised light measured at the output face of the "light mixer", and for different values of its length, from 30 mm up to 57 mm, while the square section remains constant ($18 \times 18$mm$^2$).

These figures would be in favour of a 50 mm length "light mixer". They indicate also some "interference" effects, that are certainly due to the square section of the "light mixer". Such a depletion is clearly evident on the Figure (33) with a contour level representation.

Nevertheless, to be more quantitative, one should look at the Figures (34) where are represented the variations of the renormalised PMT response as a function of the x (y) coordinate, and for different fixed values of the other coordinate. From these curves, 30 and 35 mm long "light mixers" could be certainly excluded. But it appears that, if the edge behaviour is better for the 50 mm long "light mixer", the central response is more uniform in the case of the 43 mm long "light mixer". One should also keep in mind the effect of light attenuation and Cerenkov emission increase with the length. So we fix to 43 mm the length of the "light mixer" as a good compromise.

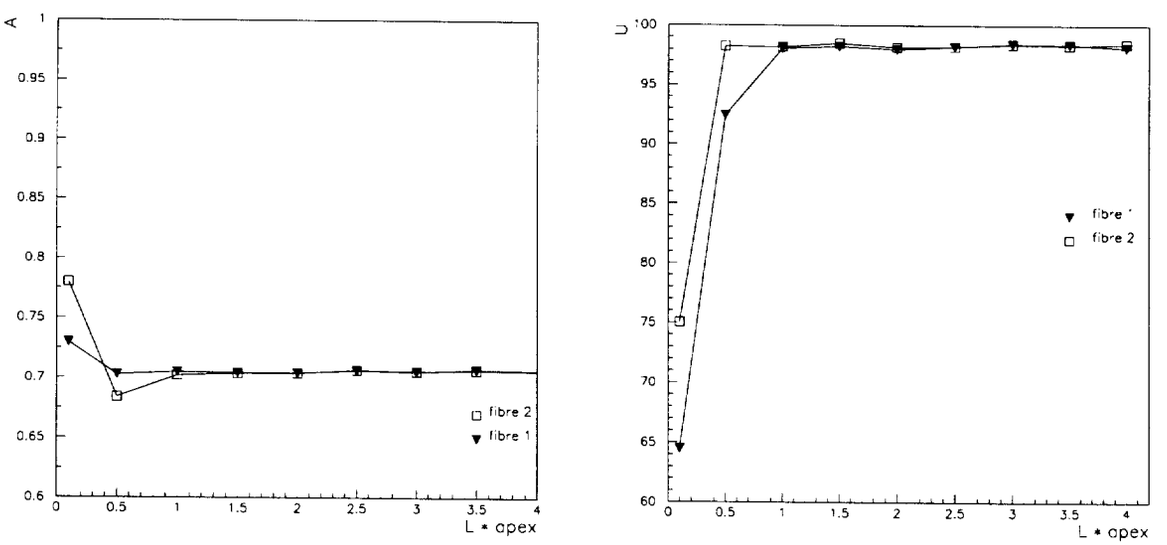


*Figure 31 : Monte Carlo results on the acceptance and uniformity of PMT response as a function of the mixer length. Left part of the figure shows the ratio (A) of photocathode light to incident light. Right part of the figure shows the uniformity (U) of illumination of the photocathode. The results are shown for fibres near (#1) or far (#2) from the center of the light mixer.*

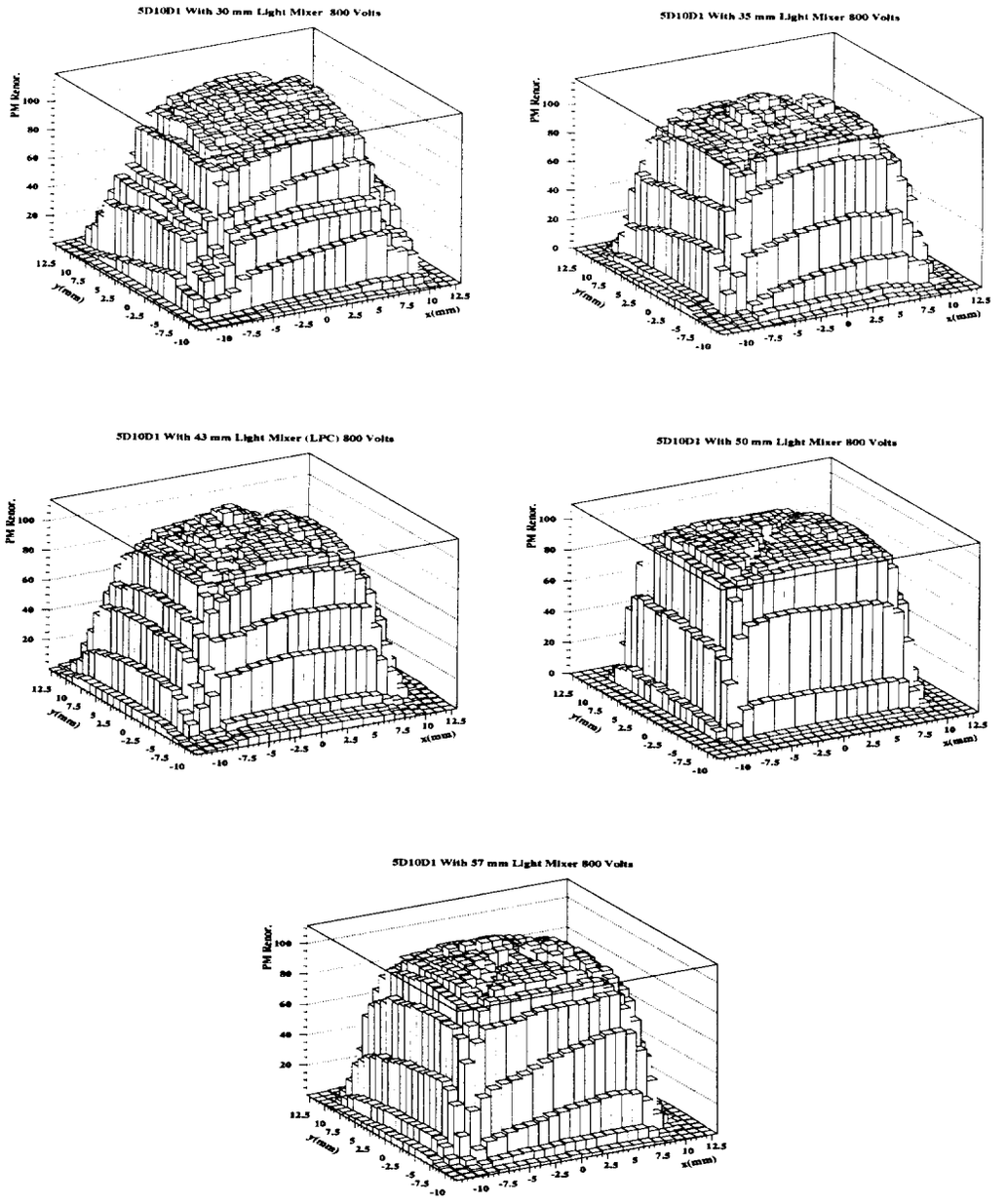


*Figures 32 : Variation of the PMT (#5D10D1) response, as a function of the x and y coordinates of a* $1 \times 1$ mm$^2$ *illuminated window of this PMT photocathode moving in front of the output face of the light mixer (the PMT is simply used as a spot photodetector). The signal of that spot photodetector after pedestal substraction is renormalised to the averaged response on a* $16 \times 16$ mm$^2$ *central square window on the output face of the light mixer. The length of the "light mixer" was 30 mm (top-left), 35 mm (top-right), 43 mm (middle-left), 50 mm (middle-right) and 57 mm (bottom).*

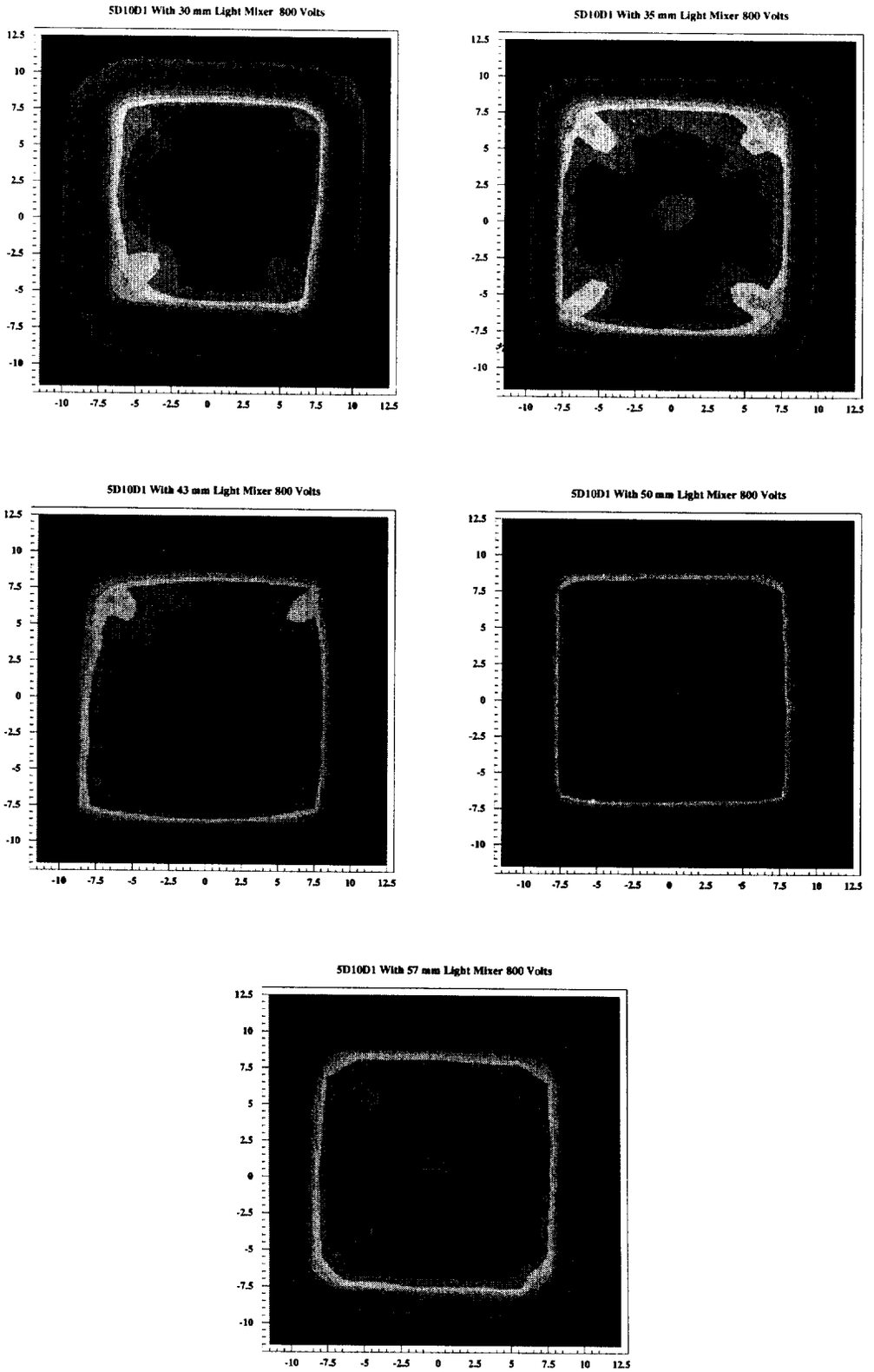


*Figure 33 : Same as on Figure (32) but with a level contour representation. Interference effects clearly grow-up when the "light mixer" length still increases.*

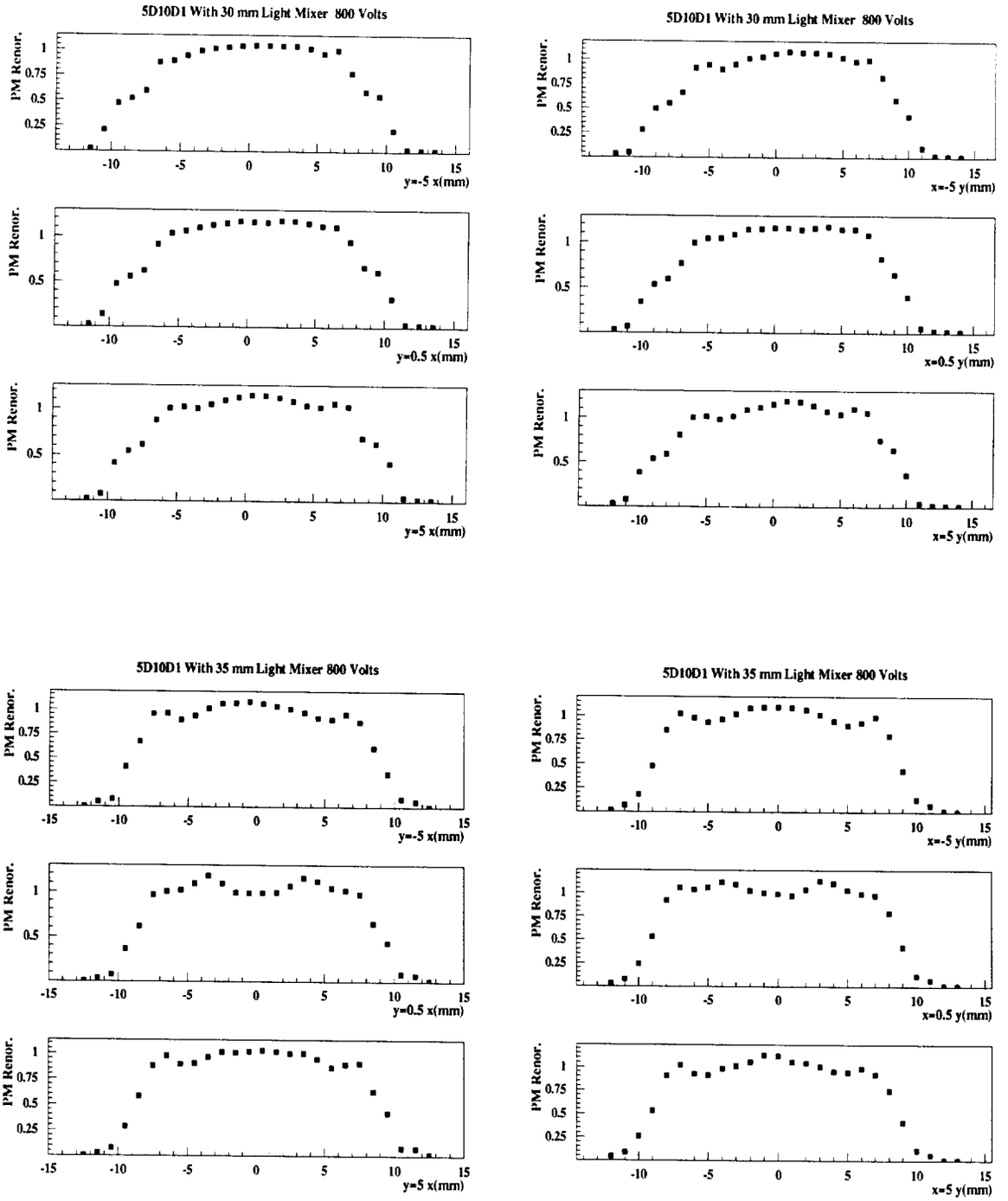


*Figure 34-a : Variation of the PMT (#5D10D1) response as a function of x (y) coordinate, and for different fixed values of the other coordinate. The signal after pedestal substraction is renormalised to the averaged response on a* $16 \times 16$ $mm^2$ *central square window on the output face of the light mixer. The length of the "light mixer" was 30 mm (top) and 35 mm (bottom).*

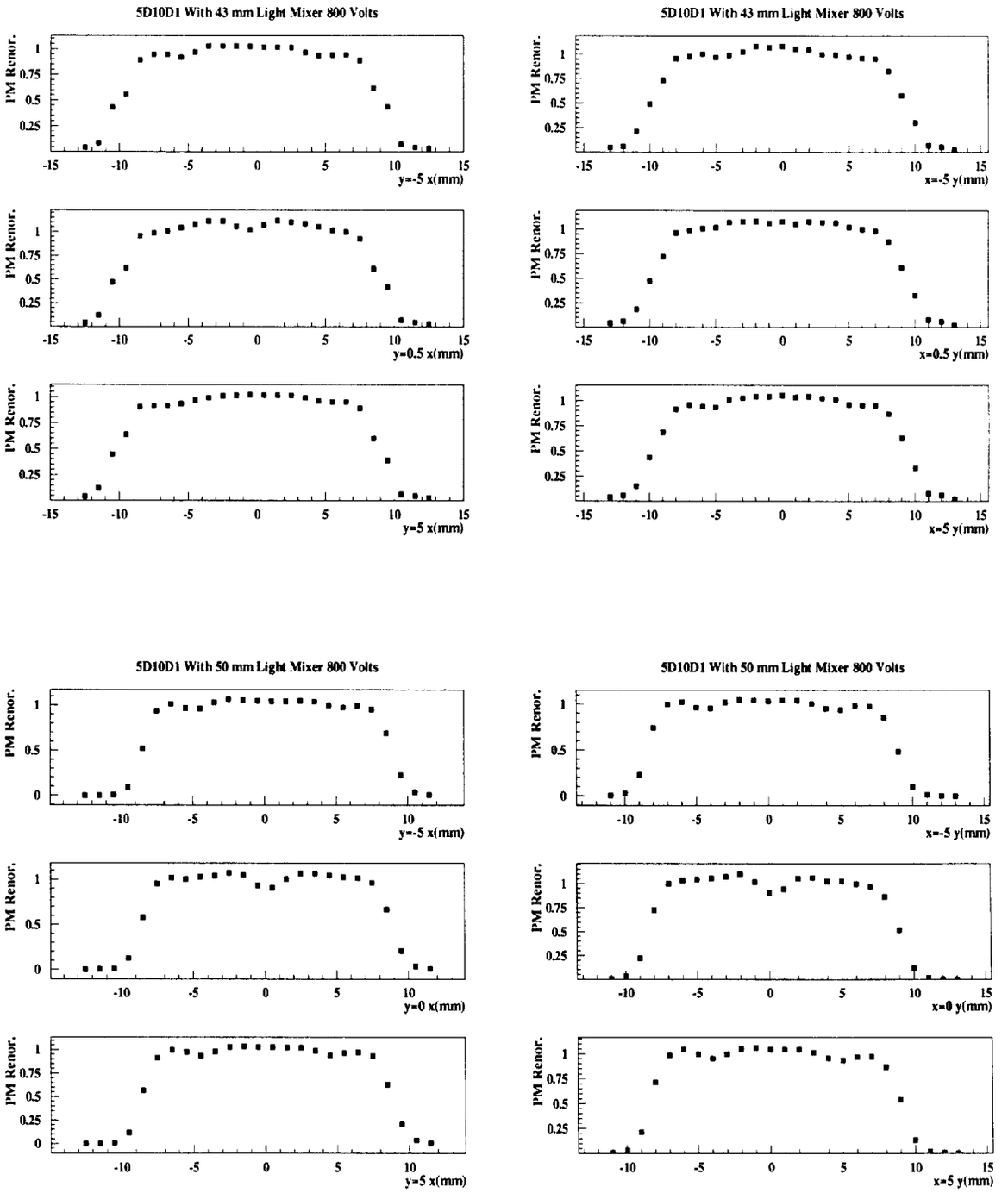


*Figure 34-b : Same as on Figure (34-a). The length of the "light mixer" was 43 mm (top) and 50 mm (bottom).*

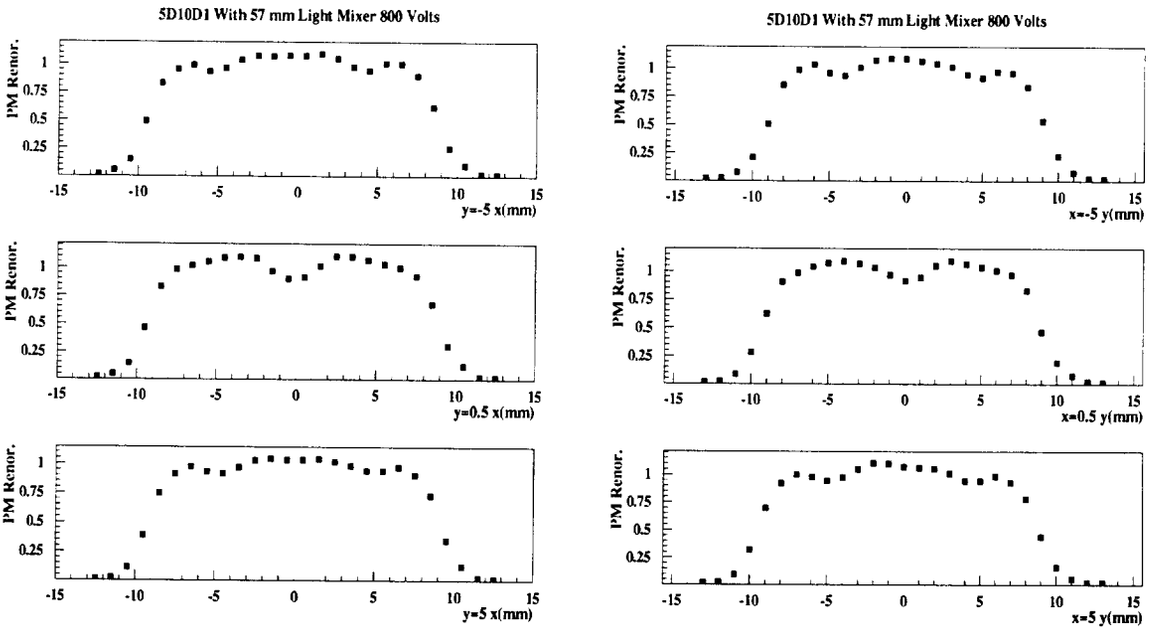


*Figure 34-c : Same as on Figure (34-a). The length of the "light mixer" was 57 mm.*

Figure (35) represents the light repartition at the 43 mm long "light mixer" output face, when the fiber points to the top left corner on the "light mixer" input face.

The corrective effect of the 43 mm long "light mixer" is demonstrated on the part a) of the Figure (36) that shows, for a typical PMT (#4L24D6), the spatial uniformity without (left) and with (right) the "light mixer". Now the "light mixer" is fixed to the PMT and the light spot position is moving at the input face of the "light mixer". Part b) of the Figure (36) represents the spatial uniformity without (top) and with (bottom) the "light mixer", as a function of the x (y) coordinate for 3 different fixed values of the other coordinate. The physical center position on the photocathode in our specific coordinate system corresponds to x = 2 mm and y =18 mm.

Once again, to be more quantitative, Figure (37) represents the distribution of the variation of the PMT response measured in a $16 \times 16$ scan. Table (4) finally summarizes the effects of the "light mixer". The maximum response ($Max(S)$) decreases from 732. down to 474. But the most significative value is the averaged value of the response ($< S >$)) which decreases from 511. to 449., i.e. by an amount of 13%. In addition, the dispersion on the $16 \times 16$ central effective window of the photocathode decreases from 17% to 3%.

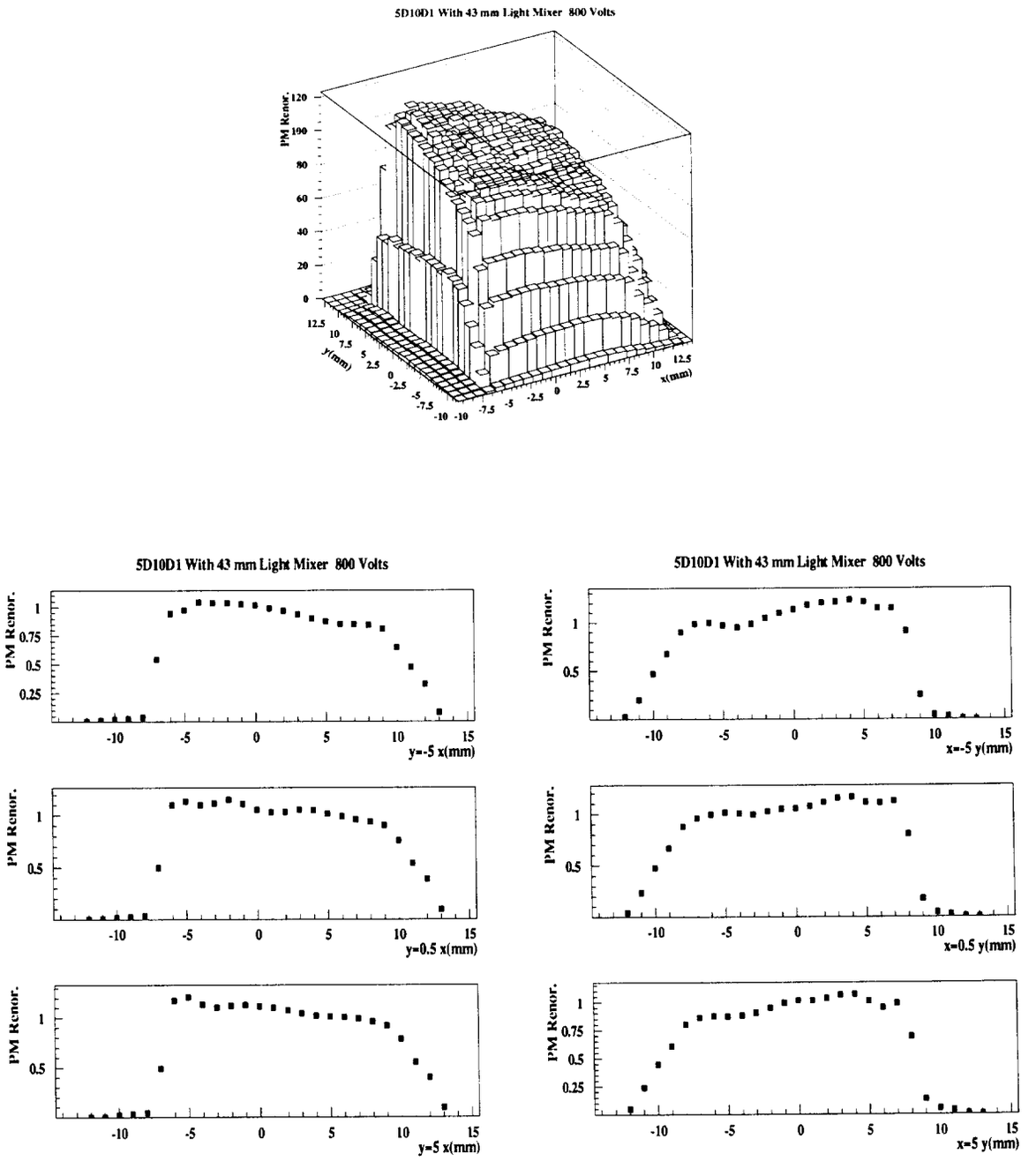


*Figure 35 : Variation of the PMT (#5D10D1) response, as a function of x and y coordinate of a* $1 \times 1$ mm$^2$ *illuminated window of this PMT photocathode moving in front of the output face of the light mixer (the PMT is simply used as a spot photodetector). The signal of that spot photodetector, after pedestal substraction is renormalised to the averaged response on a* $16 \times 16$ mm$^2$ *central square window on the output face of the "light mixer". The length of the "light mixer" was 43 mm, and the fiber points to the top left corner on the "light mixer" input face.*

| Configuration | $Max(S)$ | $< S >$ | $\sigma_S / < S >$ |
|---|---|---|---|
| Without Light Mix. | 732. | 511. | 0.168 |
| 43 mm Light Mix. | 474. | 449. | 0.026 |
| 35 mm Light Mix. | 483. | 445. | 0.042 |
| 30 mm Light Mix. | 505. | 459. | 0.054 |

*Table 4 : Maximum value, averaged value and resolution of a PMT response for three different lengths of the "light mixer".*

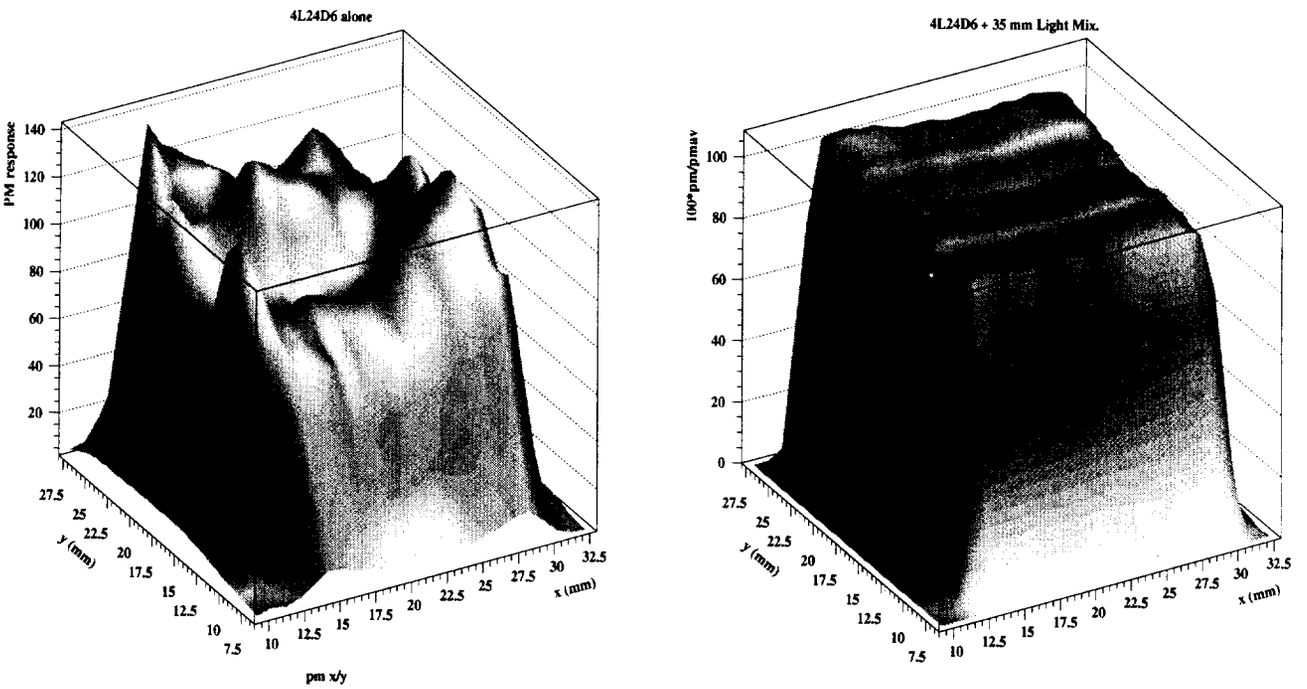


*Figure 36-a : Spatial uniformity for a typical PMT (#4L24D6), without (top-left) and with (top-right) a 43 mm long "light mixer". The signal after pedestal substraction is renormalised to the averaged response on a* $16 \times 16$ $mm^2$ *central square window on the output face of the "light mixer".*

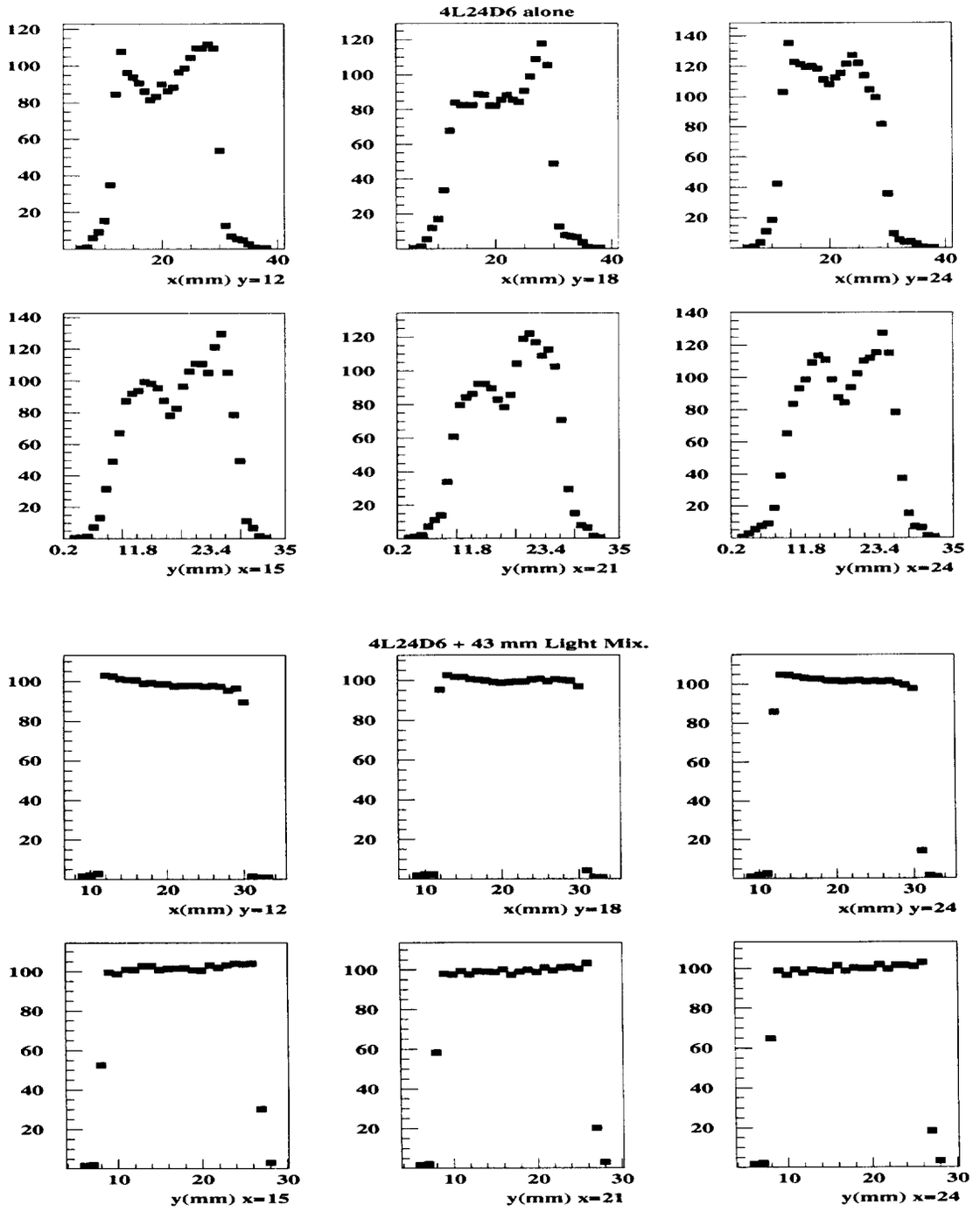


*Figure 36-b : Spatial uniformity for a typical PMT (#4L24D6), without (top-left) and with (top-right) a 43 mm long "light mixer", as a function of x (y) coordinate for 3 different fixed values of the other coordinate. The signal after pedestal substraction is renormalised to the averaged response on a* $16 \times 16$ $mm^2$ *central square window on the output face of the "light mixer".*

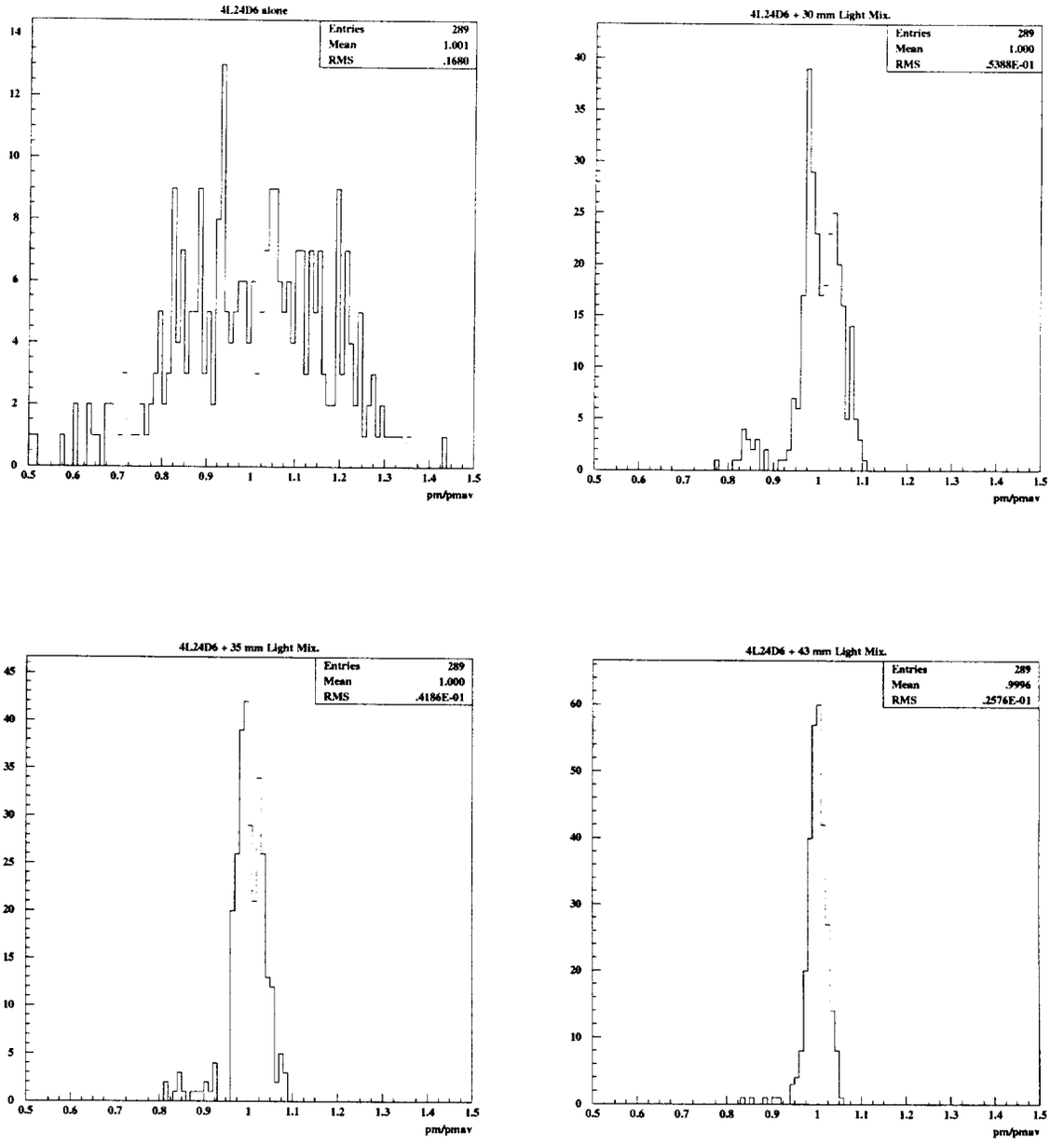


*Figure 37 : Distribution of the variation of the PMT (#4L24D6) response measured in a* $16 \times 16$ *scan of the PMT coupled without (top-left) and with a "light mixer". The length of the light mixer was 30 mm (top-right), 35 mm (bottom-left), 43 mm (bottom-right).*

# 4. Amplification

A high amplification together with a very low noise is the main characteristic of the photomultiplier. However, this amplification is very sensitive to the high voltage variation. That is why the knowledge of this dependence is primordial for the calorimeter cells calibration. For that task, one should be able to adjust very carrefully the PMT gain. But in fact, only the relative amplification dependence is needed: one increases/decreases the high voltage of $\delta$V so that the PMT amplification increases/decreases by $\delta G$.

On the other hand, as mentioned previously, the detector dynamics constraints to operate the PMT at some specific amplification with some specific high voltage repartition. To summarize one should be able to determine:

- an estimate of the amplification of the PMT as a function of the applied high voltage,

- an accurate determination of the variation of the PMT amplification like a function of the variation of the high voltage, i.e. the relative amplification.

Moreover, one should know some extra dependence on the PMT amplification like for example the effect of the voltage divider circuit, so that the final data would concern the whole PMT and divider assembly.

### 4.1 Statistics for a series of dynodes

The photoelectron current $I_{pk}$, emitted from the photocathode strikes the first dynode plane where secondary electrons are released. Then each of these secondary electrons are accelerated up to the second dynode plane, and multiplied again. So the primary photoelectron is multiplied in a cascade process from the first dynode, second dynode, ... up to the last dynode.

Let us assume that one electron impinging on the dynode $\#i$ releases, in average, $k_i$ secondaries with variance $\sigma^2_{k_i}$. The secondary emission ratio, $k_i$, is a function of the interdynode voltage. The output of the first dynode striking the second dynode produces an average gain, at the second stage, $\overline{m_2}$ with a variance $\sigma^2_{\overline{m2}}$.

Using cascade events statistics, the average gain and its variance may be related to the individual dynode statistics as follows:

$$\overline{m_2} = k_1 \times k_2 \tag{23}$$

and

$$\sigma^2_{\overline{m2}} = {k_2}^2 \sigma^2_{k_1} + k_1 \sigma^2_{k_2} \tag{24}$$

Using the same procedure up to the last stage, the gain and the fluctuations from the tenth stages are given by:

$$\overline{m_{10}} = \prod_{i=1}^{i=10} k_i \tag{25}$$

and

$$\sigma^2_{\overline{m_{10}}} = (\overline{m_{10}})^2 \times [\frac{\sigma^2_{k_1}}{k_1^2} + \frac{\sigma^2_{k_2}}{k_1 {k_2}^2} + ....\frac{\sigma^2_{k_{10}}}{(k_1 k_2 ....k_9)k_{10}^2}] \tag{26}$$

Equation (25) states the expected results: the total average gain for a series of $k$ dynodes is the product of the secondary emission yields of the individual dynodes in the series.

Equation (26) shows that the relative contribution of any state to the total fluctuation decreases with the proximity of the dynodes to the output end of the chain, i.e. the first stage contributes the most to the total variance. Moreover, the higher the first stage gain is, the less each subsequent stage contributes to the total variance. This property is an important feature and should be kept in mind when designing the PMT voltage divider configuration. Finally, the signal to noise ratio for the multiplier chain is given by:

$$\frac{\overline{m_{10}}}{\sigma_{\overline{m10}}} = [\frac{\sigma_1^2}{k_1^2} + \frac{\sigma_2^2}{k_1 k_2^2} + ....\frac{\sigma_{10}^2}{(k_1 k_2 ....k_9)k_{10}^2}]^{-1/2} \tag{27}$$

For large first stage gains, the multiplier signal-to-noise ratio is high, and most of the noise contribution comes from the first stages.

The anode current $I_a$ is given by the following equation:

$$I_a = I_{pk} \times k_1 \times k_2 \times ....k_{10} \tag{28}$$

Then:

$$\frac{I_a}{I_k} = k_1 \times k_2 \times ....k_{10} = \overline{m_{10}} \tag{29}$$

Let us calculate now $\sigma_{\overline{m_{10}}}$ in an isovoltage repartition where $k_i = k \; \forall i$. We also assume that the secondary emission follows the Poisson statistics:

$$\sigma^2_{k_i} = k_i \tag{30}$$

So that, equation (27) could be rewritten:

$$\frac{\overline{m_{10}}}{\sigma_{\overline{m10}}} = [\frac{k_1}{k_1^2} + \frac{k_2}{k_1 k_2^2} + \frac{k_{10}}{(k_1 k_2 ....k_9)k_{10}^2}]^{-1/2} \tag{31}$$

$$\frac{\overline{m_{10}}}{\sigma_{\overline{m10}}} = [\frac{1}{k_1} + \frac{1}{k_1 k_2} + \frac{1}{(k_1 k_2 ....k_{10})}]^{-1/2} \tag{32}$$

The signal-to-noise ratio of the multiplier is then:

$$\left(\frac{\sigma_{\overline{m10}}}{\overline{m_{10}}}\right)^2 = \frac{1}{k_1} + \frac{1}{k_1 k_2} + \frac{1}{(k_1 k_2 .... k_{10})} \tag{33}$$

In the case of the isovoltage repartition, the expression becomes:

$$\frac{1}{k} + \frac{1}{k^2} + \frac{1}{k^{10}} = \left(\frac{1}{k^{10}}\right)[1 + k + k^2 ... + k^9]$$

Equation (33) is now:

$$\sigma^2_{\overline{m_{10}}} = \frac{\overline{m_{10}}^2}{(k-1)} \times (1 - \frac{1}{k^{10}}) \tag{34}$$

Defining $F$ as the noise factor:

$$\sigma^2_{\overline{m_{10}}} = \overline{m_{10}}^2 \times F \tag{35}$$

where $F$ is:

$$F = \left(\frac{1}{k-1}\right)\left(1 - \frac{1}{k^{10}}\right) \tag{36}$$

Up to now only the noise contributions from the multiplier chain were considered. These results can be combined with the photocathode noise contribution in order to obtain the signal-to-noise ratio for the photomultiplier as a whole.

The average number of photoelectrons, after conversion, from the photocathode in a time $\tau$ is given by:

$$N_{p.e.} = \eta . N_\gamma \tag{37}$$

where $\eta$ is the quantum efficiency, and $N_\gamma$ is the mean number of photons impinging the photocathode. The variance of $N_{p.e.}$ is given by:

$$\sigma^2_{N_{p.e.}} = \eta . \sigma^2_{N_\gamma} \tag{38}$$

Using these expressions to describe the input to the photomultiplier chain, the average number of electrons collected at the anode can be stated as follows:

$$N_a = \eta . N_\gamma . \overline{m_{10}} = N_{p.e.} . \overline{m_{10}} \tag{39}$$

where $\overline{m_{10}}$ is given by equation (25). The variance for the output electron stream is calculated, considering that photoconversion and multiplication are cascade events and so given by:

$$\sigma^2_{N_a} = \overline{m_{10}}^2 . \sigma^2_{N_{p.e.}} + N_{p.e.} . \sigma^2_{\overline{m_{10}}} = \overline{m_{10}}^2 . \eta . \sigma^2_{N_\gamma} + \eta . N_\gamma . \sigma^2_{m_{10}}$$

where $\sigma^2_{\overline{m10}}$ is given by equation (26), and we assume that:

$$\begin{aligned} \sigma^2_{N_\gamma} &= N_\gamma \\ \sigma^2_{N_a} &= (\overline{m_{10}}^2).\eta.N_\gamma + \eta.N_\gamma.\sigma^2_{\overline{m_{10}}} \end{aligned} \tag{40}$$

Equation (40) can be rearranged as follows:

$$\sigma^2_{N_a} = N_{p.e}(\overline{m_{10}}^2 + \sigma^2_{\overline{m_{10}}}) = N_{p.e}\overline{m_{10}}^2(1+F) \tag{41}$$

together with:

$$N_a = N_{p.e}\overline{m_{10}} \tag{42}$$

The signal-to-noise ratio at the anode is:

$$\left(\frac{\sigma_{N_a}}{N_a}\right)^2 = \frac{N_{p.e}\ \overline{m_{10}}\ (1+F)}{N^2_{p.e}\ \overline{m_{10}}^2} = \frac{(1+F)}{N_{p.e}} \tag{43}$$

Finally:

$$\left(\frac{N_a}{\sigma_{N_a}}\right)^2 = N_{p.e} \times \frac{1}{1+F} \tag{44}$$

For an isovoltage repartition with an equal interdynode amplification in the multiplier chain, and neglecting the $1/k^{10}$ in equation (36), we have:

$$\left(\frac{N_a}{\sigma_{N_a}}\right)^2 = N_{p.e} \times \left(1 - \frac{1}{k}\right) \tag{46}$$

For high gain dynodes exhibiting the Poisson statistics, the signal to noise ratio at the anode is therefore given by:

$$SNR_a = \left(\frac{N_a}{\sigma_{N_a}}\right) = \sqrt{N_{p.e.}} \tag{47}$$

### 4.2 Measurement of the PMT amplification

The determination of the gain of a PMT is not an easy operation. As claimed above, it is very important to have an estimation of the HV that we should apply before any calibration on each PMT with an amplification close to $10^5$. In the following we will use three different methods for the measurement of the amplification of the PMT: a DC current method, a "one photoelectron" mode method, and a pulsed mode method. After the description of these three methods, we will compare their results for some PMTs of the generation #2.

• **DC current method**

One calculates the PMT amplification using a two steps measurement, from the ratio of the anode luminous sensitivity to the cathode luminous sensitivity. But in order to determine the cathode or the anode luminous sensitivity, as shown in expression (1), one should know exactly the light flux intensity. Nevertheless, it does not care whether it is assumed that the PMT is operating with a constant light source (true on a short time scale). Using this assumption, the photocathode current ($I_{pk}$) is equal to:

$$I_{pk}(v) = L \times S_{pk}(v) \tag{47}$$

where $L$ is the light flux, $S_{pk}$ the photocathode luminous sensitivity measured with the voltage $v$ between the photocathode and the first dynode.

With a complete voltage divider configuration, and the same light flux, the anode current is:

$$I_a(V) = G \times I_{pk}(v) = L \times S_a(V) \tag{48}$$

where $G$ represents the PMT amplification, and $S_a$ the anode luminous sensitivity with the overall voltage $V$. Moreover, if $v$ is the voltage equivalent to the one which is applied between the photocathode and the first dynode in the complete configuration:

$$G = \frac{S_a(V)}{S_{pk}(v)} = \frac{I_a(V)/L}{I_{pk}(v)/L} = \frac{I_a(V)}{I_{pk}(v)} \tag{49}$$

To prevent a too high anode current (10 nA $\times$ $10^5$ = 1000$\mu$A), we decrease the light flux by operating with a neutral filter of known attenuation ($T_a$ between 500 and 1000). Then:

$$G = \frac{T_a \times I_a(V)}{I_{pk}(v)} \tag{50}$$

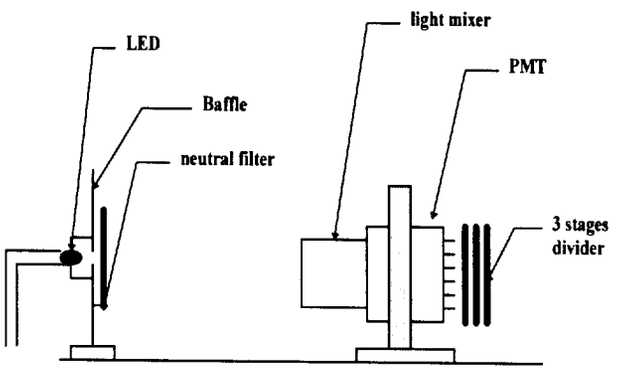


*Figure 38: Experimental set-up used for the amplification measurement. This measurement is achieved in a two steps procedure using the "three-stages" dividers.*

As shown on Figure (38), all the measurements are done with a light mixer in front of the PMT and a baffle to avoid the light reflection problems. The voltage divider was specific to that measurement ("three-stages" divider). Its main characteristic was that it consists of 3 parts. Plugging part #1 and #2, one obtains the configuration shown on Figure (38). Adding part #3 results in the normal voltage divider configuration with the high voltage repartition.

This method has been used many times and especially to the set of 15 R5900 tested in Clermont previously to their use in Module 0. The amplification curves are shown on Figure (39). These results indicate that a PMT amplification of $10^5$ is achieved with a PMT applied voltage in the range 650 to 725 Volts. The measurements were performed with the same voltage divider, so the variations in the set of PMTs are mainly due to the PMT characteristics.

**• "One photoelectron" method**

The PMT absolute gain could also be measured, at least for some values of the HV, using the "one photoelectron" mode. In that specific mode, one assumes that the mean number of photoelectrons, after conversion in the photocathode and before multiplication, is less than 1. Considering one event with $N_{p.e.}$ photoelectrons, the charge at the PMT anode in Coulomb is:

$$Q(C) \;=\; N_{p.e.} \times G \times 1.6 \times 10^{-19} \tag{51}$$

The main limitation of the method is that, in order to get the charge above the noise, the gain of the PMT should be very high, and the PMT noise should be very low. Moreover, it is obvious that the photoelectron collection efficiency is also a factor of limitation with such a low number of photons. That is why the accuracy of this method is limited, nevertheless it could be a useful cross-check of the other methods.

The experimental difficulty is first to achieve a light source delivering for each event a limited number of photons. This experimental set-up is shown on Figure (40). The light flux impinging on the light mixer is adjusted within the distance of the light source. The PMT signal is converted by a charge ADC [5] with a 12 bits dynamic range and a sensitivity of $50fC$/counts. The PMT is equiped with a 43x18x18 mm$^3$ light mixer, and a baffle to avoid any light reflection problems. A LED is used as a pulsed light source with a diffuser to reduce the light flux. The PMT is operated with an equilibrate voltage repartition, i.e. the 1:1:1:...1:1:1 configuration.

Assuming that one defines a position corresponding to a very low photon flux intensity, one should verify that the recorded charge peak corresponds really to $N_{p.e.}$ =1. In fact, the probability distribution function of photoelectrons is a Poisson distribution function: some events corresponds to $N_{p.e.} = 0$, and some others correspond to $N_{p.e.} \geq 1$. If the main recorded peak corresponds to $N_{p.e.} = N > 1$, increasing the distance induces a lower light flux and consequently reduces the ratio of events with $N_{p.e.} = N$. By this way the peak will move to another channel corresponding to $N_{p.e.} = N' \leq N$.

[5] LECROY 1182

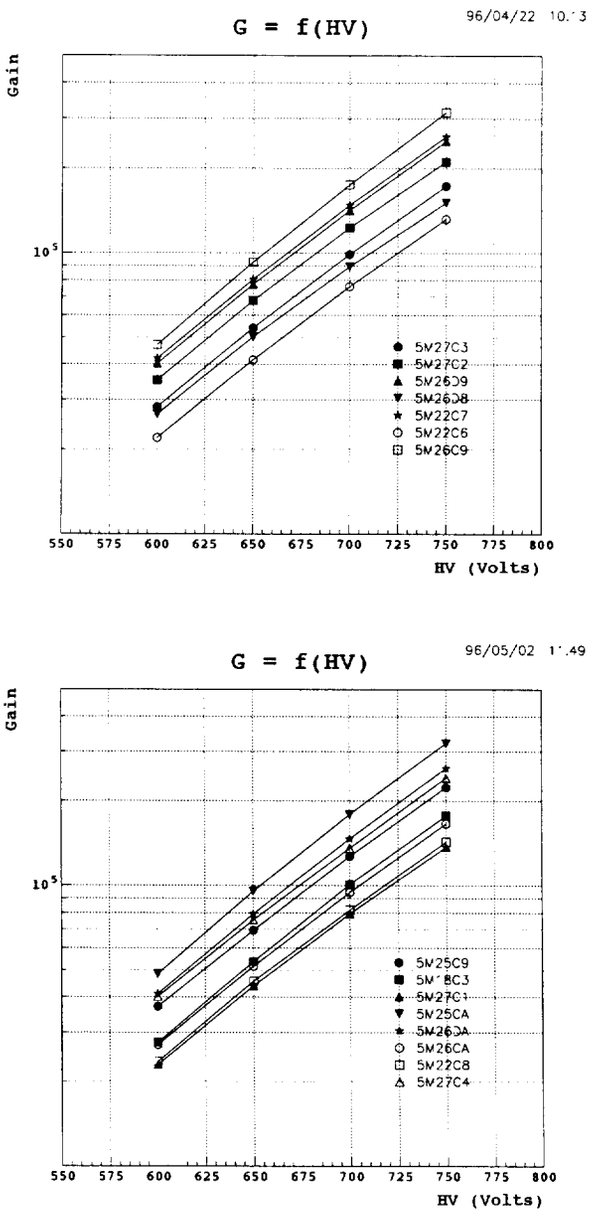


*Figure 39: Amplification of the set of 15 R5900 tested in Clermont previously to their use in Module 0, and determined using the "three-stages" divider with a 2.5:2.5:1:1-1:1:2.5:2.5 configuration.*

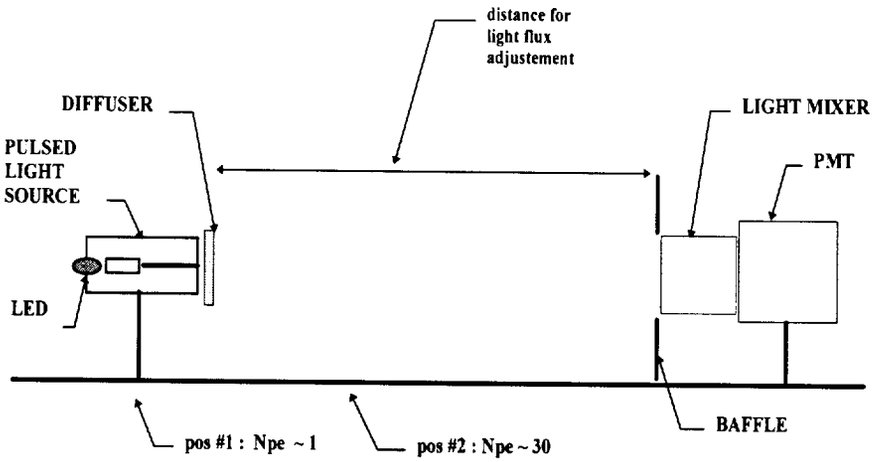


*Figure 40: Experimental set-up used for one photoelectron mode. A LED is used as pulsed light source with a diffusor to reduce the light flux. Moreover, this flux is adjusted within the distance of the light source. The PMT is equiped with a* $43 \times 18 \times 18$ $mm^3$ *light mixer and a baffle to avoid any light reflection problems.*

On the other hand, if the main peak corresponds to $N_{p.e.} = 1$, increasing the distance will only increase the fraction of event with $N_{p.e.} = 0$, so that the main peak will decrease in amplitude but will stay at the same channel. Repeating the measurements for different values of the PMT voltage establishes some calibration, i.e., the channel number of the one photoelectron peak for the different values of the voltage.

The experimental spectra are fitted with the following expression:

$$F(x') = \alpha_7 \, exp^{(-\alpha_8 x')} + \sum_{j=1}^{j=4} \frac{\alpha_j}{\sqrt{2\pi j \alpha_5}} exp^{-\frac{(x'-j\alpha_6)^2}{2j\alpha_5}} \qquad (52)$$

where $x'$ is the pedestal substracted ADC channel. The $N_{p.e.} = 1$ contribution channel is defined by the fitted parameter $\alpha_6$.

Figure (41) shows the experimental spectra, together with the results of the fit, for the PMT #5D10D1 (generation #2) at 3 different PMT voltage values: 900, 800 and 750 Volts.

In the configuration using the 1:1:1:...1:1:1 repartition the interdynode gain $k$ should be the same at each stage. So using measured data in "one photoelectron" mode, we calculate the values of the PMT overall gain, interstage gain $k$ and corresponding interstage voltage $V_d$ equal to HV/11 for the 1:1:1...1:1:1 configuration.

Such a calibration is impossible for too low values of the PMT voltage (less than 850 Volts). Nevertheless one could define a second position (#2) corresponding to a larger number of photoelectrons (at least $N_{p.e.} \sim 30$). It is possible to estimate the mean $N_{p.e.}$ in this position #2 from spectra recorded in that position at some high value of the

PMT voltage, and using the position #1 peak position at this same PMT voltage to calibrate the position #2 peak.

Figure (42) shows the experimental spectra recorded in position #2, together with the results of the fit, for this same PMT, at 4 different PMT voltage values: 1000, 950 900 and 850 Volts.

Moreover, the signal-to-noise ratio at the anode output of an ideal equal interdynode gain PMT is given by the expression (46). Using this expression and the measured data, we could have an other indication of the mean number of photoelectron in position #2.

These two different estimations of the photoelectron number are indicated in Table (5) for the different values of the PMT voltage: $N'_{p.e.}$ corresponds to the position #2 estimated from the position #1 measured at same voltage. $N''_{p.e.}$ corresponds to $N_{p.e.}$ estimated from fitted spectra in the position #2 and equation (46).

At sufficient high values of the PMT voltage, $N_{p.e.}$ should be constant. However, it could be first affected by the uncertainty from the method, especially in the position #1 measurement. Besides, when increasing too much the high voltage (950 Volts), the PMT extra noise from the effect of the too high electric fields inside the multiplier disturbs the simple relation between the anode signal and $N_{p.e.}$.

From the averaged value of $N_{p.e.}$ (=32) estimated previously in position #2 at some high values of the PMT voltage, one could calculate for the fitted spectra on the whole range of PMT voltage, the overall gain $G$, the interdynode gain $k$ corresponding to the interdynode $V_d$, and $N_{p.e}$ given directly from equation (46). This last value is quite constant above 700 Volts, indicating by the way, that the PMT efficiency is almost achieved for this value of the voltage. All these data are sumarized in Table (6).

| HV | $G$ | $k$ | $V_d$ | $N'_{p.e}$ | $N''_{p.e}$ |
|---|---|---|---|---|---|
| 950 | $1.33 \times 10^7$ | 5.16 | 86.36 | 34.6 | 32.26 |
| 900 | $1.00 \times 10^6$ | 5.01 | 81.82 | 31.8 | 32.19 |
| 800 | $4.20 \times 10^6$ | 4.61 | 72.73 | 31. | 31.76 |
| 750 | $2.80 \times 10^6$ | 4.41 | 68.18 | 27.1 | 29.9 |

*Table 5 : Results of measurements using fitted spectra in position #1 for PMT # 5D10D1. G is the estimated gain in the isovoltage repartition, k is the corresponding interdynode amplification. $N'_{p.e.}$ and $N''_{p.e.}$ are the two different estimations of $N_{p.e.}$: $N'_{p.e.}$ corresponds to position #2 calibrated from position #1 measured at same voltage, $N''_{p.e.}$ corresponds to $N_{p.e.}$ estimated directly from fitted spectra in position #2 and equation (46).*

| HV | $G$ | $k$ | $V_d$ | $N''_{p.e}$ |
|---|---|---|---|---|
| 1000 | $1.98 \times 10^7$ | 5.366 | 90.91 | 31.96 |
| 950 | $1.44 \times 10^7$ | 5.198 | 86.36 | 32.05 |
| 900 | $1.0 \times 10^7$ | 5.012 | 81.82 | 31.07 |
| 850 | $6.60 \times 10^6$ | 4.807 | 77.27 | 30.63 |
| 800 | $4.07 \times 10^6$ | 4.581 | 72.73 | 30.5 |
| 750 | $2.38 \times 10^6$ | 4.341 | 68.18 | 30.05 |
| 700 | $1.31 \times 10^6$ | 4.09 | 63.64 | 30.8 |
| 650 | $6.84 \times 10^5$ | 3.833 | 59.09 | 29.30 |

*Table 6 : Variation of the PMT # 5D10D1 gain G, estimated from position #2 illumination and assuming* $< N_{p.e.} >= 32$. *Last column indicates the estimation of* $N_{p.e.}$ *using directly fitted spectra in position #2 with equation (46). For HV above 700 Volts,* $N''_{p.e.}$ *is almost constant, indicating that the PMT efficiency is achieved. Above 900 Volts,* $N''_{p.e.}$ *increases again.*

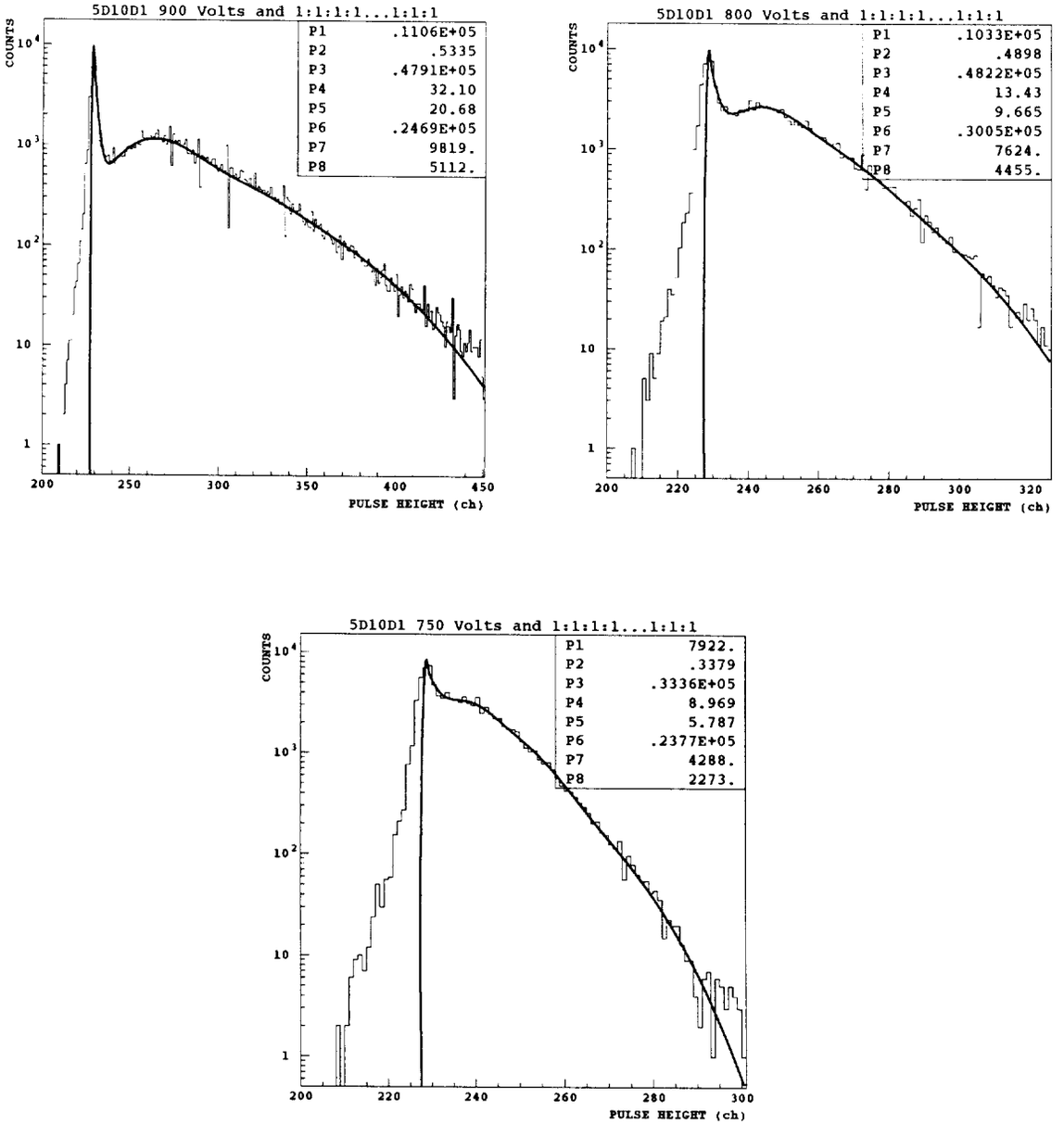


*Figure 41 : One photoelectron spectra of PMT #5D10D1, with light illumination in position #1 corresponding to $N_{p.e.} = 1$. The photoelectron spectra is fitted with expression (52). PMT HV is 900 Volts, 800 Volts and 750 Volts. The parameter $P_4$ of the fit corresponds to the one photoelectron contribution to the spectra (parameter $\alpha_6$ in expression (52)).*

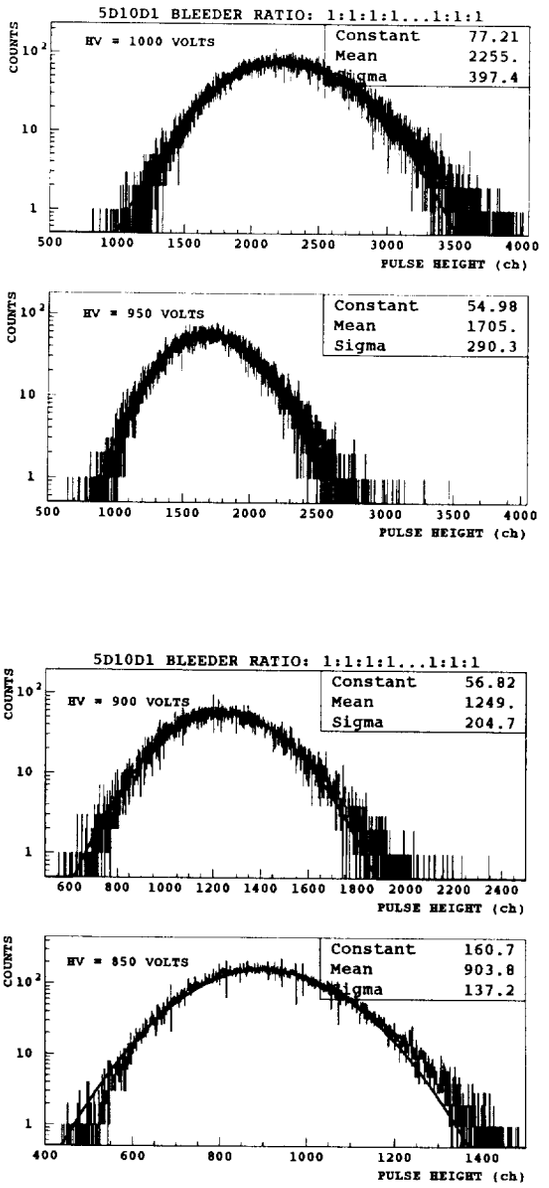


*Figure 42 : Spectra of PMT #5D10D1, with light illumination in position #2 corresponding to some tens of photoelectrons, and for different HVs: 1000 Volts, 950 Volts, 900 Volts and 850 Volts.*

Using the previous estimated values of the interstage gain $k$ , the variation of $k$ as a function of $V_d$, could be fitted in the range of $V_d$ from 700 Volts up to 900 Volts (which corresponds to a rather constant extracted values of the number of photoelectrons). One obtains:

$$k = -0.378910^{-3} V^2 + 0.1053 V - 1.073 \quad (53)$$

In order to cross-check the validity of the $k$ parametrisation, experimental measurements had been also performed at different HV values and for the same PMT (#5D10D1), but with a different high voltage repartition: 1.5:1.5:1.5:...1.2:1.5:1.8. Figure (43) shows some of the measured spectra with this new voltage repartition.

Table (7) indicates what are the interdynode voltages with this configuration ($HV = 14V_d$) and for the various HV values. Using the parametrisation of the interdynode gain $k$ as a function of $V_d$ given by equation (53), one calculates the corresponding interdynode gain $k$ for each dynode.

Finally using the estimated $k$, we could obtain the overall PMT gain $G$, for each HV value. In Table (8), these predicted values of $G$ are compared with the experimental one for the 1.5:1.5:1.5:...1.2:1.5:1.8 configuration. The experimental values for the 1.5:1.5:1.5:...1.2:1.5:1.8 configuration are determined, applying the same method like above, i.e. position #2 peak calibrated from position #1 measurements.

| HV repartition with 1.5:1.5:1.5:...1.2:1.5:1.8 | | | | | | | | | | | |
|---|---|---|---|---|---|---|---|---|---|---|---|
| HV | D1 | D2 | D3 | D4 | D5 | D6 | D7 | D8 | D9 | D10 | A |
| (Volts) | $k_1$ | $k_2$ | $k_3$ | $k_4$ | $k_5$ | $k_6$ | $k_7$ | $k_8$ | $k_9$ | $k_10$ | |
| 1000 | 107.1 | 107.1 | 107.1 | 71.4 | 71.4 | 71.4 | 71.4 | 71.4 | 85.7 | 107.1 | 128.6 |
| | 5.86 | 5.86 | 5.86 | 4.51 | 4.51 | 4.51 | 4.51 | 4.51 | 5.17 | 5.86 | |
| 900 | 96.4 | 96.4 | 96.4 | 64.3 | 64.3 | 64.3 | 64.3 | 64.3 | 77.1 | 96.4 | 115.7 |
| | 5.56 | 5.56 | 5.56 | 4.13 | 4.13 | 4.13 | 4.13 | 4.13 | 4.79 | 5.56 | |
| 800 | 85.7 | 85.7 | 85.7 | 57.1 | 57.1 | 57.1 | 57.1 | 57.1 | 68.57 | 85.7 | 102.9 |
| | 5.17 | 5.17 | 5.17 | 3.70 | 3.70 | 3.70 | 3.70 | 3.70 | 4.37 | 5.17 | |
| 700 | 75. | 75. | 75. | 50. | 50. | 50. | 50. | 50. | 60. | 75. | 90. |
| | 4.69 | 4.69 | 4.69 | 3.25 | 3.25 | 3.25 | 3.25 | 3.25 | 3.88 | 4.69 | |
| 600 | 64.3 | 64.3 | 64.3 | 42.9 | 42.9 | 42.9 | 42.9 | 42.9 | 51.43 | 64.3 | 77.1 |
| | 4.13 | 4.13 | 4.13 | 2.75 | 2.75 | 2.75 | 2.75 | 2.75 | 3.34 | 4.13 | |

*Table 7 : Interdynode voltage for PMT #5D10D1 with the 1.5:1.5:1.5:...1.2:1.5:1.8 voltage repartition, and corresponding $k_i$ calculated from (53).*

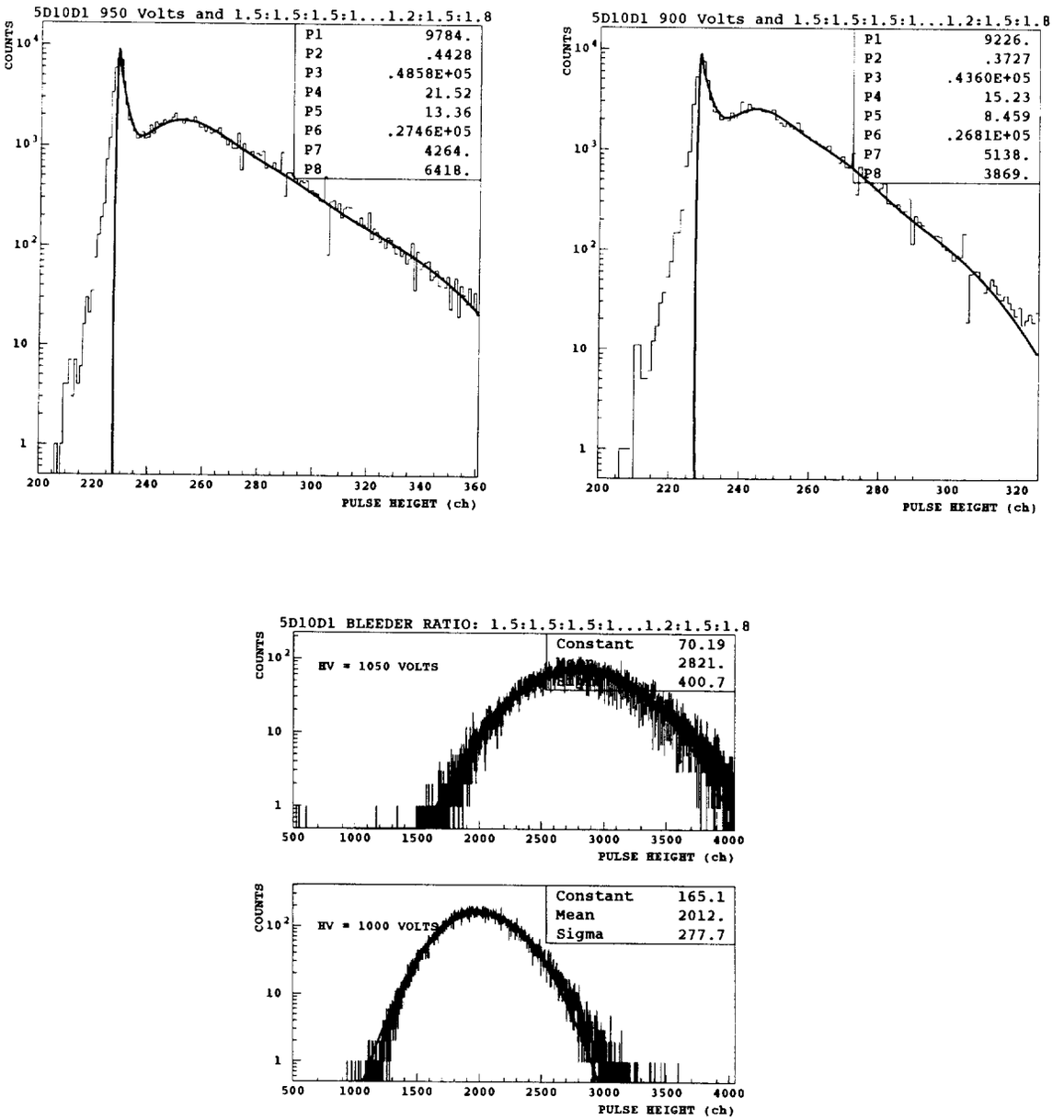


*Figure 43 : Spectra with light illumination in position #1 (top) and #2 (bottom). The HVs are 950 Volts and 900 Volts with repartition 1.5:1.5:1.5:...1.2:1.5:1.8.*

| HV ($Volts$) | Predicted $G$ | Measured $G$ | $R$ |
|---|---|---|---|
| 1000 | $1.1410^7$ | $1.3010^7$ | 0.87 |
| 950 | $8.1010^6$ | $8.5510^6$ | 0.95 |
| 900 | $5.5010^6$ | $5.5110^6$ | 1.00 |
| 850 | $3.5610^6$ | $3.5010^6$ | 1.02 |
| 800 | $2.1810^6$ | $2.0210^6$ | 1.08 |
| 750 | $1.2610^6$ | $1.1610^6$ | 1.09 |
| 700 | $6.8010^5$ | $6.2510^6$ | 1.09 |

*Table 8 : Comparison between the measured PMT (#5D10D1) amplification and the estimated one in the 1.5:1.5:1.5:...1.2:1.5:1.8 voltage repartition, using the interdynode amplification $k_i$ estimated from equation (54). R is the ratio of the predicted G to the measured one. Its averaged value is 1.01, with a dispersion of 8%.*

| PMT # | DC method | 1 p.e. method | $R$ |
|---|---|---|---|
| 5D10D4 | $3.11 \times 10^6$ | $2.51 \times 10^6$ | 1.24 |
| 5D07F2 | $1.76 \times 10^6$ | $1.65 \times 10^6$ | 1.07 |
| 5D12D1 | $2.54 \times 10^6$ | $2.41 \times 10^6$ | 1.05 |
| 5D12D3 | $3.88 \times 10^6$ | $3.13 \times 10^6$ | 1.25 |
| 5D11D3 | $1.71 \times 10^6$ | $1.87 \times 10^6$ | 0.91 |
| 5D06F3 | $2.16 \times 10^6$ | $2.26 \times 10^6$ | 0.96 |
| 5D10D1 | $2.97 \times 10^6$ | $2.81 \times 10^6$ | 1.06 |

*Table 9 : Comparison between the measured amplification of some PMTs of generation #2 with the two methods: the DC method and the "one photoelectron" method. The voltage repartition is 1.5:1.5:1.5:...1.2:1.5:1.8 and the applied voltage is 800 Volts. The averaged ratio (R) of the two estimations is 1.08 with a dispersion of* 12%.

As a conclusion, we compare in Table (9) the PMT amplification measurements using the two methods, for some PMTs of generation #2:

- The "one photoelectron" method allows first to estimate the amplification of the PMT only for the high range of the HV.

- The "one photoelectron" method is not a so accurate method since it is strongly disturbed by PMT or electronics noise which increases with the HV.

- Nevertheless, the "one photoelectron" method allows to cross-check, in an absolute way, the other estimations of the PMT amplification for some values of the HV.

- Moreover, "one photoelectron" spectra could give other indications on the PMT characteristics in the use of some more sophisticated expressions for the fit of the "one photoelectron" spectra; especially when using the Polya parametrisation for the secondaries statistics.

- The DC method is also not so safe since the measurement strongly depends on the quality of the experimental setup, particularly in the accurate determination of the neutral filter attenuation. The accuracy of that method is roughly 30%.

- The determination of the variation of the interdynode amplification as a function of the interdynode voltage allows to calculate the noise factor $F$.

**• Pulsed mode**

An estimation of the PMT amplification could also be achieved in a pulsed mode from the statistics of the PMT signal. This is done usually using the distribution of the anode signal, i. e., the signal-to-noise ratio at PMT anode. This method is derived from equation (46), in a simple form, since the charge measured by the ADC (in channels) is proportional to $N_a$. When the following assumptions are fullfilled:

- The electronic induced noise is very low so that the ADC does not increase the signal-to-noise ratio. Otherwise, the pedestal noise could disturb the efficiency of the method especially when measuring a low voltage amplification.

- The noise factor ($F$) is not taken into account.

The number of photoelectrons can be estimated,

$$N_{p.e.} = \left( \frac{< M > - Ped}{\sigma} \right)^2 \tag{54}$$

where $< M >$ ($\sigma^2$) is the mean (variance) of the ADC distribution, and $Ped$ is the ADC pedestal. Knowing the number of photoelectrons, the gain $G$ of the PMT is directly obtained from the PMT output charge $Q$ using:

$$N_{pe} \times G \times 1.6 \times 10^{-19} = Q \tag{55}$$

Figure (44) represents the variation of the gain versus the PMT applied voltage for 6 of the R5900 used in Module 0. The systematic uncertainty on the experimental determination of $N_{pe}$ is of the order of 2%, and the incertainty on $Q$ measurement due to the ADC is of the order of 4%

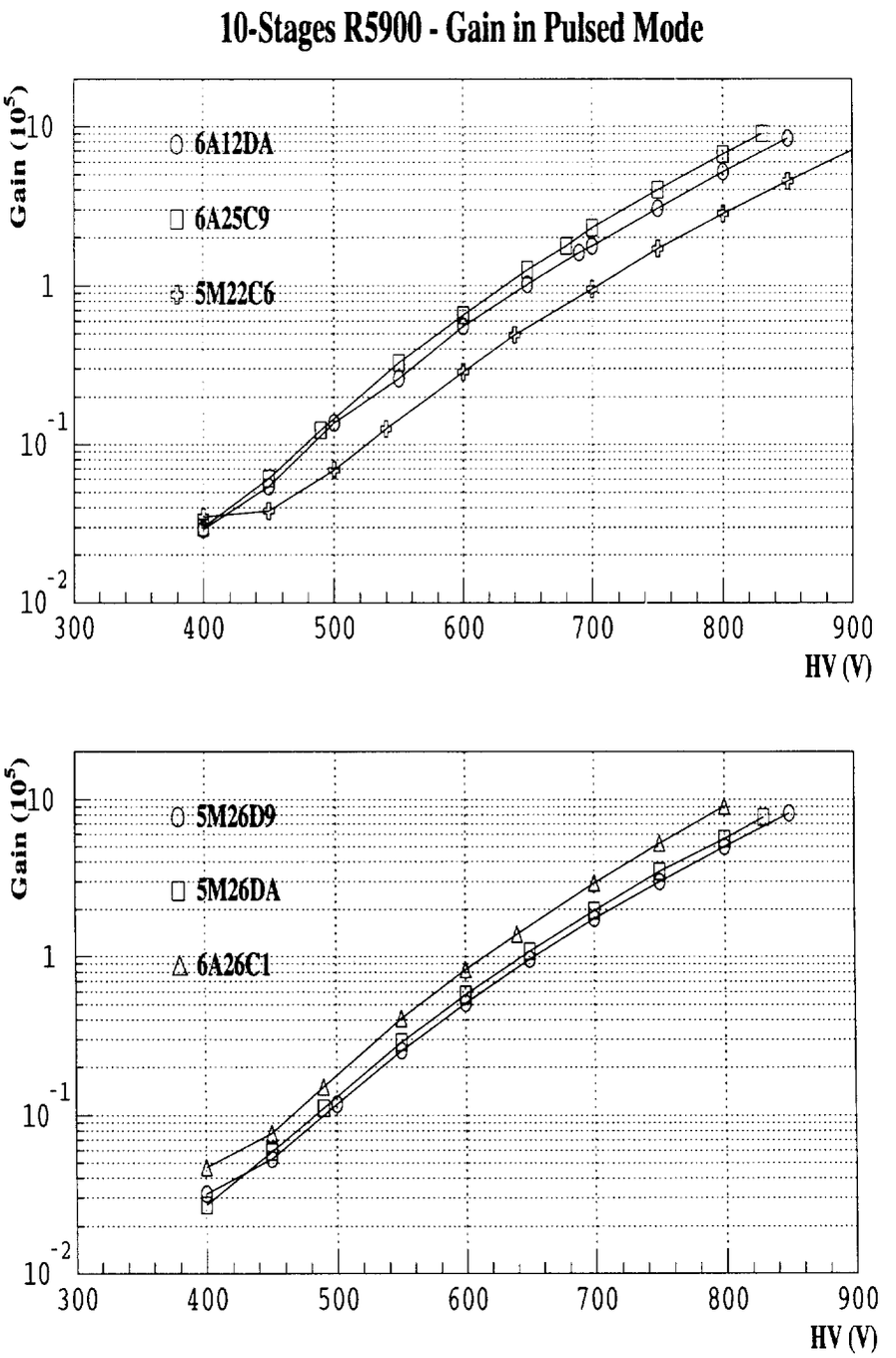


*Figure 44 : PMT amplification in pulsed mode derived from the statistics of the PMT signal, i.e., estimating the number of photoelectrons from equation (54).*

In Table (10) are reported the high voltages for the nominal gain of $10^5$. In the third column are also reported the corresponding DC measured amplifications. It appears a discrepancy since there is, on the average, a factor 1.45 between the two different methods. Such a discrepancy could partially come from some systematic errors that affect the both methods and that are very difficult to control on such a set-up. Nevertheless, the huge difference between the results could also come from the simplification of the $N_{pe}$ estimation.

When taking account the noise factor (equation (44)), expression (54) becomes:

$$N'_{p.e.} = \left(\frac{< M > -Ped}{\sigma}\right)^2 = N_{p.e.} \times (\frac{1}{1 + F}) \tag{56}$$

$$G_{Meas.} = (\frac{Q}{1.6 \times 10^{-19} \times N'_{p.e.}}) \tag{57}$$

$$G_{Meas.} = \left(\frac{Q}{1.6 \times 10^{-19} \times N_{p.e.}}\right) \times (1 + F) = G \times (1 + F) \tag{58}$$

and so the noise factor corrected amplification ($G$) is:

$$G = \frac{G_{Meas.}}{(1 + F)} \tag{59}$$

It remains to estimate the noise factor for the 2.5:2.5:1—1:2.5:2.5 repartition. With that configuration, one should calculate:

$$\frac{1}{k_{2.5}} + \frac{1}{(k_{2.5})^2} + \frac{1}{(k_{2.5})^2 k} + \ldots\ldots \frac{1}{(k_{2.5})^3 k^7} \tag{60}$$

or with notation $k_{2.5} = k'$ and $k_1 = k$:

$$\frac{1}{k'} + \frac{1}{(k')^2} + \frac{1}{(k')^2 k} + \ldots\ldots \frac{1}{(k')^3 k^7} \tag{61}$$

Equation (61) could be written:

$$[\frac{1}{k'} + \frac{1}{(k')^3 k^7}] + [\frac{1}{(k')^2} + \frac{1}{(k')^2 k} + \ldots \frac{1}{(k')^2 k^6}] \tag{62}$$

$$\frac{1}{k'}[1 + \frac{1}{(k')^2 k^7}] + \frac{1}{(k')^2}[1 + \frac{1}{k} + \ldots \frac{1}{k^6}] \simeq \frac{1}{k'} + \frac{1}{(k^6)(k')^2}[1 + \ldots k^6] \tag{63}$$

Equation (33) is now:

$$\sigma^2_{\overline{m_{10}}} = \overline{m_{10}}^2 \left(\frac{1}{k'} + \frac{1}{(k^6)(k')^2} \frac{(1 - k^7)}{(1 - k)}\right) \tag{64}$$

and the noise factor is:

$$F = \left(\frac{1}{k'} + \frac{1}{(k^6)(k')^2}\frac{(1-k^7)}{(1-k)}\right) \tag{65}$$

finally:

$$F \sim \frac{1}{k'}\left[1 - \left(\frac{k}{1-k}\right)\frac{1}{k'}\right] \tag{66}$$

The variation of the interdynode amplification ($k$) as a function of the interdynode voltage ($v$) could be parametrised as:

$$k = \alpha\, v^{\beta} \longrightarrow log(k) = \beta log(v) + log(\alpha) \tag{67}$$

together with:

$$k' = \alpha\,(2.5 \times v)^{\beta} \longrightarrow log(k') = \beta(log(v) + log(2.5)) + log(\alpha) \tag{68}$$

since

$$G = k'^3 \times k^7 \tag{69}$$

$$log(G) = 10\beta log(V) + 10log(\alpha) + \beta(3log(2.5) - 10log(17))$$
$$log(G) = \beta' log(V) + log(\alpha') \tag{70}$$

$$G = \alpha' \times V^{\beta'}$$

with

$$\beta' = 10\beta \text{ and } log(\alpha') = 10log(\alpha) + \beta(3log(2.5) - 10log(17))$$

Considering all the PMTs used in Module 0, the mean value of the parameter $\beta'$ is equal to $8.328 \pm 0.048$, with an r.m.s. of 0.39. The values are seen to have only a small dispersion, and so correspond to the typical performance of the multipliers. As $\beta' = 10 \times \beta$, we used this averaged value to determine first $\alpha$, then the $k$ and $k'$ values for each of the 6 PMTs, starting from the DC amplification measured at the nominal HV, and finally the noise factor from expression (66).

The data reported in the last column of the Table (10) correspond to the noise factor corrected amplification, and could be compared to the DC amplification measurements. There remains a systematic difference of 15% between the two set of data, but once again the amplification determination is very sensitive to systematics that are very difficult to control.

| PMT # | HV | $G_{DC}$ ($\times 10^5$) | $k_1$ | $k_{2.5}$ | $F$ | $G'$ ($\times 10^5$) |
|---|---|---|---|---|---|---|
| 6A12DA | 650 | $(0.68 \pm 0.2)$ | 2.420 | 5.190 | 0.256 | 0.800 |
| 6A25C9 | 630 | $(0.73 \pm 0.2)$ | 2.437 | 5.227 | 0.253 | 0.798 |
| 5M26D9 | 655 | $(0.70 \pm 0.2)$ | 2.427 | 5.206 | 0.255 | 0.797 |
| 5M26DA | 645 | $(0.66 \pm 0.2)$ | 2.417 | 5.184 | 0.256 | 0.796 |
| 6A26C1 | 615 | $(0.67 \pm 0.2)$ | 2.416 | 5.183 | 0.256 | 0.796 |
| 5M22C6 | 705 | $(0.70 \pm 0.2)$ | 2.427 | 5.206 | 0.255 | 0.797 |

*Table 10 : Nominal high voltages corresponding to the nominal gain of* $10^5$*, as measured in pulsed mode for 6 of the R5900 that had been used in Module 0. The third column reports the corresponding DC measured amplification.* $k_1$ *and* $k_{2.5}$ *are the interdynode amplifications,* $F$ *is the noise factor, and finally* $G'$ *is the noise corrected pulsed mode derived amplification*

### 4.3 Temperature effect on PMT amplification

In order to estimate the PMT gain variation with the temperature, one used a dedicated cooling and heating system that is able to evacuate or to add heat dissipated by the electronic, and so maintains the local temperatures within 1° C.

The experimental setup is shown on Figure (45). The light, produced by a pulsed blue LED, is split into two different light beams. One of these light beam is used for monitoring the light source by the way of a photodiode. The second light beam is focused into a large acceptance "Liquid-fiber" which transports the light to the PMT test box where is located a R5900 under test. The box temperature is stabilized externally and monitored by a temperature probe. The local temperature in the box is recorded for each event (LED pulse).

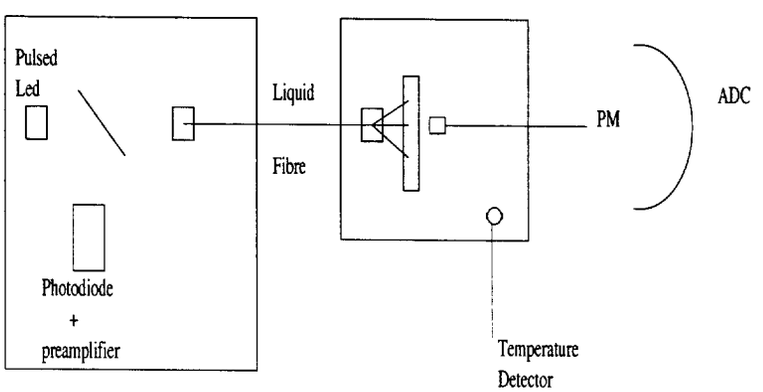


*Figure 45 : Experimental set-up used for the test of the temperature effect on the PMT amplification. The PMT box temperature is regulated within 1° C, and is recorded for each event for the offline analysis.*

Let us call $Pm(\Theta)$ the response to a light pulse of the R5900, measured by a charge ADC and $Ph(\Theta)$ the output of the photodiode in response to the same light pulse. The relative gain variation is estimated using the following expression:

$$D(\%) = 100 \times \frac{(Pm(\Theta)/Ph(\Theta)) - (Pm(\Theta_0)/Ph(\Theta_0))}{(Pm(\Theta_0)/Ph(\Theta_0))} \tag{71}$$

where $Pm(\Theta_0)$ and $Ph(\Theta_0)$ are the response of the photomultiplier and the photodiode respectively, measured at 20° C. The photomultiplier has been operated at a high voltage corresponding to a gain of $10^5$. The results are presented in Figure (46). It clearly appears that the variation of the gain is not important. The variation is about 1% per 5° C.

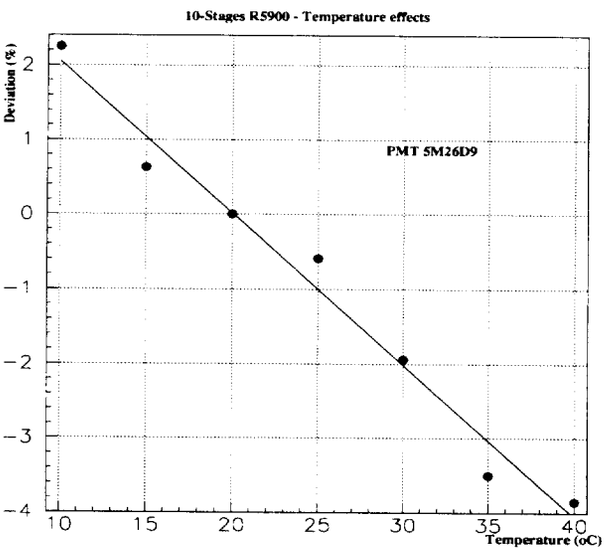


*Figure 46 : Temperature effect on the amplification of a typical R5900. The gain variation is of the order* 0.2% *per* 1° *C.*

### 4.4 Pile-up effect on the PMT amplification

These measurements were done in order to reproduce the PMT conditions in the ATLAS detector. In the worst-case scenario of an average of 20 minimum bias events at each bunch crossing , one will have an anode current of the order of 2 $\mu A$. So to estimate what could be the PMT amplification variation with this DC light component, we test the PMT with the set-up shown in Figure (47).

The DC background is produced by a LED operated in a DC mode. The DC light is directly added at the input side of the light mixer. The tests have been performed with 4 different anode current values: 100 $nA$, 1 $\mu A$, 2 $\mu A$ and 4 $\mu A$.

A pulsed LED is used to simulate the calorimeter light pulse. The amplitude of that pulse is modified by the way of a set of neutral filters with different attenuations. The PMT anode charge is converted by an ADC, so that a precise determination of the amplification could be achieved. The PMT anode current could also be measured on the scope. The PMT voltage has been set to the nominal value in order to have the nominal amplification.

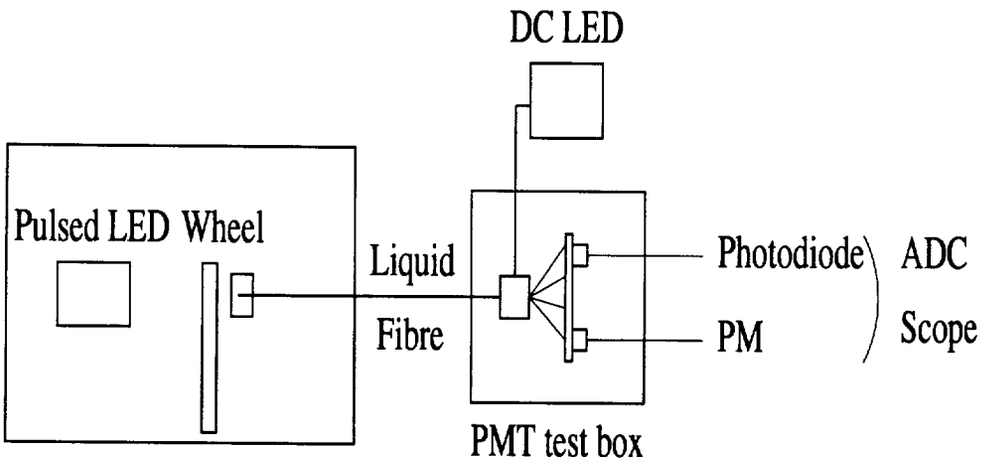


*Figure 47 : Experimental set-up used for the test of the pile-up effect on the PMT amplification. DC light is adjusted first using the photodiode monitoring, then pulsed light is adjusted using a set of neutral filters with different attenuations.*

Figures (48) and (49) represent the variation of the amplification of the PMT versus the anode current for 7 of the R5900 used in Module 0, and for the different values of the background current.

Reading each curve on the horizontal axis scale, gives access to the linearity variation of the PMT as a function of the pulse amplitude with DC light added.

Reading on the vertical axis scale at constant anode current, gives access to the effect on the PMT amplification with the growing DC light.

The variation of the gain is sizeable. For the extreme conditions of the experiment ($I_{DC} = 4\ \mu A$) the variation is about 4 %.

The explanation of the gain increase is the following. If one assumes that the dynode voltages are derived from a resistive divider across a stabilized power supply, the anode current $I_a$ tends to lessen the potentiel between the last dynode and the anode. This variation can be ignored if the output current is small. However, when the incident light level is increased, i.e., when an intense DC current circulates through the PMT, the voltage distribution of each dynode varies a lot as shown on Figure (50). Because the overall cathode to anode voltage is kept constant by the HV source, the loss of the interdynode voltage at the latter stages is redistributed to the previous stages so that there is an increase of the amplification in the first stages.

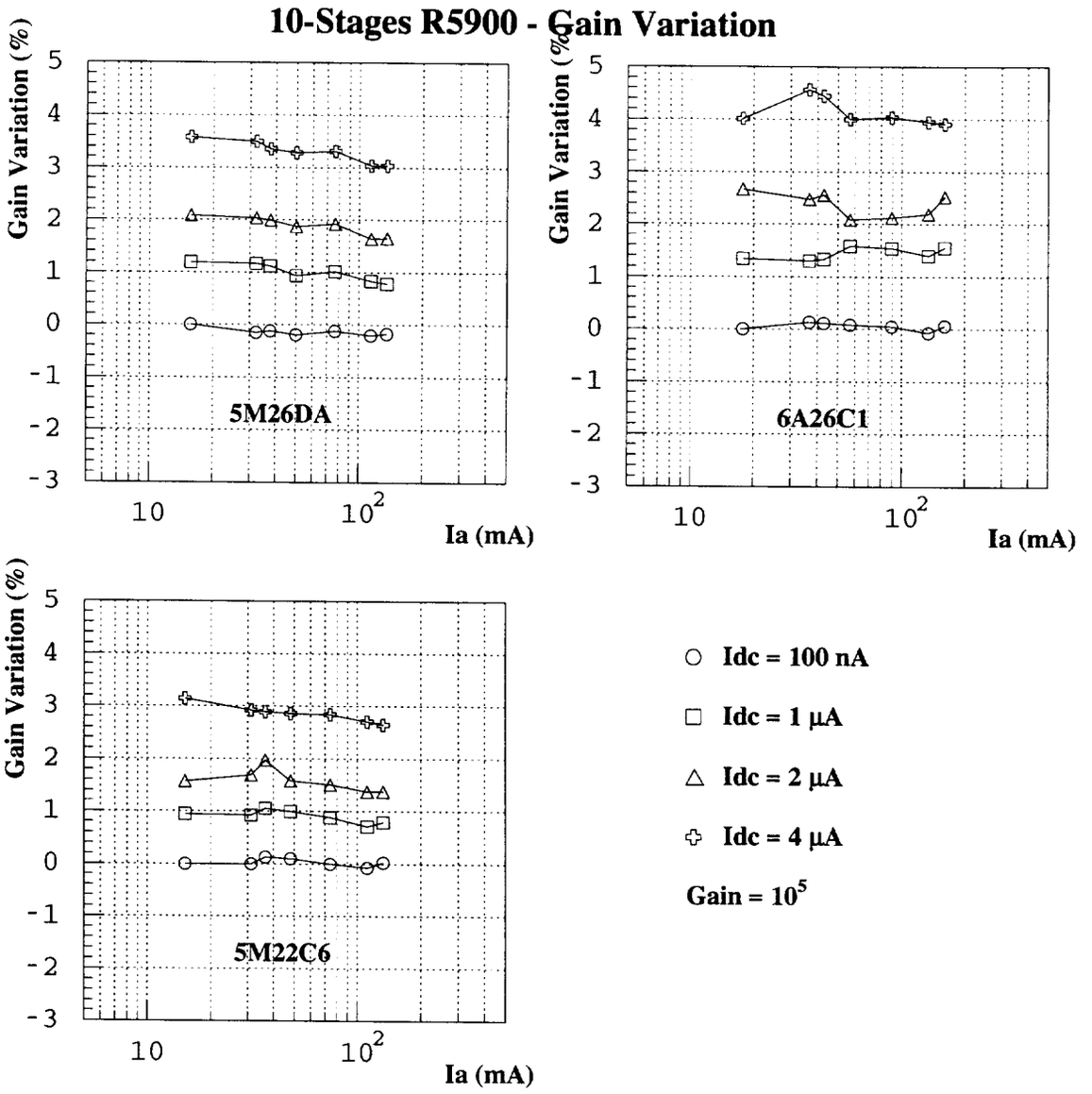


*Figure 48 : Variation of the gain versus the anode current for different values of the DC background current.*

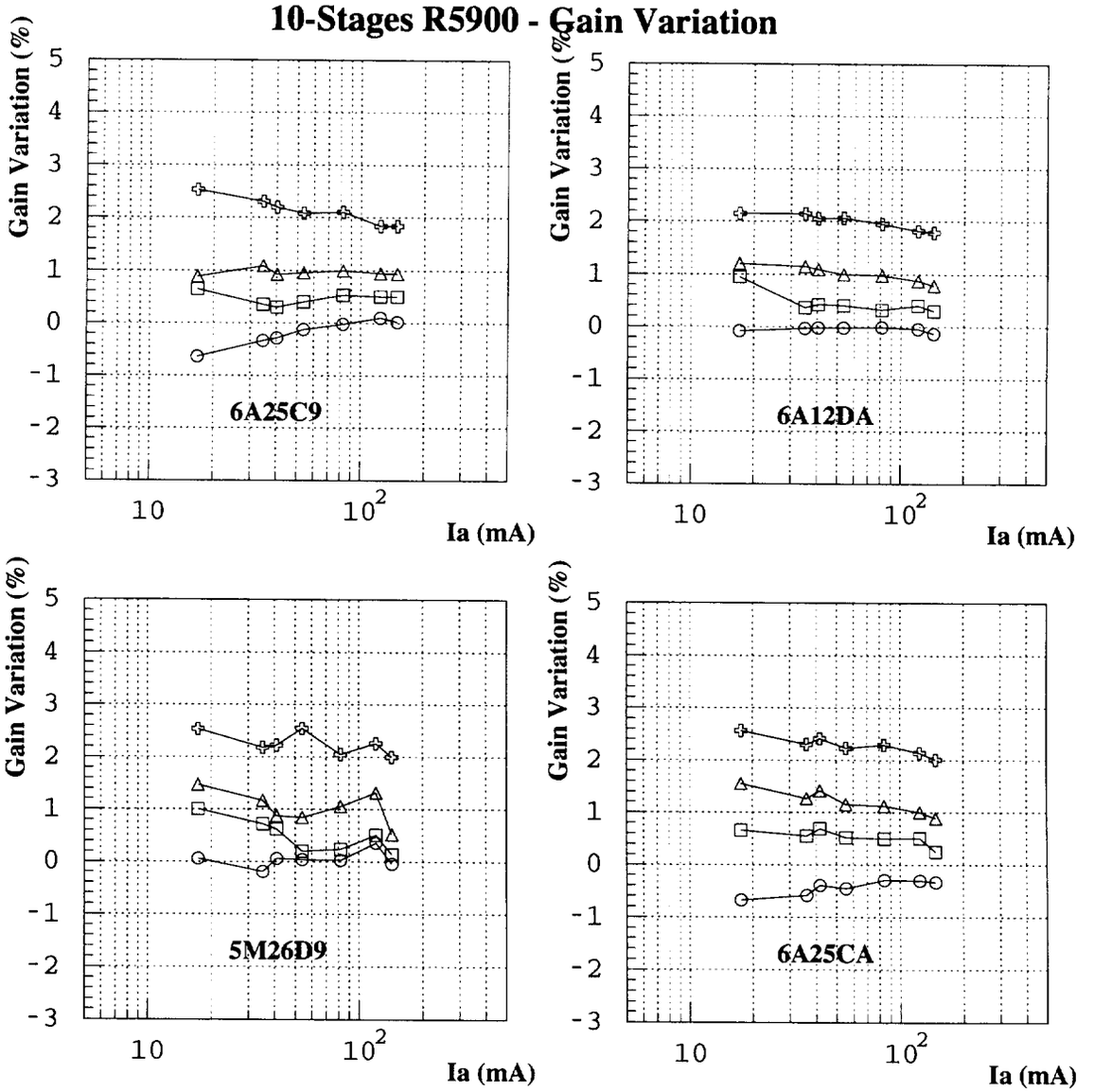


*Figure 49 : Variation of the gain versus the anode current for different values of the DC background current.*

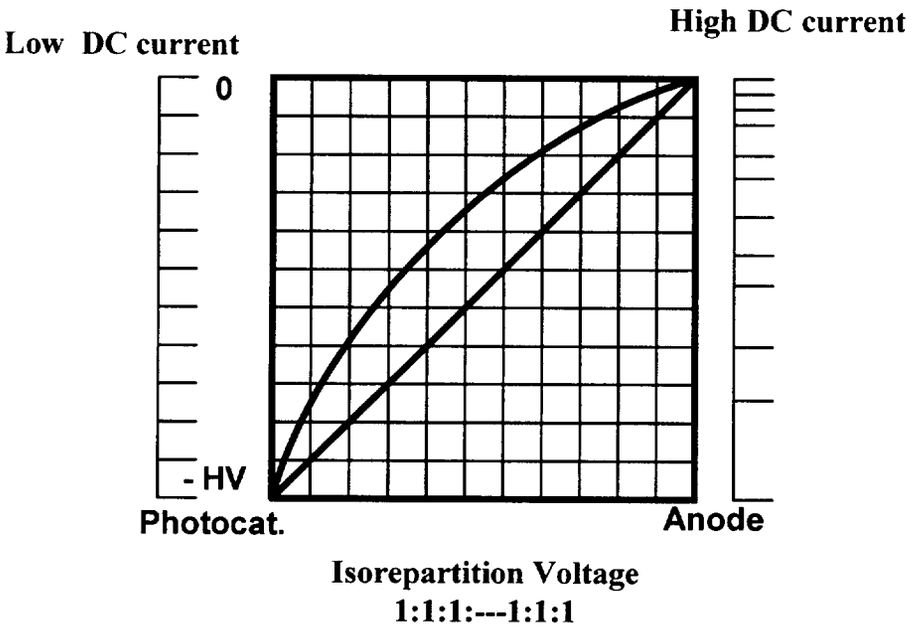


*Figure 50 : Variation of the interdynode repartition with the 1:1:1.:...1:1:1 configuration when the anode current grows-up to an excessive high value. The left axis scale shows the isorepartition of the HV between the photocathode and the anode. The right axis scale indicates that, with a high DC current, anode to dynode #10 voltage increases (no amplification), meanwhile the photocathode to dynode #1 voltage decreases (smaller amplification).*

### 4.5 Relative amplification parametrisation

The amplification curves of the set of PMTs used in the Module 0, with the standard divider (2.5:2.5:1.0 ...1.0:2.5:2.5) are well reproduced by fitting the gain G versus the PMT overall voltage V with the usual law:

$$G = \alpha \times V^{\beta} \tag{72}$$

Considering all of PMTs used in Module 0, the mean value of the parameter $\beta$ is equal to :

$$< \beta > = \ 8.328 \pm 0.048 \text{ with an r.m.s. of } 0.39 \tag{73}$$

The averaged value of $\beta$ corresponds to the typical performance of a 10-stage multiplier. The average HV which corresponds to the nominal gain of $10^5$ is equal to $665 \pm 79$ V. Therefore these PMTs need rather low HV values. Moreover, it follows that an adjustment of the gain at a level of 0.5% requires a stabilization of the HV with an accuracy of 0.4 V.

# 5. Dark current

In the Figure (51) are shown the dark currents of 15 R5900 used in Module 0, as a function of the applied voltage. The dark currents has been measured with the same voltage divider circuit, corresponding to a 2.5:2.5:1–1:2.5:2.5 repartition. In fact this measurement should be done for each PMT associated with its specific voltage divider circuit.

Most of the PMTs have an anode dark current lower than 100 pA for a HV lower than 750 Volts, while the #5M22C6 presents a sharp increase dark current above 700 Volts. For that PMT the nominal amplification of $10^5$ is obtained at 725 Volts.

Without that PMT (tagged as bad) the averaged value of the dark current at nominal voltage is equal to:

$$< I_{dc} >_{10^5} = 35.71\ pA \tag{74}$$

with a dispersion of 12.5%. We also evaluate the gradient of the relative variation of the dark current at nominal value of the PMT voltage on a voltage variation of 25 Volts: the mean variation for the set of PMTs (without the # 5M22C6) is:

$$< \frac{1}{I_{DC}} \frac{\Delta I_{DC}}{\Delta V} > = 0.62\% \tag{75}$$

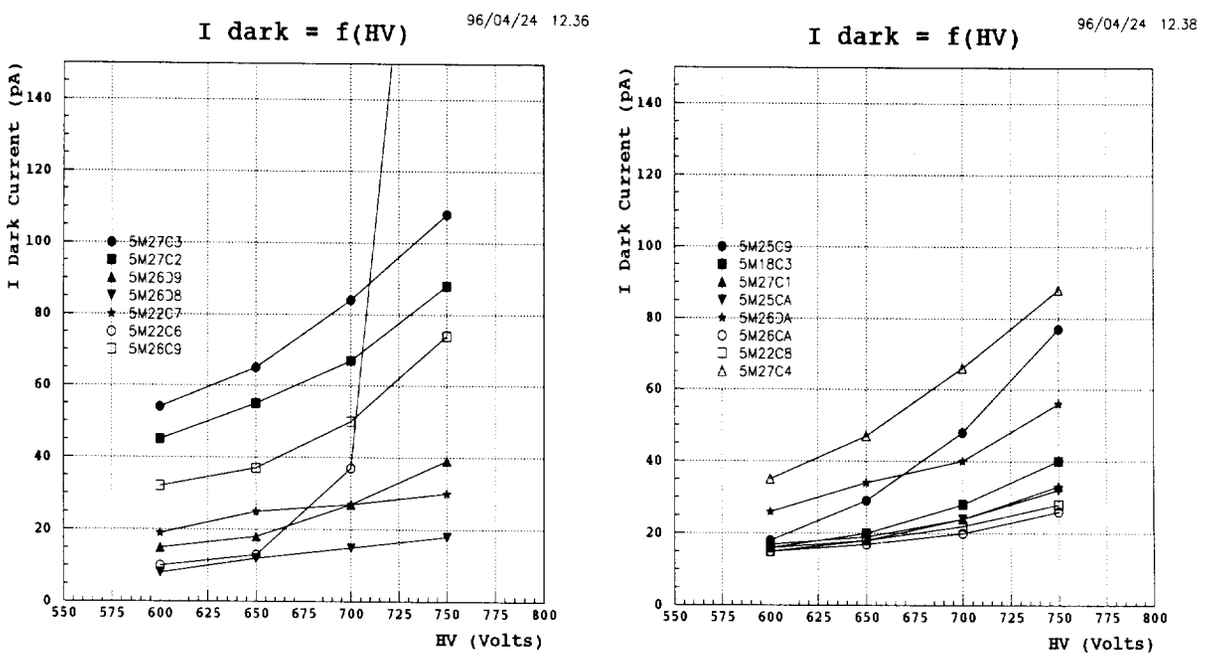


*Figures 51: Dark current (pA) as a function of HV (Volts), measured on a set of 15 R5900 used on Module 0 with a 2.5:2.5:1–1:2.5:2.5 repartition.*

# 6. linearity

Generally, a PMT provides a good linearity for the anode output current over a wide range of incident light levels. However, if the incident light amount is too large, the output begins to deviate from the ideal linearity. The anode linearity is limited by two factors; the space charge effect and the bleeder circuit configuration.

In the former case, as claimed in the previous section, the averaged DC current ($I_a$) flowing in the anode could affect the PMT linearity when growing-up to excessive high value.

In a pulsed mode operation when an intense light pulse enters the PMT, due to the amplification, a large current flows in the latter dynode stages, increasing the charge density in the dynode structure. For that reason, the pulse linearity deviation due to the charge density effects depends as well on the peak as on the width of the anode current. That space charge effects depend also on the electric field strentgh between each dynode. A corrective action to overcome the space charge effect and so to achieve a better linearity is generally to apply higher values of the voltages to the final stages so that the electric field strentgh between each dynode is enhanced. But one should take care about the interdynode voltage tolerance. In any case the PMT linearity limitation is very dependent on the interdynode voltage repartition.

### 6.1 First estimation of the R5900 linearity using a pulsed LED

The experimental set-up used for a first estimation of the R5900 linearity, and using a pulsed LED is shown on Figure (52).

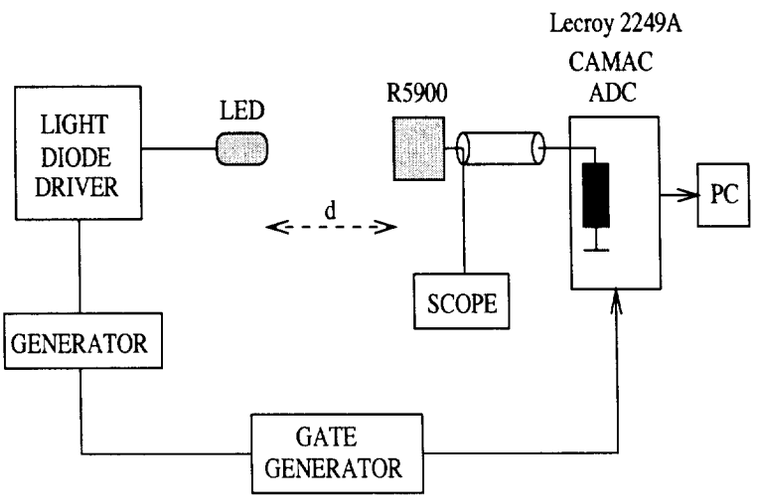


*Figure 52 : Experimental set-up used for a first estimation of R5900 linearity .*

The LED, operating in a double pulsed mode, is used to provide higher and lower pulse amplitudes, in a constant ratio ($\sim 4$).

The distance between the LED block and the PMT can be modified in order to adjust the luminous flux impinging the photocathode. The ratio between the higher and lower pulse amplitudes remains constant, independently from the distance between the light source and the illuminated PMT.

The PMT responses to these light pulses are the charges $Q_1$ and $Q_2$ respectively. Let us call $Q_{01}$ and $Q_{02}$ the charges corresponding to the lowest luminous flux, i.e. the largest distance between the PMT and the LED. The ratio of $Q_{02}/Q_{01}$ can be used as a reference. So, for each LED position, we first measure the charge ratio using a charge ADC. We also measure the PMT anode current on a digital scope by looking at the amplitude of the 30 ns wide higher pulse and we deduce the anode current $I_{p2}$.

When the LED light source is brought close to the PMT, the anode output current increases and starts to deviate from the linearity. The saturation will usualy occurs first at the output current $I_{p2}$ that corresponds to the higher pulse light. Thus the ratio between the two recorded charges has the following relation:

$$Q_2/Q_1 < Q_{02}/Q_{01} \tag{76}$$

and the deviation from the linearity of the PMT at the anode current $I_{P2}$ is estimated by the following formula:

$$D(\%) = 100 \times \frac{(Q_2/Q_1) - (Q_{02}/Q_{01})}{(Q_{02}/Q_{01})} \tag{77}$$

Nevertheless, if the non linearity also occurs for the lower light level, the previously discussed method is no more valid.

First tests with that set-up indicate some disturbances for very low anode currents. So we assume that roughly no deviation from linearity occurs below an anode current of 5 mA and we start the linearity measurements above 5 mA anode current.

This assumption was checked by measuring the lower part of the linearity curve, using a preamplifier. Then, we measure the high intensity part of the curve without the preamplifier. We performed the measurements to have a common part in the two cases in order to cross-check the continuity of the curve. The result are shown in Figure (53) with a PMT voltage equal to 800 Volts. That confirms that one can take the $5mA$ anode current data as a reference point. This choice is kept for the results presented in that subsection.

The Hamamatsu method for measuring the PMT linearity is roughly equivalent to the above described method. In fact Hamamatsu calculates the deviation from the linearity using the anode current amplitude instead of the charge. However, we have to keep in mind that the non linearity could appear first looking at the pulse amplitude rather than at the charge of the signal. In Figure (53) is shown the comparison between the Clermont linearity measurements and the Hamamatsu results for the 1:1:1:...:1:1:0.5 repartition, and with a PMT voltage equal to 800 Volts.

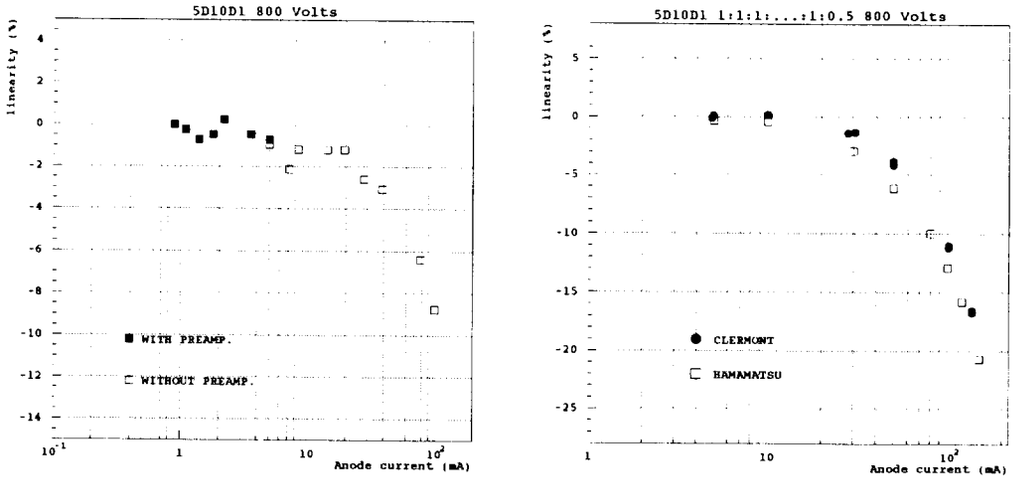


*Figures 53 : R5900 linearity (PMT # 5D10D1 of the second generation) as a function of the anode current: On the left part, open squares (full squares) correspond to measurements done without (with) the preamplifier. PMT voltage was set to 800 Volts, and the voltage repartition was 1:1:1:...:1:1:1. On the right part is presented a comparison between the Clermont linearity measurements and the Hamamatsu results for the same voltage repartition at 800 Volts.*

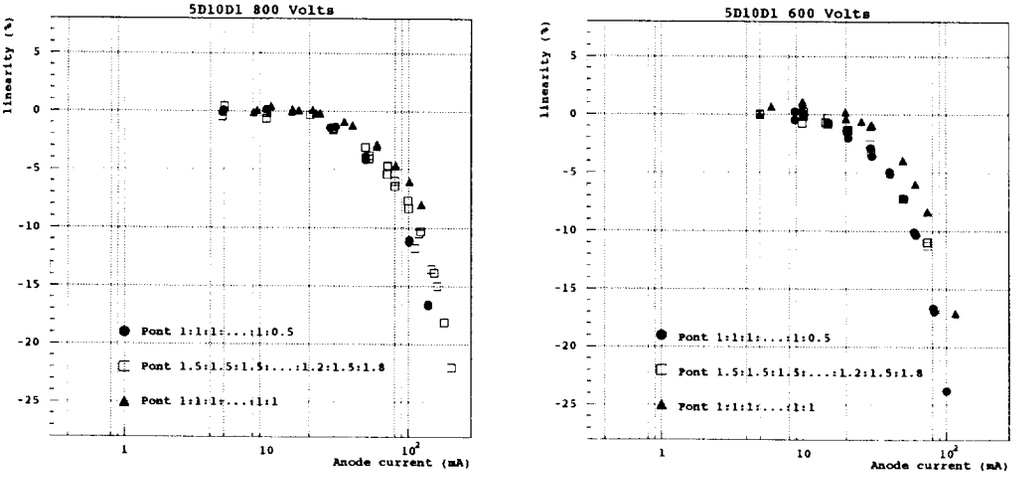


*Figure 54 : R5900 linearity (PMT # 5D10D1 of the second generation), as a function of the anode current for three different voltage repartitions: open squares correspond to the 1.5:1.5:1.5:1:...:1.2:1.5:1.8 configuration, full circles to the 1:1:1:...:1:1:0.5 configuration, and full triangles to the 1:1:1:...:1:1:1 configuration. On left part, PMT voltage was set to 800 Volts, on right part to 600 Volts.*

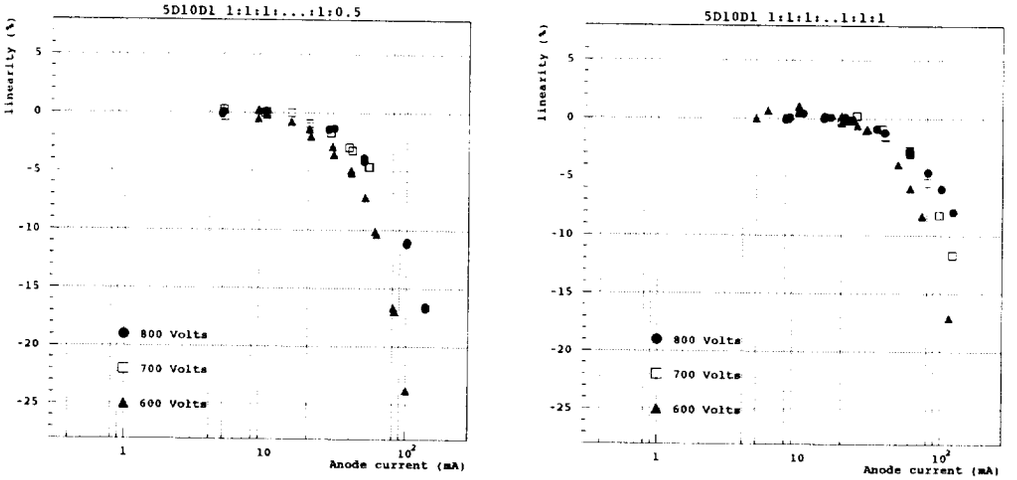


*Figure 55 : R5900 linearity (PMT # 5D10D1 of the second generation), as a function of the anode current for three values of the PMT voltage: open squares correspond to 700 Volts, full circles to 800 Volts, and full triangles to 600 Volts. On the left part the 1:1:1:...:1:1:0.5 voltage repartition was used, and the 1:1:1:...:1:1:1 on the right part.*

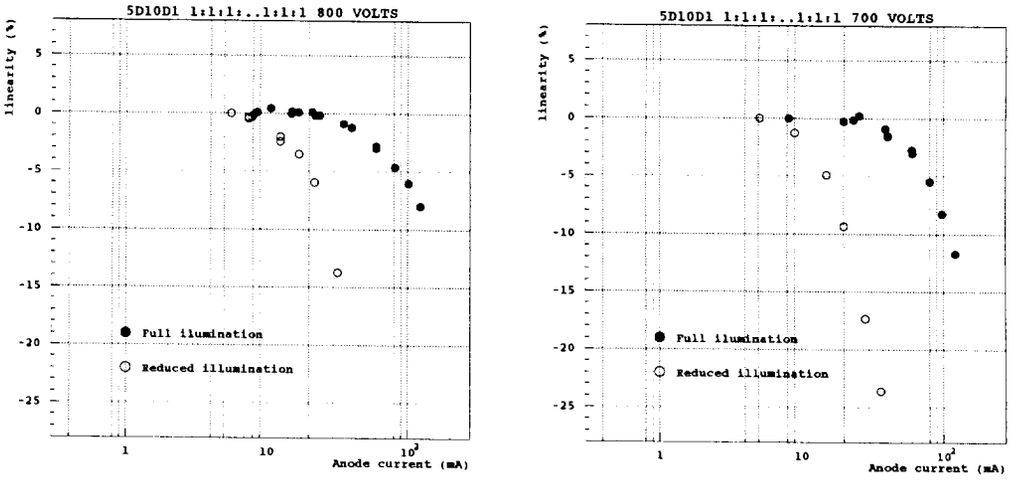


*Figure 56 : R5900 linearity (PMT # 5D10D1 of the second generation), as a function of the anode current for the 1:1:1:...:1:1:1 voltage repartitions: open symbols correspond to a reduced illumination of the PMT photocathode (5 × 5mm square spot), full symbols correspond to a full illumination of the PMT photocathode. PMT voltage was set to 800 Volts for the left part, and 700 Volts for the right part.*

As a first conclusion, the previous figures indicate that with a gain of $10^6$ and an isorepartition of the voltage between dynodes, the 2% linearity range corresponds roughly to a 30 mA anode current.

Moreover, Figures (54) and (55) show that this limit is not so dependent on the voltage repartition between the dynodes, but clearly and naturally depending on the PMT amplification.

The way the light is impinging the photocathode is also very important as shown on Figure (56). In this case, the light spot on the photocathode was reduced by using a smaller light mixer $5 \times 5$ mm$^2$. In such a configuration, it appears that the linearity is damaged, especially at low voltages. It is due to the fact that themetal channel dynode structure has a very small electrical cross-talk, so that the electron density becomes important. At low voltages, this density effect could not be overcome by the electric field strength. That is why, in the linearity measurements, we use a $43 \times 18 \times 18$ mm$^3$ light mixer in front of the photocathode.

### 6.2 Linearity measurement using a pulsed Laser

The previous method has the clear disadvantage of no providing a real reference measurement of the light: if the light intensity is too large, even the low pulse could be affected by the non linearity effect.

That is the reason why we performed another method for the linearity measurements using a Ytrium Lithium Fluoride (YLF) laser as light source. This laser was the one dedicated to the calibration and monitoring system of the TILECAL prototypes. The main characteristics are summarized in Table (11), and the general set-up is shown in Figure (57).

| **Output characteristics** | |
|---|---|
| Wavelength (nm) | 523 |
| Max. Pump Power (W) | $2 \times 1$ |
| Max. energy per pulse ($\mu$J) | $2 \times 20$ |
| Pulse width (ns) | $< 15$ |
| Beam diameter (mm) | 0.58 |
| Beam divergence (mrad) | 0.7 |
| **Output stability** | |
| Energy rms | 4% |
| Energy 3 $\sigma$ | $\pm$12% |

*Table 11: The YLF Laser performances and its main characteristics.*

The core of this system is a frequency doubled YLF solid-state laser [6], both externally triggerable and modulated, fully computer controlled. The produced light pulses have characteristics similar to the light delivered by particles in the calorimeter.

During a period, the laser is driven to produce trains of 16 adjusted light pulses of increasing intensity, spanning the PMT dynamic range. The intensity of each pulse is measured by photodiodes [7] operating as laser monitors.

The absolute stability of the photodiodes and the associated electronics (preamplifier) is controlled using $\alpha$ particles [8] from an americium radioactive source.

A small capacitor is used in parallel with the photodiode to inject calibrated charge in the photodiode preamplifier and so to measure the linearity of the electronics behind the photodiode.

The laser system could be operated in different modes:

- Pedestal measurements of the photodiodes in the two VME system (Laser and DAQ crates).
- Calibration of the photodiodes by the $\alpha$ source.
- Photodiode channel linearity by calibrated charge injection.
- Normal laser operation with a VME controlled generation of 16 different intensity pulses.

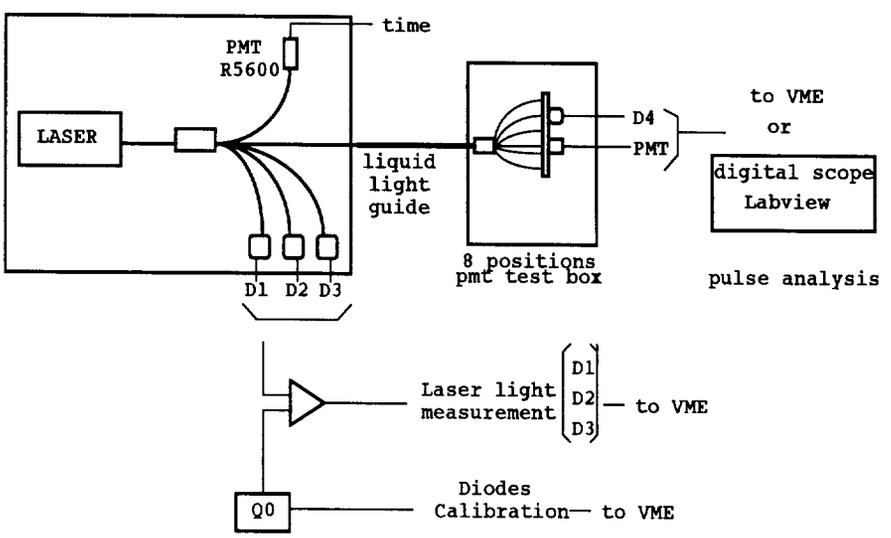


*Figure 57 : Block diagram of the Laser system used as a modulated and adjustable light source for the PMT linearity measurements.*

[6]Spectra Physics, model 7300

[7]large area PIN silicon Hamamatsu S2662 photodiodes

[8]85% 5.486MeV

However we have to mention that when the following measurements were performed, one of the two diodes used in order to excite the Solid State Medium of the laser was out of service, limiting the dynamical range that is accessible to the laser. In any way the limitation was not only operating on the pulse intensity but also on the pulse width which is directly correlated to the pulse intensity in that laser.

As an illustration, Figure (58) shows the 16 laser pulses recorded, respectively by one of the photodiode (D1) and the tested PMT. This PMT (#5D10D1) of the second generation was operated at 710 Volts with a voltage isorepartition (1:1:1:...:1:1:1). This specific value of the voltage corresponds roughly to an amplification of $10^6$. The pulses have been adjusted to cover fully the dynamic range. Due to both the best quantum efficiency of the photodiodes and the largest amount of the incoming light, the photodiodes spectrum (bottom) offers a better energy resolution than the PMT spectrum (top).

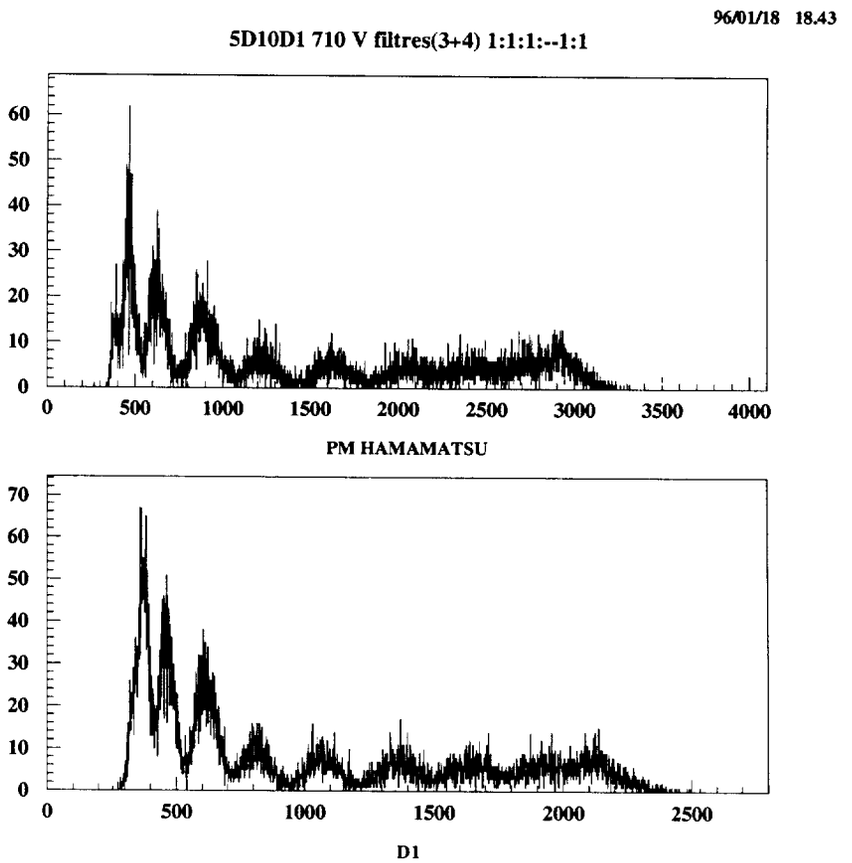


*Figure 58 : Spectra of the 16 laser pulses as recorded, respectively by one of the photodiode (D1) and the tested PMT. The PMT (#5D10D1) of the second generation was operated at 710 Volts with a voltage isorepartition (1:1:1:...:1:1:1). This specific value of the voltage corresponds roughly to an amplification of* $10^6$. *The pulses have been adjusted to cover fully the dynamic range.*

For a given adjusted laser amplitude, there are pulse-to-pulse laser fluctuations. These fluctuations contribute to enlarge the 16 light pulses. Nevertheless, measuring event by event the light pulses, all the points in the previous figure are individually used to compare the PMT and the light as recorded by the photodiodes.

As the PMT gain is known and as long as the PMT is linear, the PMT anode charge could be expressed directly as a function of the number of photoelectrons before amplification. This is used in Figure (59) which represents the ratio PM/D1 as a function of the number of photoelectrons before amplification. The ratio PM/D1 had been renormalized to one for the lowest light pulse, where the pulse-to-pulse fluctuation increase since for the diode the statistics becomes very low in comparison with the intrinsic diode noise.

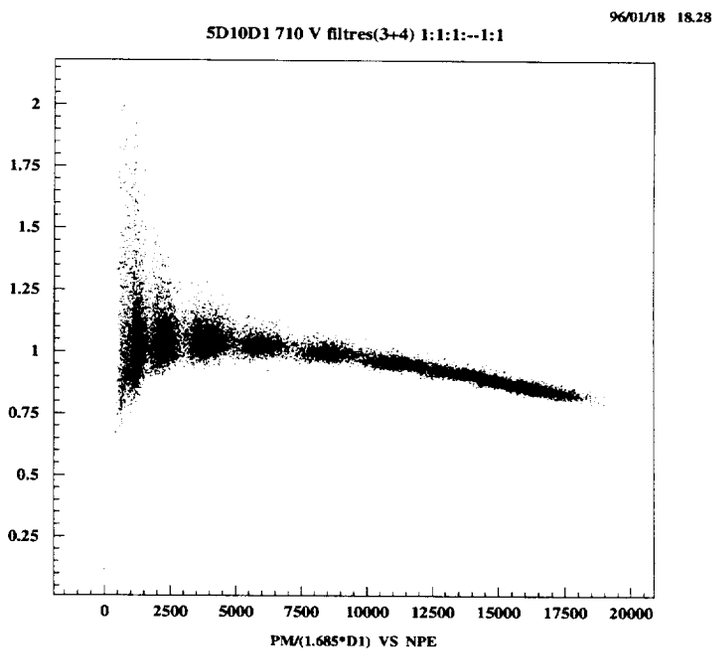


*Figure 59 : Ratio (PM/D1) of the PMT (#5D10D1) response over signal of one of the laser photodiode (D1), as a function of the PMT number of photoelectrons before amplification, and assuming a full linearity. The ratio PM/D1 has been renormalized to one of the lowest light pulse. The PMT was operated at an amplification of* $10^6$ *(710 Volts with a 1:1:1:...:1:1:1 voltage repartition).*

Figure (60) shows the comparison, for PMT #4*M*02*D*1 operated at an amplification of $10^6$ with 1:1:1:—1:1:1 voltage repartition, between the linearity measurements achieved at Clermont with the LED or the laser system and by Hamamatsu in Japan. For the Laser method, the anode current has been estimated using the PMT pulse width (the laser pulse widths are slightly different for each of the 16 amplitudes).

The three curves are comparable, especially the Hamamatsu and Laser results. This gives some confidence in our linearity measurement method that will be used now for the linearity optimisation.

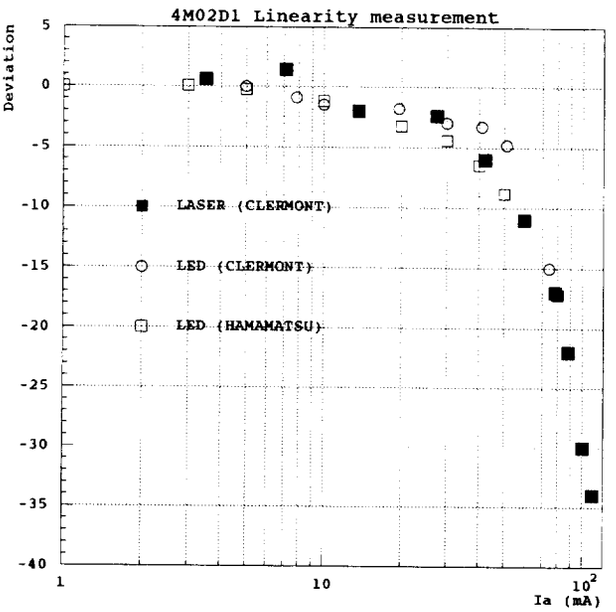


*Figure 60 : Comparison, for PMT #4M02D1 operated at an amplification of* $10^6$ *with the 1:1:1:—1:1:1 voltage repartition, between linearity measurements achieved at Clermont with the LED or the laser system and by Hamamatsu in Japan. For the Laser method, the anode current has been estimated using the PMT pulse width (the laser pulse widths are different for each of the 16 amplitudes).*

### 6.3 Improvement of the linearity

As claimed above, a corrective action to overcome the space charge effect and so to achieve a better linearity is generally the use of higher values of the voltage applied to the final stages. So the divider could be optimized in such a way that the electric field strentgh between the dynodes of the final stage is enhanced, and consequently improves the linearity.

Figures (61) to (65) represent the ratio PMT/D1 (indicating the linearity deviation) measured with the laser setup, using the PMT #5D10D1 and with different voltage repartitions and amplifications. In each configuration, the ratio variation is shown as a function of the photoelectrons number before amplification, and the ratio is renormalised to one of the lower part of the $N_{p.e.}$ range. One should keep in mind that this curve indicates only qualitatively the linearity deviation since as soon as the PMT is in a non linear mode, the number of photoelectrons before amplification is no longer simply related to the PMT anode current.

• Figure (61) corresponds to a 1:1:1:1–1:1:1 repartition. On top, the PMT amplification is $10^5$ with two different ranges of the photoelectrons number. For $N_{p.e.}$ = 70K, the deviation linearity is $-10\%$. On bottom, the PMT amplification is $10^6$.

• Figure (62) corresponds to a 1.5:1.5:1:1–1.2:1.5:1.8 repartition. For $N_{p.e.}$ = 70K and an amplification of $10^5$, the deviation linearity is $-5\%$.

• Figure (63) corresponds to a 2.5:1:1:1–1:1:2.5 repartition. For $N_{p.e.}$ = 70K and an amplification of $10^5$, the deviation linearity is $-9.5\%$.

• Figure (64) corresponds to a 2.5:2.5:1:1–1:2.5:2.5 repartition. For $N_{p.e.}$ = 70K and an amplification of $10^5$, the deviation linearity is $-4.5\%$.

• Figure (65) corresponds to a 1:1:1:1-0.5-1:1:1 repartition. For $N_{p.e.}$ = 70K and an amplification of $10^5$, the deviation linearity is $-7.8\%$

The improvement in linearity from the configuration illustrated by the Figure (61) to the configuration illustrated by the Figure (64) appears clearly. Finally, the Figure (64) corresponds to a 1:1:1:1-0.5-1:1:1 repartition, i.e., with a so-called "gain killer". In that last configuration, the linearity is worse than in the 2.5:2.5:1:1–1:2.5:2.5 repartition.

In addition, we check in that configuration, that the PMT amplification does not depend on the location of the "gain killer" stage.

So at the nominal amplification of $10^5$, the best configuration corresponds to the 2.5:2.5:1:1–1:2.5:2.5 repartition. Such a voltage repartition has many advantages. As this 10-stages PMT are designed to operate typically with an amplification of $10^6$, a lower amplification induces rather low high voltages (500-600 Volts). As claimed above it could lead to a bad PMT efficiency, since the interdynode voltage is of the order of 44 Volts. With the 2.5:2.5:1–1:2.5:2.5 configuration the overall high voltage is increased of roughly 100 volts, so that the voltage on the first stage is now of the order of 100 Volts, and by the way improve the light collection efficiency.

Figure (66) represents the linearity deviation of a set of 5 PMTs, used in the Module 0, measured with the 2.5:2.5:1:1–1:2.5:2.5 voltage repartition at the nominal amplification. For these measurements, the experimental set-up is the one presented on Figure (45): the variation of the pulsed light amplitude is achieved using a set of different attenuation neutral filters. The 2% linearity deviation corresponds to a PMT anode current range of 30 to 60 mA, and with a pulse width of 17 ns, in a photoelectron range of 32K to 64K.

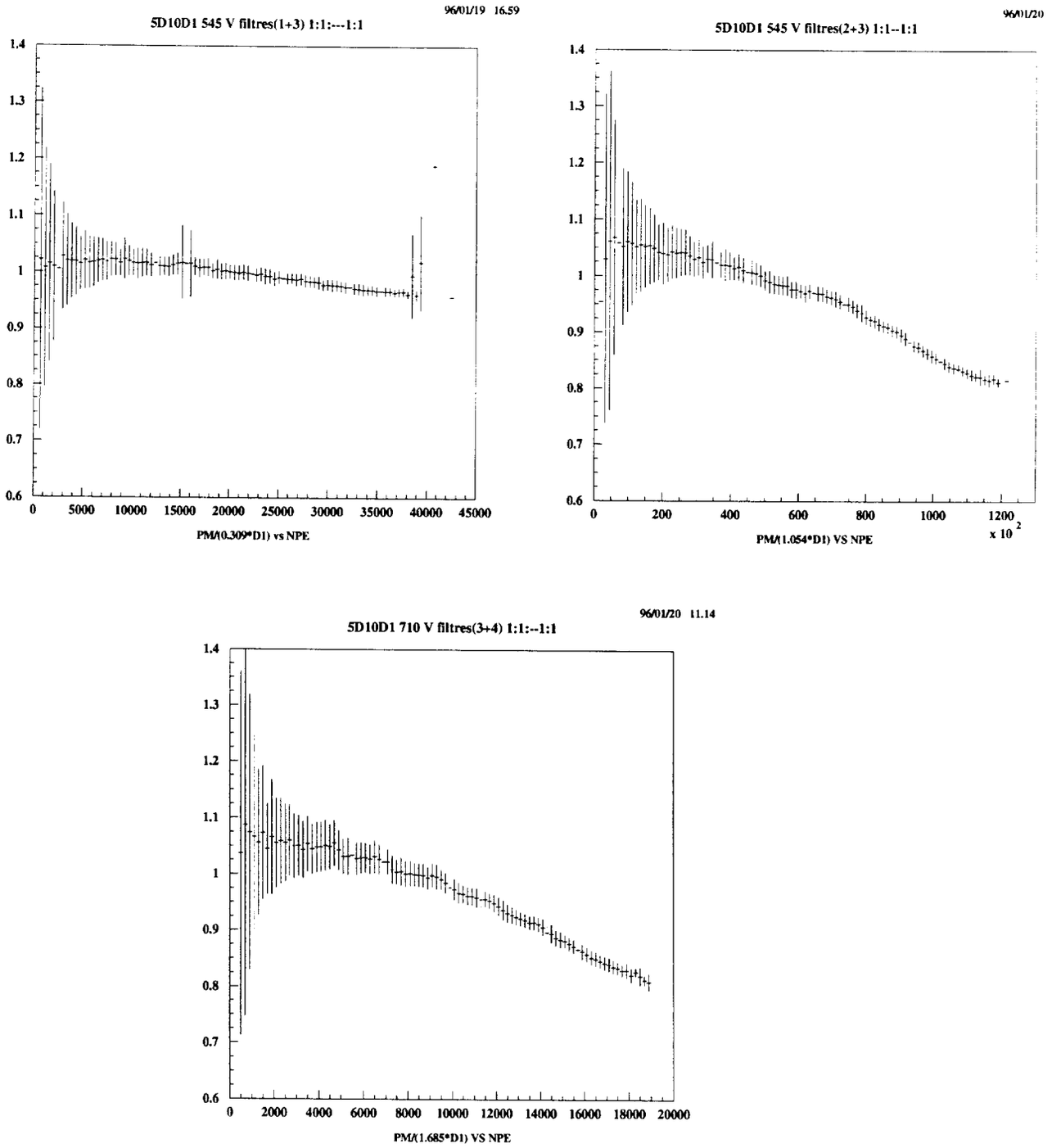


*Figure 61 : Differential linearity curves with a 1:1:1:1–1:1:1 voltage repartition. Top figures correspond to a PMT amplification of* $10^5$ *with two different ranges in* $N_{p.e.}$*. Bottom corresponds to an amplification of* $10^6$*.*

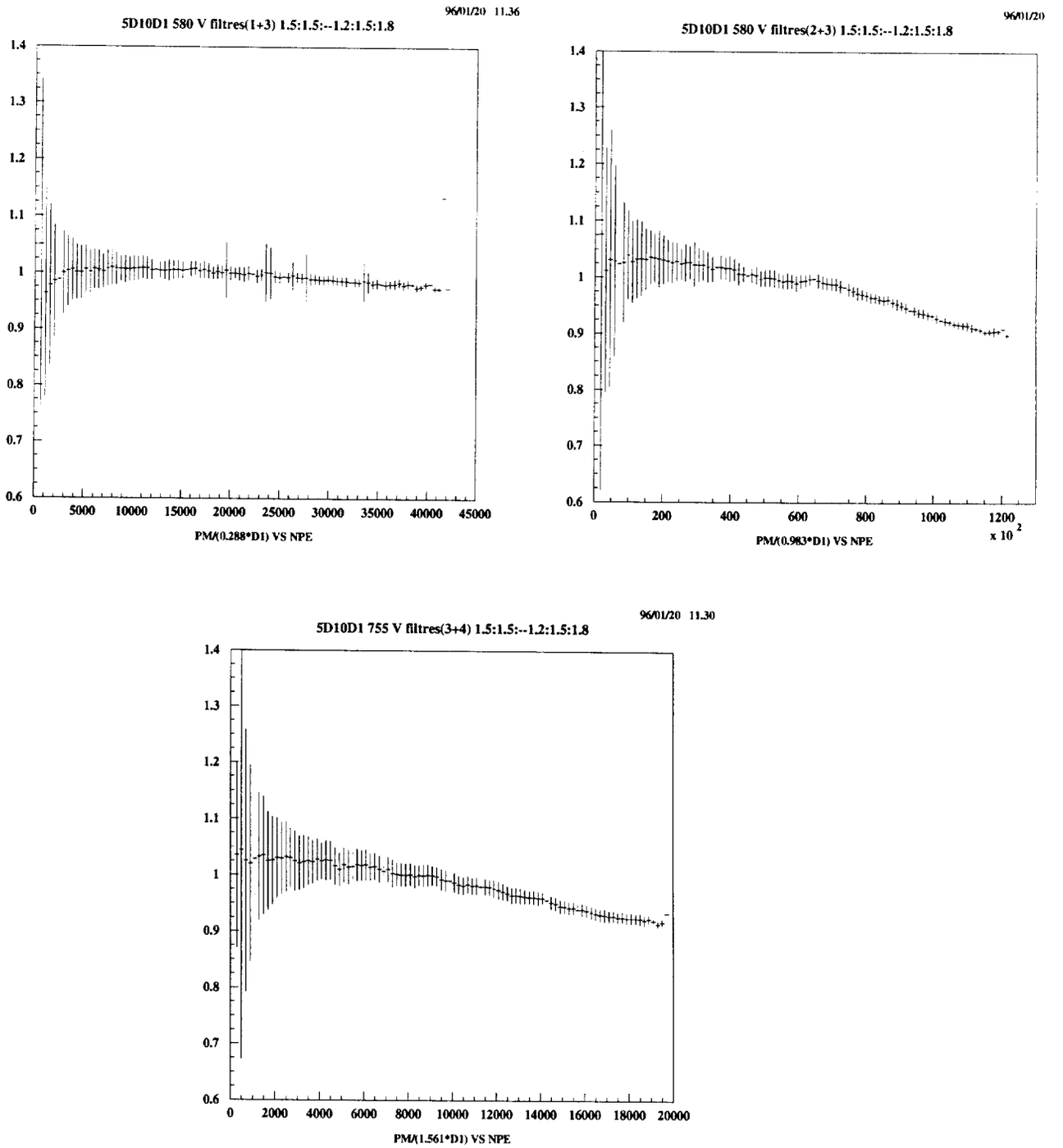


*Figure 62 : Differential linearity curves with a 1.2:1.5:1.8:1–1.5:1.5 repartition. Top figures correspond to a PMT amplification of* $10^5$ *with two different ranges in* $N_{p.e.}$*. Bottom corresponds to an amplification of* $10^6$*.*

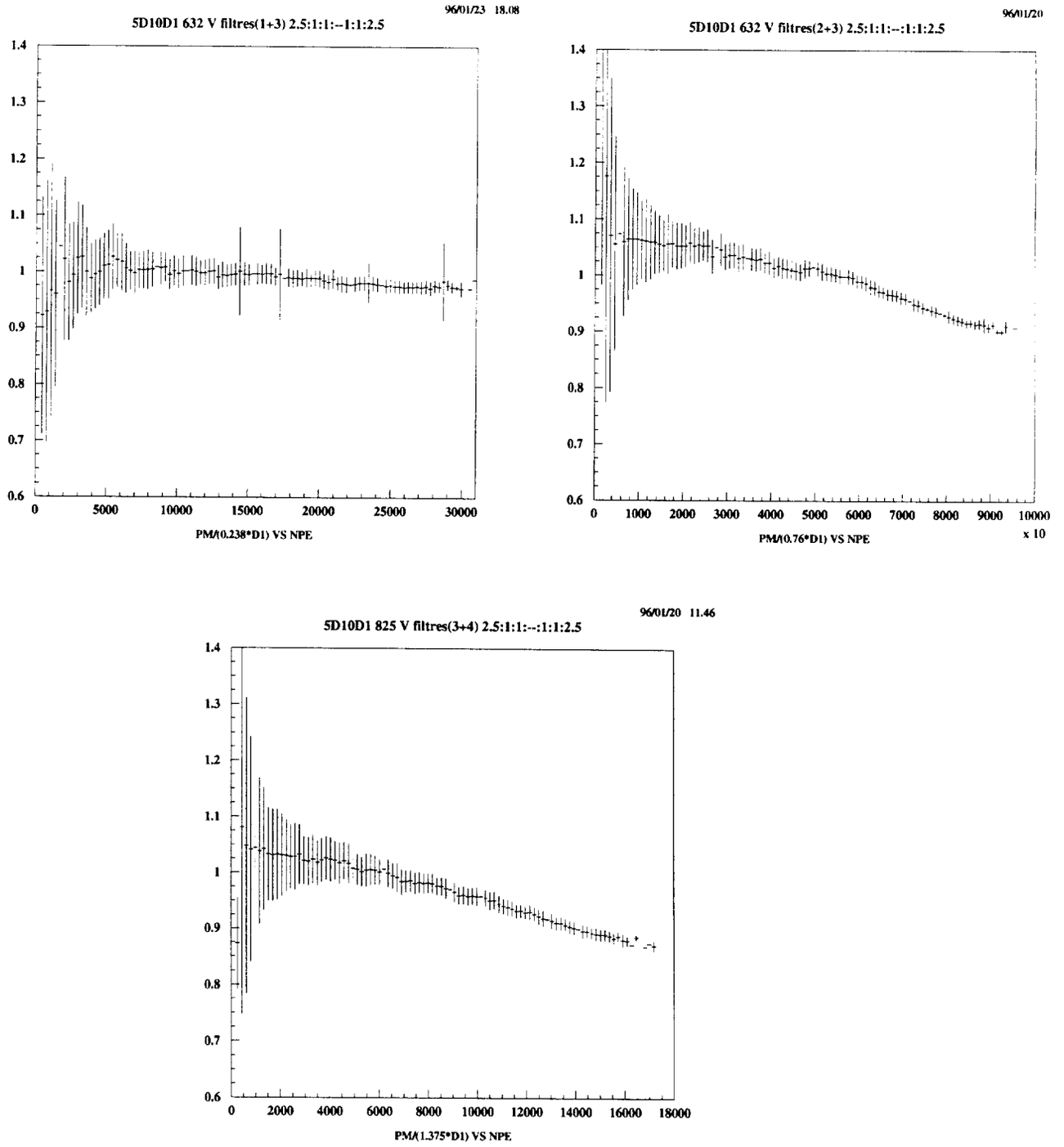


*Figure 63 : Differential linearity curves with the 2.5:1–1:2.5 repartition. Top figures correspond to a PMT amplification of* $10^5$ *with two different ranges in* $N_{p.e.}$*. Bottom corresponds to an amplification of* $10^6$*.*

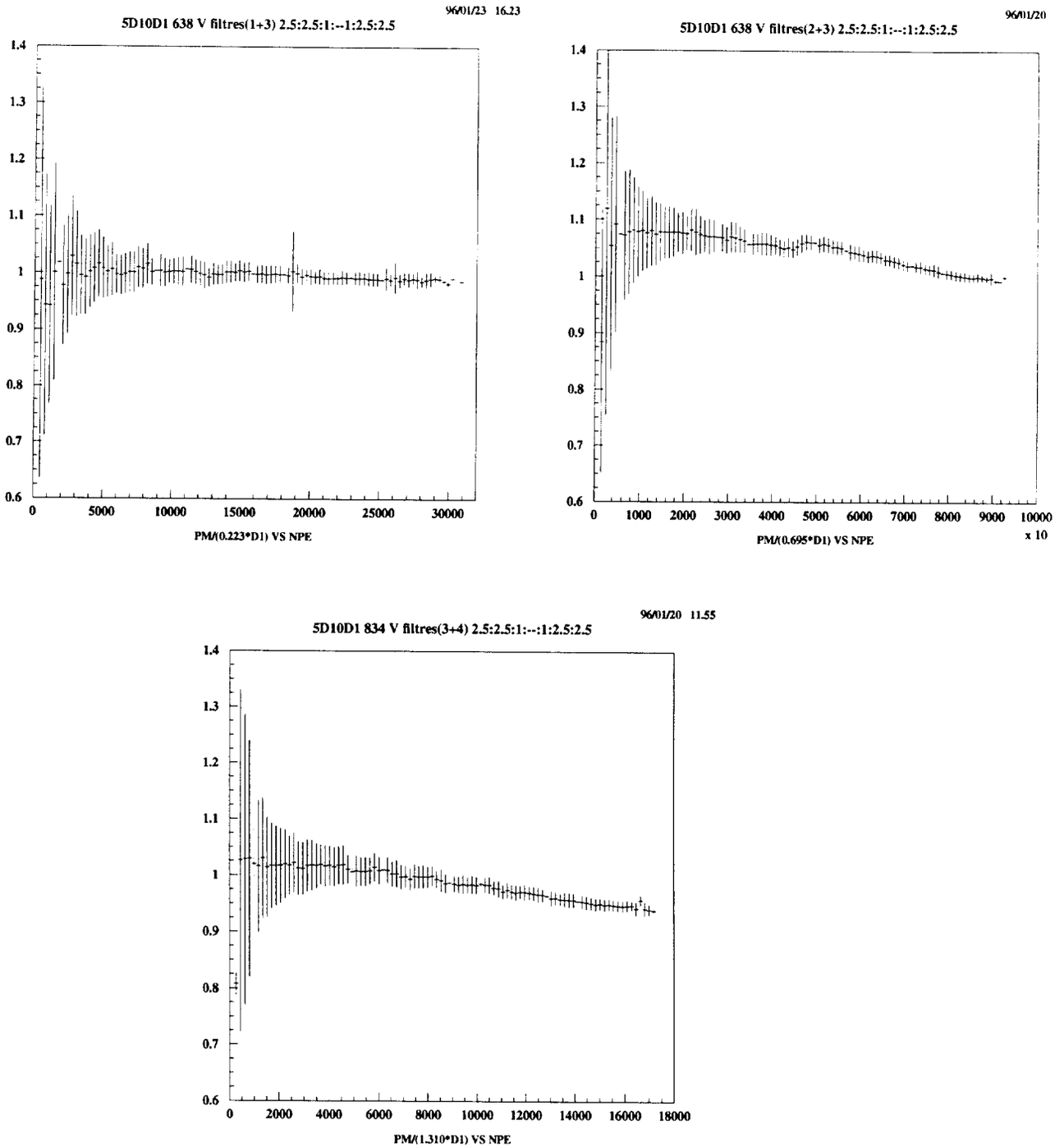


*Figure 64 : Differential linearity curves with the 2.5:2.5:1–1:2.5:2.5 repartition. Top figures correspond to a PMT amplification of* $10^5$ *with two different ranges in* $N_{p.e.}$*. Bottom corresponds to an amplification of* $10^6$*.*

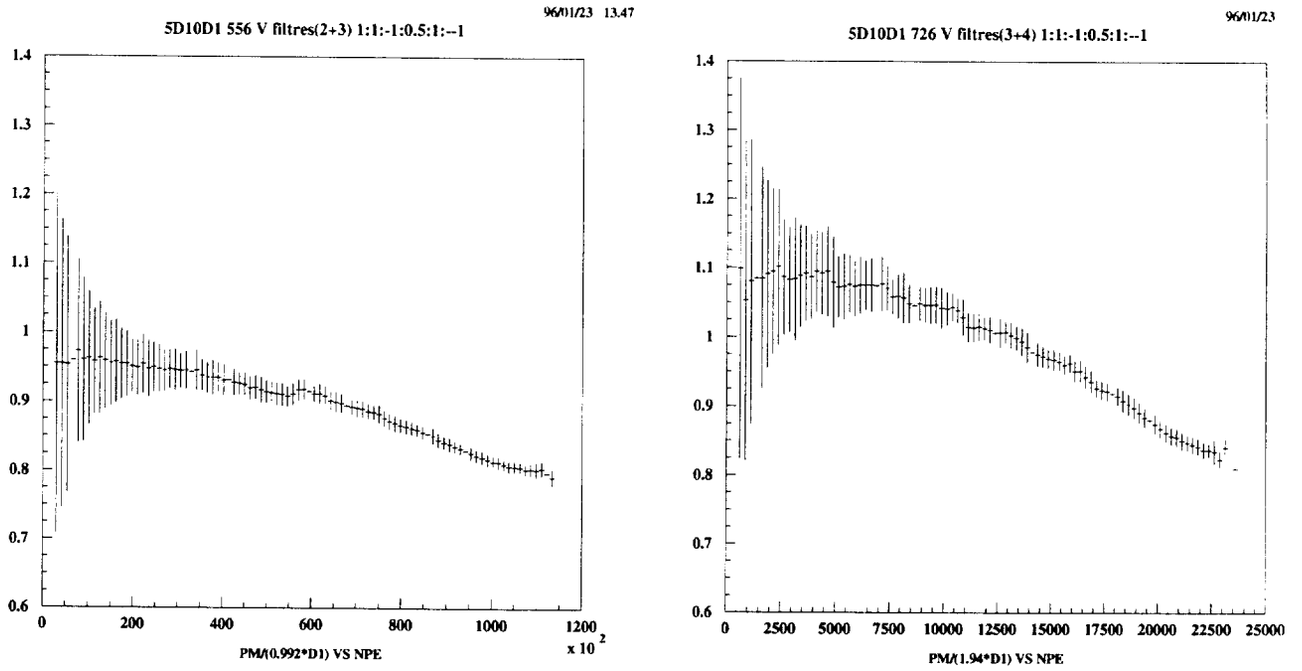


*Figure 65 : Differential linearity curves with the 1:1:1-0.5-1:1:1 repartition. Top figures correspond to a PMT amplification of* $10^5$ *with two different ranges in* $N_{p.e.}$*. Bottom corresponds to an amplification of* $10^6$*.*

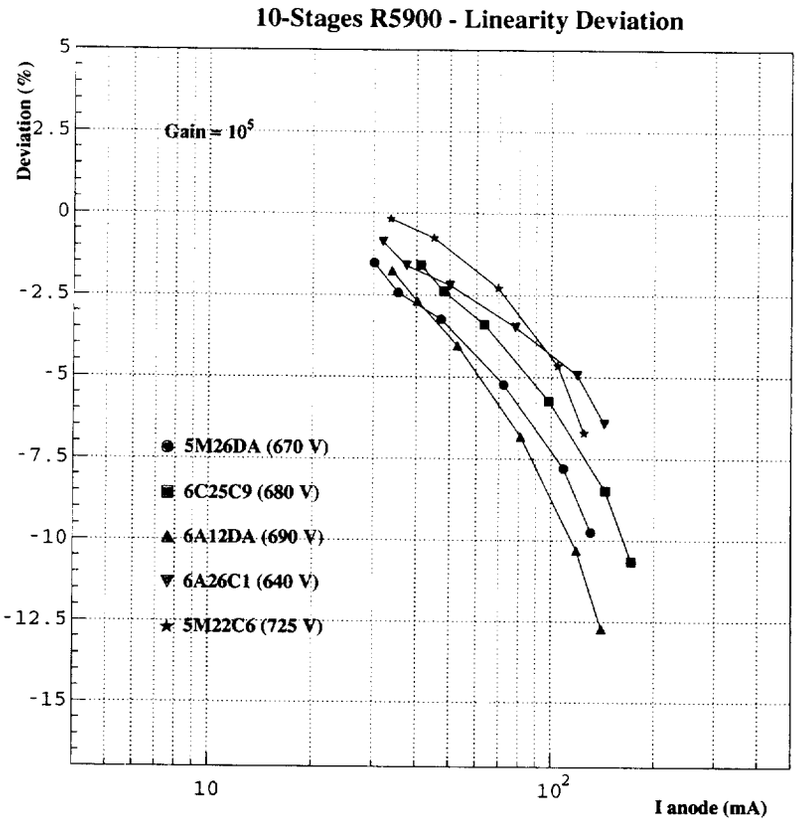


*Figure 66 : Linearity deviation of a set of 5 PMTs, used in Module 0, measured at the nominal amplification, with the 2.5:2.5:1:1–1:2.5:2.5 voltage repartition. For these measurements, the experimental set-up is the one presented on Figure (44): the variation of the pulsed light amplitude is achieved using a set of different attenuation neutral filters. The 2% linearity deviation corresponds to a PMT anode current range of 30 to 60 mA, and with a pulse width of 17 ns, in a photoelectron range of 32K to 64K. 50 K photoelectron with an amplification of* $10^5$ *corresponds to a resulting PMT anode current equal to 50 mA*

# 7. Magnetic sensitivity

As required in the calorimeter light read-out specifications (Section 1.4), a magnetic shielding is necessary to avoid the effects of the residual magnetic fields on the PMT. In order to provide a large safety factor, the goal was first to have a maximum gain variation of about 1% for a field of 500 Gauss in every direction.

The R5900 magnetic sensitivity studies have been done at CERN and at Clermont-Ferrand without and with shielding. The main results correspond to the gain variation for several field directions ($\phi$ and $\alpha$ angles). The angles definitions are shown on Figure (67):

- the $\phi$ angle is related to the (x,y) grid structure.
- the $\alpha$ angle is related to the PMT z-axis.

We define the limit for the maximum gain variation to be below 1.4% (in absolute value), with 0.4% coming from the relative accuracy of the measurements. The maximum authorized fields will correspond to these limits.

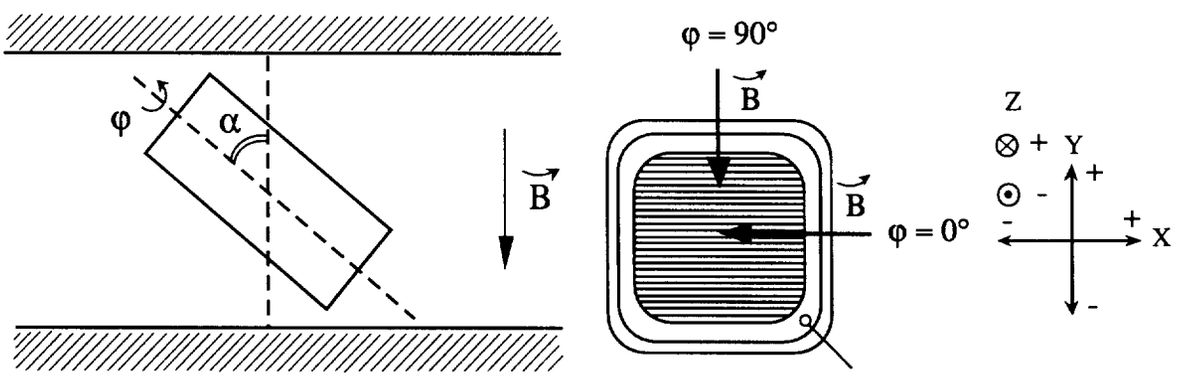


*Figure 67 : Definition of the angles $\phi$ and $\alpha$ and referential used to test the R5900.*

### 7.1 R5900 Magnetic field sensitivity without shielding

The measurements of the effects of the magnetic field on the bare PMT allow to achieve the optimization of the shielding. The effect of fields perpendicular to the PMT z-axis ($\alpha = 90°$) with various $\phi$ angles, in the B ranges of about (0, 200 gauss) and ($\pm$35 gauss) are shown respectively in part a) and b) of Figures (68).

Along the y-direction, ($\alpha = 90°$ and $\phi = 90°$), the results are always within the 1.4% specifications, independently on the field direction. In the x-direction ($\alpha = 90°$ and $\phi = 0°$)) the sensitivity is strongly increased and an asymmetry appears between the negative and positive fields. That is a direct effect of the grid structure. Nevertheless, the specifications are reached roughly for fields in the range $\pm$5 gauss, easily managed by the $\mu$-metal shielding. For a larger field of about 100 gauss, the loss of efficiency can reach 60%.

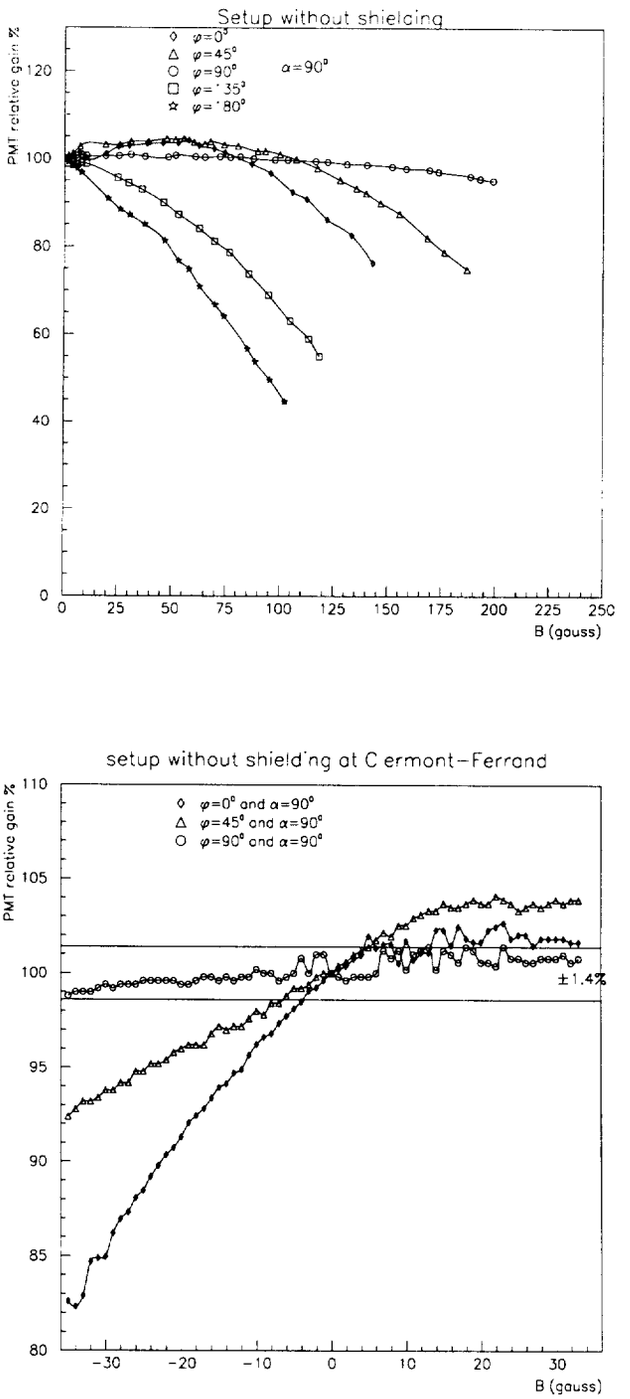


*Figure 68 : Effect of the magnetic fields on a bare R5900 PMT: a) and b) Field perpendicular to the z-axis ($\alpha = 90°$) with various $\phi$ angles, in the B ranges of about (0, 200 gauss) and ($\pm 35$ gauss), respectively.*

The Figure (69) compares the effect of fields perpendicular ($\alpha = 90°$) and parallel ($\alpha = 0°$) to the z-axis. The behaviours are different, but the PMT is rather less sensitive to the fields parallel to the z-axis.

Only one R5900 PMT has been tested, but the measured behaviours are similar to the one observed when testing the R5600 PMTs. In fact the magnetic field effects only depend on the metal channel dynodes structure, which are roughly equivalent for the two types of PMTs. From the R5600 tests one conclude that there is never a huge fluctuation from a sample to another one in a set of PMT.

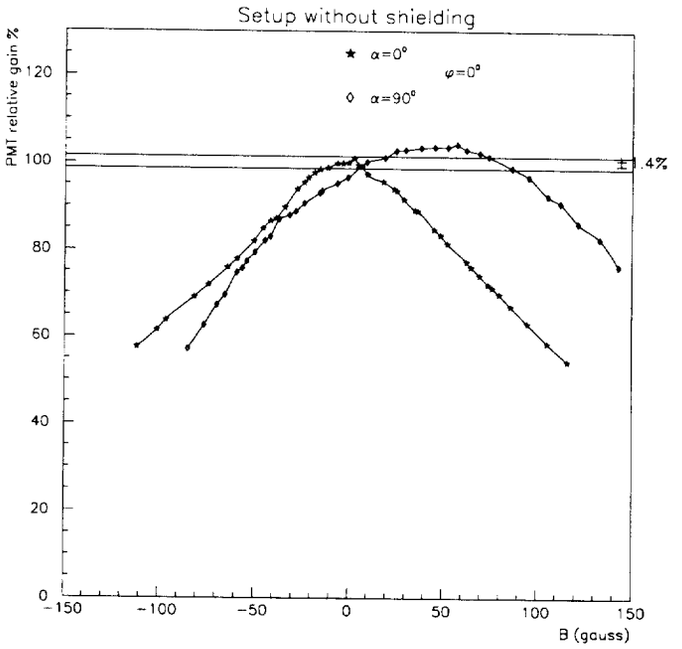


*Figure 69 : Effect of magnetic fields on bare R5900 PMT: Field parallel to the z-axis ($\alpha = 0°$) and field perpendicular to the z-axis ($\alpha = 90°$), in the B range of about ($\pm$100 gauss).*

### 9.2 R5900 Magnetic field sensitivity with shielding

The set-up corresponding to the optimum shielding is shown on the Figure (70). The optimization of the shielding clearly depends on the light mixer length, and so on the light uniformity constraint. Moreover, the overal size (length and external diameter) of the iron cylinder in addition depends upon the available space inside the drawer system.

The use of the end-cap and front iron ring that are closed as much as possible to the magnetic shielding cylinder results directly from the tests. The final design of the PMT "Block" must take into account other constraints such as the mechanical tolerances, the design of the 3-in-1 PMT base and the cabling to the outside world.

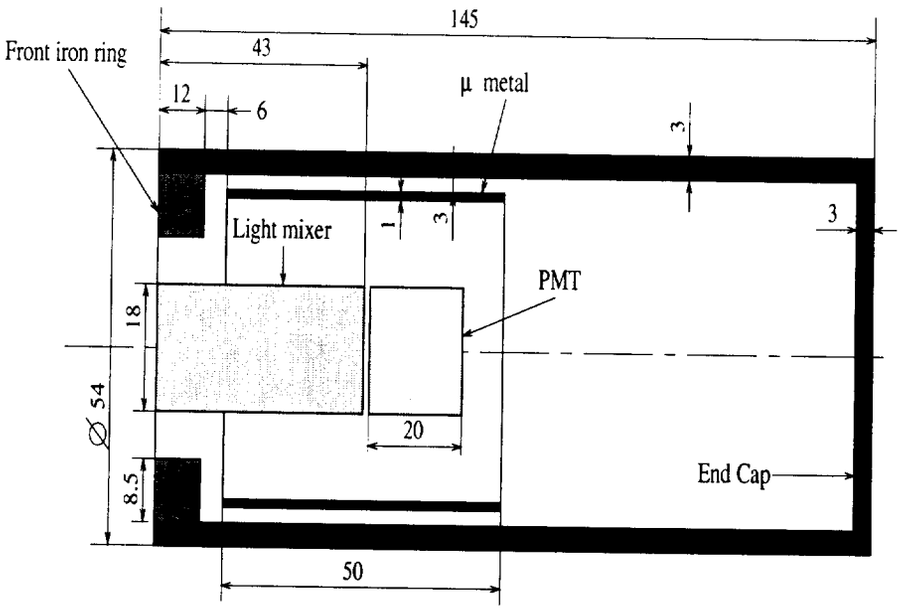


*Figure 70 : Optimum shielding design. Dimensions are given in mm.*

The magnetic fields sensitivity of two different R5900 PMTs (# 5M26DA and 6A12DA), with the final design of the shielding are shown on Figure (71):

a) effect of a longitudinal field ($\alpha = 0$).

b) effect of a transverse field ($\alpha = 90°$) with different orientations ($\phi$).

These figures indicate clearly that after shielding the results are independent from the tested PMT, and that, within the 1.4% specifications, the shielding is efficient up to 800 and 250 gauss, respectively, for transverse and longitudinal magnetic fields.

One should compare the resulting limits to the estimated fields in the ATLAS environment. As summarized in Table (12), the full magnetic simulations taking into account the effects of the two solenoid and toroid contributions, show that the longitudinal components are lower in the worst case than the transversal one. The ratio of the fields corresponding to the limits of shielding to the largest simulated values defines some safety factors. This safety factor is in any case above 40, and even larger in the longitudinal direction.

| | Simulation limit (*gauss*) | Shielding limit (*gauss*) | Safety factor |
|---|---|---|---|
| $B_{\perp}$ | $< 20$ | $\leq 800$ | $\geq 40$ |
| $B_{//}$ | $< 5$ | $\leq 250$ | $\geq 50$ |

*Table 12: Compilation of magnetic field limits on the R5900, using a gain variation of* 1.4% *for the limit definition in the shielding tests, and the full magnetic filed simulation.*

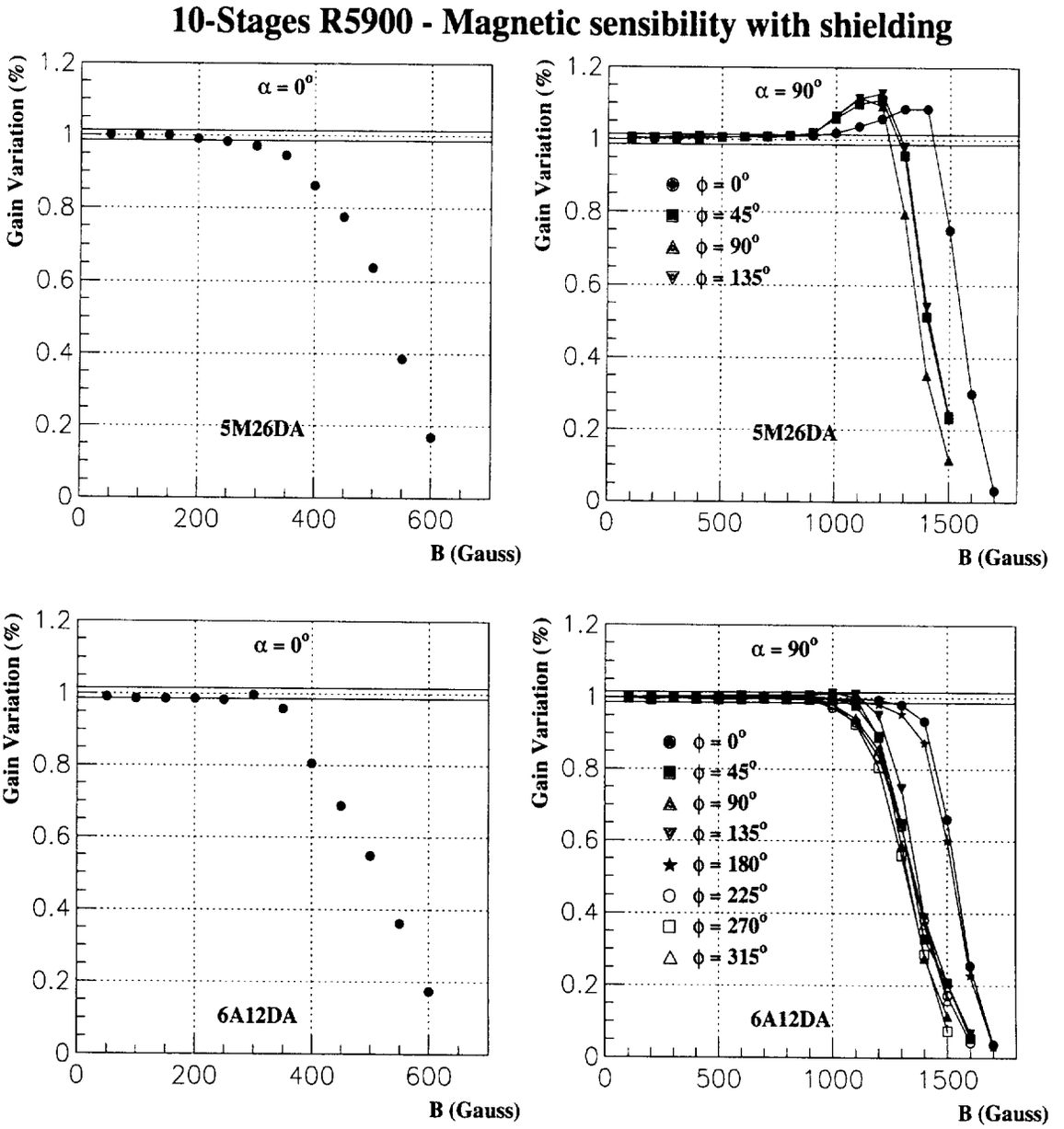


*Figure 71 : Effects of magnetic fields on shieldied R5900 PMT, for two PMTs (# 5M26DA and 6A12DA): a) field parallel to the z-axis ($\alpha = 0°$)in the range (0, 600 gauss). b) field perpendicular to the z-axis ($\alpha = 90°$), with various $\phi$ angles, in the range (0, 1600 gauss).*

# 8. Voltage divider optimisation

The voltage divider provides first the correct interdynode voltages for the photomultiplier. As shown in section 6.3, it could be used also to insure a good linearity of the anode output current over a wide range of incident light levels when operating the PMT with its nominal amplification of $10^5$.

The other design criteria are the light collection efficiency and the reduction of the space charge effects.

The divider acts also as a socket for the PMT, it supports the board (3-in-1 board) where are implanted the integrator, the shaper and the services and controls.

The choice of resistors in the voltage divider is first governed by the value of the DC current that flows in the voltage divider. This DC current is estimated using a factor of 100 above the mean anode current. In the calorimeter, the mean anode current is mainly due to the pile-up events that occur at each bunch-crossing. Using the worse configuration, i.e., on average 40 pile-up events at each bunch crossing, one could find an average anode current of the order of 2 $\mu$A. This value induces a voltage divider current equal to 200 $\mu$A.

In an isovoltage repartition (1:1:—-1:1) with a typical high voltage of 650 Volts for the nominal amplification, the increment value of the divider resistor is equal to 295 k$\Omega$. The corresponding interdynode voltage is equal to 60 Volts.

In the pulsed mode operation, an intense light induces a large current flow in the last dynode stages, affecting considerably the voltage repartition, and then changing the PMT response. To prevent such a problem, decoupling capacitors can be connected to the last stages. These capacitors supply the photomultiplier tube with an electric charge during the pulse duration and restrain the voltage drop between the last dynodes and the anode.

So, if the pulse width is short enough, it is possible to derive an estimate of the capacitor. Let us suppose that output pulse charge $Q_0$ corresponds to 800 pC with a pulse duration of 15 ns, the charge stored in a capacitor C is $Q = C \times V$. In order to achieve a good linearity, we used the following constraint:

$$Q(= C \times V) >> 100 \times Q_0 \tag{78}$$

together with an average interdynode voltage V equal to 60 Volts (1:1:1:1—1:1 repartition), one estimates that C should fullfill the following condition:

$$C >> 1.3\text{nF} \tag{79}$$

Figure (72) represents the design for the voltage divider with the 2.5:2.5:1–1:2.5:2.5 configuration, used for test of the Module 0. Last stages capacitors (C1, C2, C3) has been choosen equal to 22 nF. This value corresponds to a standard low cost product in SMD components.

Moreover, one has a large safety factor in comparison to the estimation. Resistors R1 to R11 are metal film ship resistors with a 1% precision. The resistor between the HV and the photocathode with the corresponding capacitor (10 nF) is used to reduce the pick-up noise coming from the high voltage. The value of this resistor (10 kohm) has been choosen as a trade-off between the efficiency of the RC filtering and a drop of the applied high voltage. A small value resistor is used to separate the high voltage ground and the analog ground of the 3-in-1 board.

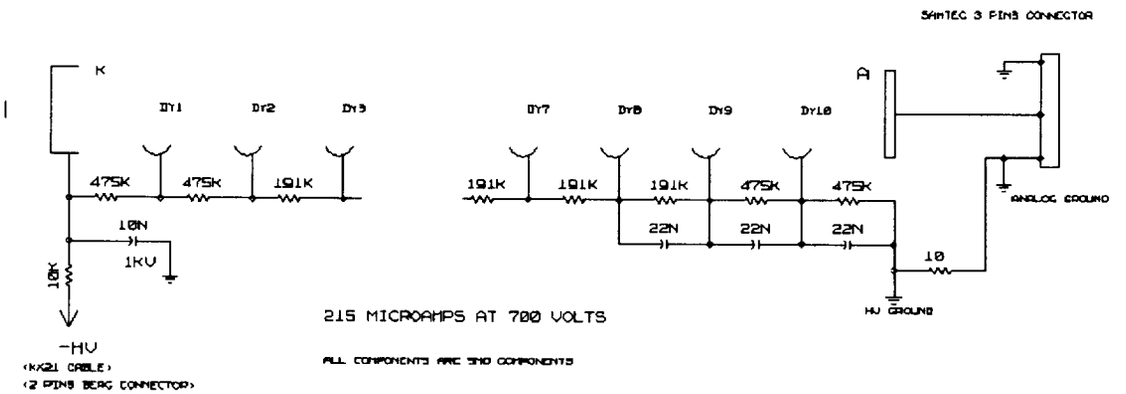


*Figure 72 : Design for the voltage divider with the 2.5:2.5:1–1:2.5:2.5 configuration, used for the test of Module 0.*

# 9. Conclusions

The 10-stages R5900 PMT satisfies the requirements of the TILECAL readout system presented in section 1.

• The magnetic field shielding is very easy to achieve with an important safety factor ($> 40$), since the R5900 is itself rather insensitive to magnetic field.

• The spatial uniformity of the R5900 is now good, and the addition of a 43 mm "Light mixer" is sufficient to garantee that the PMT response is independent on the impinging point of the light on the photocathode, and so on the illuminated tiles.

• The R5900 quantum efficiency at 480 nm is of the order of 16.4 % with a dispersion of 6.2 %. This is a quite normal value for a standard bialkali photocathode, since it corresponds to a quantum efficiency of $\sim$ 21% at 400 nm.

• The R5900 collection efficiency is achieved for low values of the voltage between the photocathode and the first dynode: $\sim$ 20 (40) Volts for a photocathode current of 10 nA (30 nA). By the way, the PMT efficiency is reached over a large range of voltages.

• The R5900 dark current at an amplification of $10^5$ is of the order of few tenth of pA.

• The R5900 is almost insensitive to the temperature since the variation of the amplification is of the order of 0.2 % per $1°C$.

• Operating the R5900 in realistic conditions, i.e., with a DC light added component simulating the pile-up effect, a $2\mu A$ DC anode current corresponds a 2% variation of the PMT amplification.

• In the dynamic range going up to 50K photoelectrons, the 2% deviation linearity is achieved for most of the R5900. Due to fluctuations, some PMTs could have a larger values but in any cases below 5%. This results from the optimisation of the voltage divider with a 2.5:2.5:1–1:2.5:2.5 configuration.

The 2.5:2.5:1–1:2.5:2.5 configuration is due mainly to the fact that this R5900 is a 10-stages PMT, and that the dynamics for the TILECAL assigns the nominal amplification ($10^5$) well below the standard one ($10^6$), for which the nominal operating conditions is 800 Volts. It is the reason why we are studying a specific 8-stages R5900.